NUCLEIC ACID-PROTEIN HYBRID MATERIALS

A Dissertation

Presented to the Faculty of the Graduate School

of Cornell University

In Partial Fulfillment of the Requirements for the Degree of

Doctor of Philosophy

by

Thua Nguyen Nhi Tran

May 2012

NUCLEIC ACID-PROTEIN HYBRID MATERIALS

Thua Nguyen Nhi Tran, Ph. D.

Cornell University 2012

DNA nanotechnology was used to interface with proteins through DNA-protein hybrid molecules for protein detection and protein intracellular delivery. EZZ protein, which can bind to almost all IgG antibodies, was selected to be conjugated to DNA linker. Different methods of DNA-protein conjugation were used to develop universal adapters between IgG antibodies and DNA. Using DNA nanobarcodes, which is based on the color ratios of two colors rather than using different colors, a library of IgG-based nanobarcodes were generated through a simple mixing step. The IgG-based nanobarcodes were used as a platform to simultaneously detect target proteins in different systems, including microbead-based, membrane-based, and tissue-based. Moreover, for the first time, a new concept of using DNA transfection reagents was introduced to deliver proteins intracellularly with great efficiency.

BIOGRAPHICAL SKETCH

Born and raised in a peaceful coastal city, Vung Tau City, in southeastern Vietnam, Thua Tran grew to love the immense ocean and dreamed one day she would go beyond the horizon to learn more about the world. After finishing her bachelor's degree in Microbiology and Molecular Biology, she was accepted to a tenure track position at the Department of Environment within Ho Chi Minh City University of Natural Sciences. While pursuing a master's degree in Environmental Sciences, Thua won the Vietnam Education Foundation (VEF) Fellowship Award, created by the US Congress and funded by the US Federal Government, for a Ph.D. degree at Cornell University. This gave her the great opportunity to fulfill her childhood dream of going beyond the Pacific Ocean's horizon, where she experienced a totally new life in Ithaca, New York. After many long years with tremendous support from advisors, family, and friends, she completed her Ph.D. degree in Bioengineering with pride and satisfaction.

To my parents, my sister, and my loved ones

ACKNOWLEDGMENTS

No words could describe how grateful I am for the tremendous help, support, and guidance that I have been receiving in life and during the years at Cornell University. Without those, I would definitely not be here and could not have completed my Ph.D. degree.

My first teachers, whom I could never thank enough, were my parents, who taught me to be honest, sincere, strong, and independent. Without the opportunity for a good education, they transferred their love of knowledge and their dreams of higher education to help me fly high and far. I am glad that I could fulfill their dreams and make them proud of me.

It is said that there are always opportunities, but you must know where to find them and when to catch them. I would like to thank the U.S. Government and Vietnam Education Foundation (VEF) for giving not just me, but hundreds of other fellows like me, the opportunities to meet great people, to learn, and to contribute to the greatness of knowledge.

However, I would never be able to complete my Ph.D. degree without the countless support and guidance in many years from Professor Dan Luo, my academic advisor and the chair of my committee. I am also indebted to Professor John March, and Professor John Lis for their advice, understanding, and for always making themselves available for me whenever I needed them.

I also deliver my thanks to all members in Luolabs for their technical help, suggestions and discussions, especially Mark Hartman, Natt Kiatwuthinon, Jason

Kahn, and Shawn Tan, who were also good friends and made my years in Luolabs more fun and memorable. Thanks also to Jinhui Cui and Chuanying Xu for their hard work and intensive help. I also sincerely thank Dr. Hisakage Funabashi for being a great mentor during my first years in Luolabs, and who also had strong influences on me about science and work ethics.

Moreover, I am grateful for the technical help from Carol Bayles and Johanna M. Dela Cruz in the bioresource center, Lavanya Gowri Sayam in the flow cytometry facility in Vet school, Dr. David Latulippe from Professor Harold Craighead's group, Dr. Abdullah Ozer from Professor John Lis' group, and Dr. Faping Duan from Professor John March's group.

I will also never forget the kindness, friendliness, support, and smiles from all of the professors and staff of the BEE department, especially Nancy Fairchild, who has gone through many "troubles" with me, but always smiling and encouraging to me.

And thanks to my Vietnamese "gang" and awesome housemates, especially Markus Brink and Jahan Dawlaty, who were like big brothers to me and who helped me adapt to the new environment from the very first days that I lived in the Gamma Alpha co-op science house, and to Brendan Holt and Andy Poshadel for their good friendships and for all the fun with pool games, movies, guitar playing, English teaching, etc. You all made me feel at home, and made the years in Ithaca less painful and less homesick.

For those whom I could not name here, my sister, cousins, relatives, old friends, new friends, my loved ones, you are always in my heart for even the smallest

things that you have done for me. Thanks to everyone's support, the story of my student life is now ended and a new chapter of my life is beginning. I'll keep all the lessons and memories in mind as I continue on the journey ahead.

TABLE OF CONTENTS

LIST OF FIGURES

LIST OF TABLES

CHAPTER 1: INTRODUCTION

The concept of bringing two or more different materials to work together, to create so-called “hybrid” materials with new characteristics and applications, is an interesting and exciting development in materials science. This work will describe how DNA and protein are brought together to serve as one material, with the properties, advantages, and functions of both nucleic acid and protein. In addition, I will describe applications of DNA-protein hybrid materials, as well as discuss the potential of the field.

The structure of the dissertation includes six chapters. Chapter 1 will introduce the background for a general understanding about this work and related fields including DNA nanotechnology, DNA-protein conjugation, protein detection, and protein delivery. Chapter 2 and 3 will talk about the different methods of making DNA-protein hybrid materials, and their characterization. Chapter 4 and 5 will focus on the applications of protein detection and protein delivery, respectively. Finally, Chapter 6 will wrap up with conclusions and open up to discussions and future directions.

1.1. DNA As Generic Materials For Nanotechnology

DNA has been well known as the genetic material of life since it was first discovered. However, since the early 1980s, Seeman introduced a new concept of using DNA as a generic material, creating rigid, artificial branched DNA junctions[1] as building blocks to construct geometrical DNA nanostructures[2, 3]. Using the most basic and important property of DNA, Watson-Crick base pairing, Seeman and his group produced unnatural two, three, four-armed branched DNA junctions using double-crossover (DX)[4], triple-crossover (TX)[5], and paranemic-crossover (PX)[6] motifs. Inspired by these motifs, additional designs such as parallelograms[7], four-by-four-structures[8], and three-, five-, and six-point star motifs[9-11] have been developed and assembled into 2D nanoarrays [12-14], 3D-nanoarrays[15-17], and DNA nanodevices[18, 19], as shown in Figure 1.1. More recently, Rothemund has presented the "DNA origami" concept (Figure 1.2) as a novel approach to create arbitrary patterns, such as a star or smiley face[20]. Later, DNA origami became widely used to form more complicated structures[21, 22] or a DNA box with a controlled lid[23]. For more details about recent developments in structural DNA nanotechnology, please read the excellent reviews [18, 24-28].

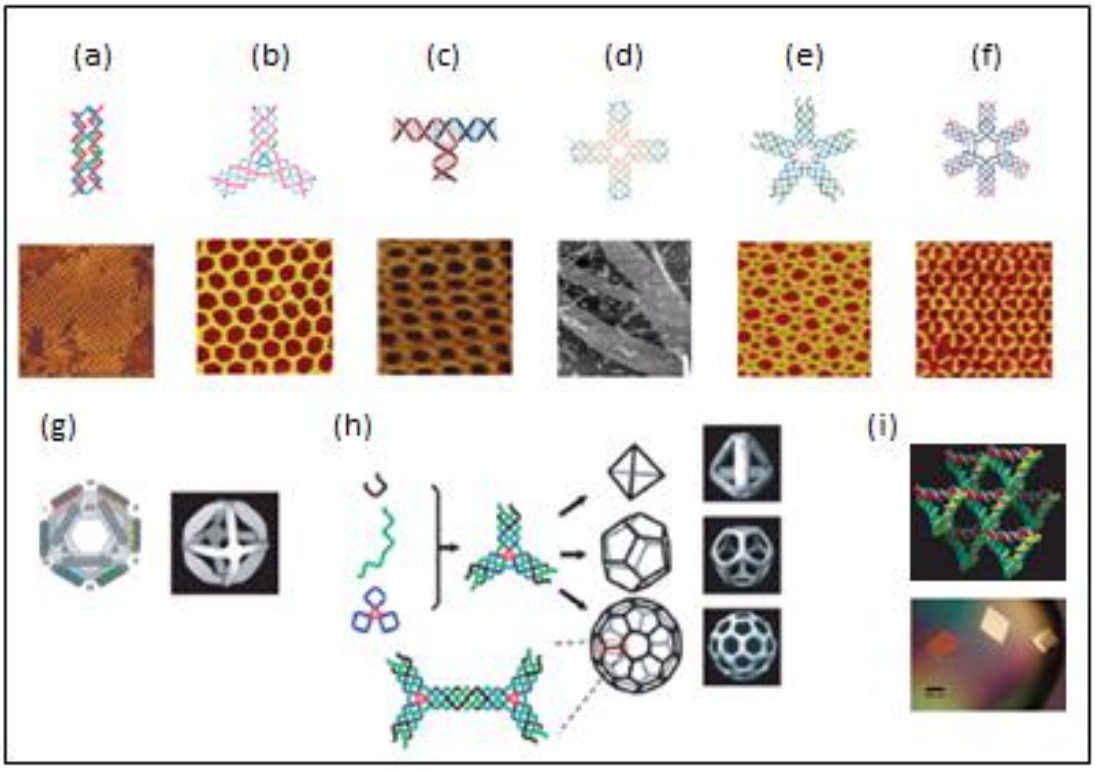

Figure 1.1. General motifs of structural DNA nanotechnology. (a-f) 2D DNA nanostructures formed from double-crossover (DX)[12], three-point-star[9], T-junction[29], four-by-four junction[8], five-point-star[10], and six-point-star motifs[11], respectively. (g) The first 3D DNA octahedron nanostructure assembled by DX motifs.[30] (h) Hollow polyhedron 3D structures assembled by three-point-star motifs.[17] (i) The first 3D DNA crystal (bottom) formed by the tensegrity triangle (top).[16]

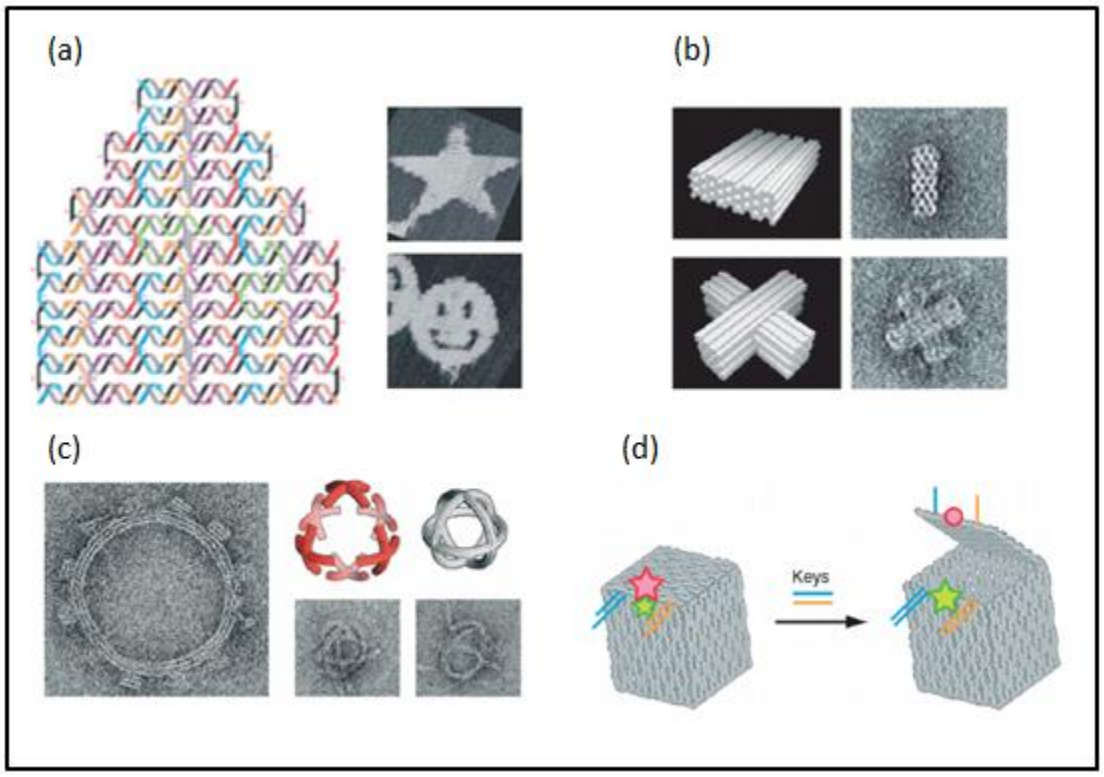

Figure 1.2. DNA origami. (a) 2D DNA nanostructures made by DNA origami. (b-c) 3D DNA origami[21, 22]. (d) DNA box based on DNA origami.[23]

However, in general, structural DNA nanotechnology has existed as a mostly academic pursuit. In contrast, taking advantage of molecular biology toolkits, Luo and his group has brought "biology to materials"[31] and can be considered as one of the first groups to use branched DNA building blocks for biological and biomedical applications. Unlike Seeman and other research groups who are using complicated DX, TX, or DNA origami in their work, Luo has focused on the simple double helix DNA structure to build Y-shaped and X-shaped DNA molecules (Figure 1.3 a) as the building blocks for multifunctional materials. Moreover, using ligase to "glue" Y- or X-monomers together, rather than just based on nucleic acid hybridization[32, 33], Luo

and coworkers have formed stable dendrimer-like (DL) DNA[34], and DNA hydrogel[35], which later were used as DNA nanobarcodes for multiplexed DNA detection[36] (Figure 1.3 b), and in a DNA hydrogel for cell-free protein production ("P-gel")[35, 37] (Figure 1.4), respectively. More recently, as an alternative to ligase, they have used photocrosslinker-modified DNA to generate DNA nanospheres for drug delivery[38]. Moreover, attaching different functional moieties to the molecular branched building blocks, they created multifunctional nanoarchitectures from anisotropic, branched and crosslinkable building blocks (ABC monomers)[39] (Figure 1.3b). This material was utilized in a pathogen detection system in which photo-polymers were generated only in the presence of a specific DNA sequence, and was also used as a biocompatible nanovector to deliver both drugs and tracers simultaneously. In addition to interacting with biological systems, DNA could also be used to interact with non-biological systems such as gold nanoparticles, allowing for enhanced control of the self-assembly of highly ordered nanoparticle arrays[40-42].

In summary, DNA is an excellent material for a range of applications due to its many unique properties. As mentioned above, Watson-Crick base pairing is highly sequence specific, which makes DNA hybridization rationally designable and programmable. Another great property of DNA is its precisely controlled dimensions at the nanoscale, so it can be produced with the exact length as desired. One base is about 0.34 nm in length and 2 nm in diameter, and the helical periodicity of double helix DNA is 10–10.5 nucleotide pairs, or 3.5 nm per turn. Moreover, unlike most polymers or other soft materials, DNA has a persistent length of 50 nm or 1 nm for double stranded or single stranded DNA, respectively, so by simply adjusting the

number of base pairs to tune the length, we can get either a rigid or flexible fragment of DNA. In addition, our work takes advantage of molecular biology toolkits to manipulate DNA. DNA can be cut specifically, chopped nonspecifically, linked, or amplified by more than 4000 different enzymes, including restriction enzymes, nucleases, ligases, and polymerases. Furthermore, DNA is non-toxic, biocompatible, and biodegradable. Finally, DNA can be modified with variety of chemical groups, nanoparticles, polymers, fluorophores, or (as the main focus of this dissertation) proteins. Combining all of these properties above makes DNA not only a unique material in and of itself, but also excellent for using with other materials.

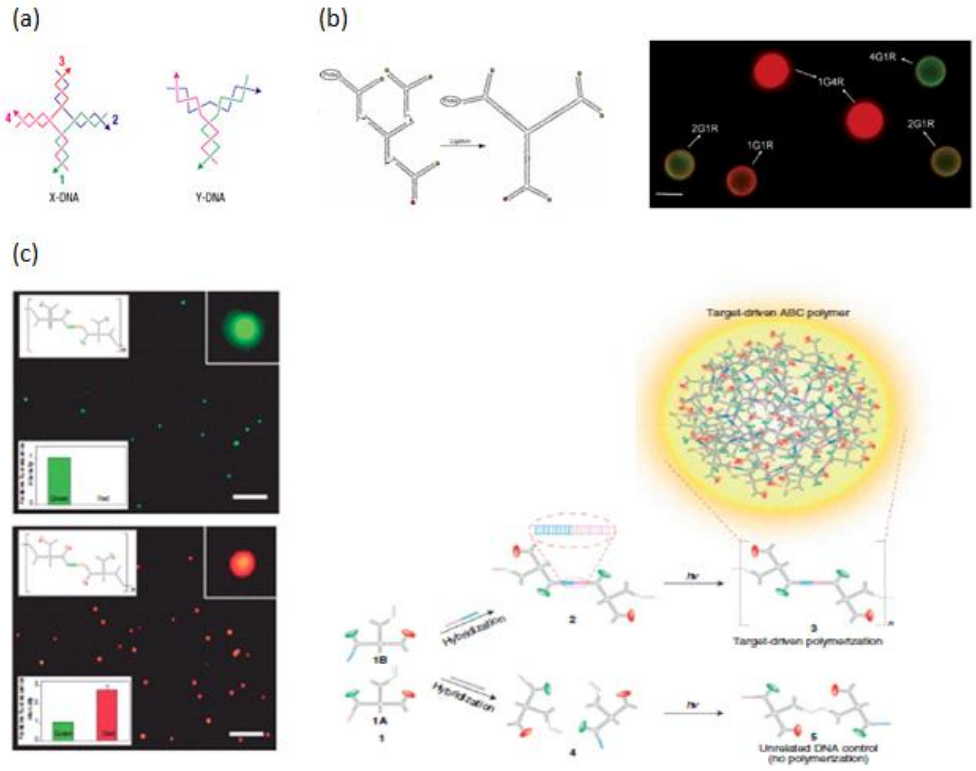

Figure 1.3. DNA as generic materials. (a) X-DNA, Y-DNA building blocks. (b) Dendrimer-like DNA based DNA nanobarcodes for multiplexed DNA detection.[36] (c) Target-driven polymerization of ABC monomers for multiplexed DNA detection.[39]

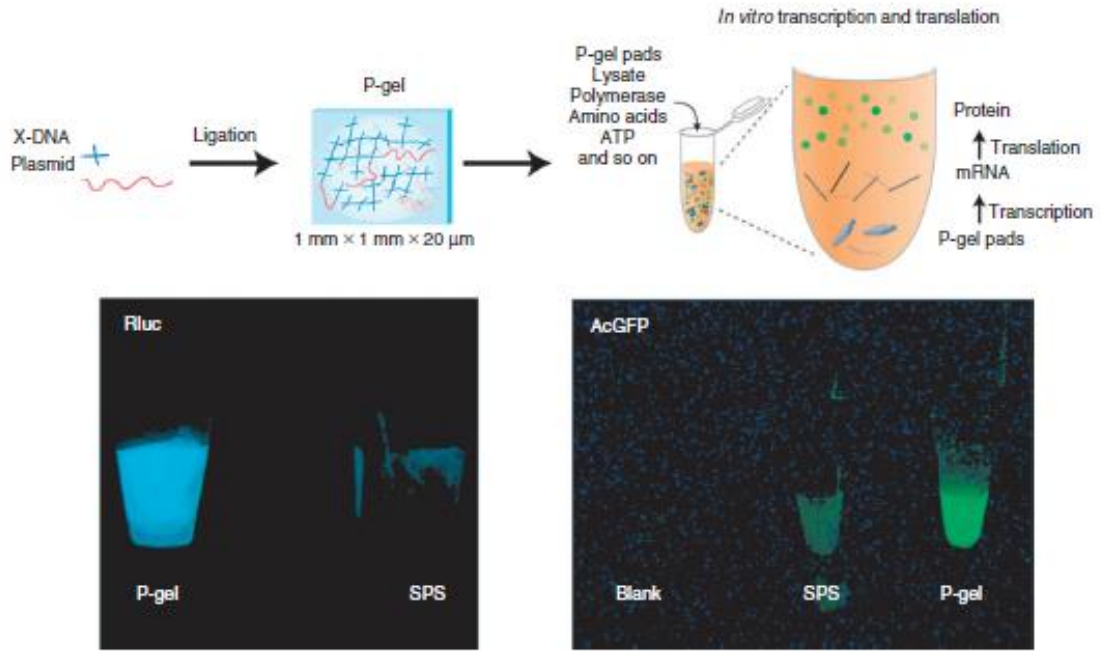

Figure 1.4. Protein-producing DNA hydrogel ("P-gel")[37]. The plasmid is incorporated into a DNA hydrogel matrix which shows greater expression of protein in a cell lysate, compared to conventional method ("SPS") of using only gene with cell lysate.

1.2. DNA Protein Hybrid Nanostructures

As mentioned above, DNA nanotechnology has been the core of many achievements of our lab. One of our goals is to explore novel uses of DNA, either by itself or combined with other materials to explore applications in many areas, including biomedicine, biological and biomedical diagnosis, environmental

monitoring, food safety, and materials. It would be extremely useful for these applications if we could interface our DNA structures with proteins. Proteins have a large spectrum of functions, from enzymatic activities, signal transduction, gene regulation to structural or mechanical functions. However, it is more challenging to modify proteins directly, compared to DNA, due to their relative instability and incompatibility with many chemical reagents or buffers. As discussed above, DNA can be easily controlled and manipulated; therefore, using DNA technology not only gives us more tools to work with proteins, but also allows us to interface proteins into bio and non-bio systems. In other words, combining proteins and DNA together would create new materials with new properties and functions.

DNA-protein hybrid materials have been mostly used for detection and for the assembly of biomolecular nanostructures. Due to the presence of two functional moieties, they have the advantages of interfacing with both nucleic acids and proteins at the same time. For example, in bioanalytic systems, one component could be used as the probe, and the other could serve as the reporter. Therefore, DNA-protein hybrid materials could be used for the detection of either DNA or proteins. For DNA analysis, enzymes such as alkaline phosphastase (AP)[43], horseradish peroxidase (HRP)[44], β-galactosidase[45], lipase[46], or esterase[47] have been used as signal amplifiers. For protein analysis, DNA has served as the reporters, and many innovative assays have been developed by taking advantage of DNA technologies such as PCR[48], RCA[49-51], and DNA microarrays[52-57]. Protein detection using DNA-protein conjugates will be discussed more below since it is one of the main focuses of this dissertation. For more details on other applications using DNA-protein conjugates, please read

these reviews.[58-62]

For the development of DNA-protein conjugation, many methods have been established to construct DNA-protein conjugates, either non-covalently or covalently. Table 1.1 summarizes some of the most current and widely used methods for DNA-protein conjugation. Depending on the purpose, either non-covalent or covalent approaches may be selected as the most appropriate. Non-covalent methods are relatively fast and easy, but can be disrupted by high temperature or denaturing conditions, and can also generate multiple DNA strands on one protein after the conjugation. This dissertation focuses primarily on covalent conjugation between DNA and proteins, particularly at a 1:1 molar ratio between DNA and protein for controlling the stoichiometry and geometry of the proteins by DNA.

Table 1.1. Summary of methods for DNA-protein conjugation

Non-covalent Coupling	**Covalent Coupling**
1. Biotin-(strept)avidin Interaction 2. Ni-NTA-Hexahistidine Interaction 3. Aptamers 4. Reconstitution of Apoenzymes	1. Bioconjugation Chemistry • Thiol • Amine • Carboxyl 2. Bioorthogonal Chemistry • "Expressed Protein Ligation" (EPL) • SNAP tag, CLIP tag, and HaloTag • "Click" chemistry

For non-covalent approaches, the most commonly used method is the biotin-streptavidin/avidin interaction. Despite its noncovalent bonding, the biotin-streptavidin/avidin interaction has an enormously high affinity with a disassociation constant K_d of about 10^{14} mol/L, which make it one of the strongest noncovalent bonds known in nature[63]. Also, there are a large number of biotin derivatives commercially available and mild biotinylation procedures make it one of the first choices to make DNA-protein conjugates. However, streptavidin exists as a tetramer. Four monomeric streptavidin proteins interacting with four biotin molecules makes it difficult, if not impossible, to control the stoichiometry of the resulting DNA–protein conjugates, and therefore it may not be used for the rational one-to-one construction of nanodevices. Also, streptavidin-biotin interactions can be disrupted by high temperature. Other non-covalent methods that have been used for protein-DNA conjugation are Ni-NTA-hexahistidine interaction[64-67], aptamers[68, 69], and some specific apoenzymes[70, 71]. Unlike biotin-streptavidin binding, Ni-NTA-polyhistidine- and aptamer-based conjugation strategies have much weaker affinities, in the nanomolar (nM) to micromolar (μM) range of K_d, which is approximately a million times lower than the biotin-streptavidin affinity. Moreover, Ni-NTA-polyhistidine interaction can be easily broken by the addition of a nickel chelator, such as EDTA or imidazole, and high temperatures will also destroy the binding between aptamers and their ligands.

For covalent methods, there are two big categories of chemistry and biochemistry reactions: bioconjugation methods, and bioothorgonal conjugation methods. The first group mostly utilizes the chemical reactions between thiol, amine,

carboxyl, and carbonyl groups which are available or can be easily modified onto proteins and DNA. The Thermo Scientific Pierce Crosslinking Technical Handbook is a good reference for choosing the chemistry and the crosslinkers for protein-DNA conjugation. Table 1.2 summarizes some of the commonly-used bifunctional crosslinkers. As implied in the name, bifunctional crosslinkers contain two functional groups which could crosslink two of the same chemical group (homo-bifunctional crosslinkers) or two different chemical groups (hetero-bifunctional crosslinkers) to generate DNA-protein hybrid molecules. Many homo-bifunctional crosslinkers are used to conjugate amine-to-amine or sulfhydryl-to-sulfhydryl groups, and these crosslinkers mostly utilize the N-Hydroxysuccinimide (NHS) ester or maleimide derivatives, respectively. For hetero-bifunctional crosslinkers, there are more choices to crosslink different groups with each other: for example, amine-to-sulfhydryl, amine-to-carboxyl, or sylfhydryl-to-carbonyl (aldehydes and ketones) groups.

Table 1.2. Commonly-used bifunctional crosslinkers

- Homo-bifunctional Crosslinkers (reagents with identical reactive groups at either end)

Crosslinking target	Crosslinker Reactive Groups, Features
Amine-to-Amine	N-Hydroxysuccinimide (NHS) ester
Sulfhydryl-to-Sulfhydryl	Maleimides

- Hetero-bifunctional Crosslinkers (reagents with different reactive groups at either end)

Crosslinking target	Crosslinker Reactive Groups, Features
Amine-to-Sulfhydryl	NHS ester / Maleimide
Amine-to-Carboxyl	Carbodiimide
Sulfhydryl-to-Carbonyl	Maleimide / Hydrazide
Amine-to-DNA	NHS ester / Psoralen

http://www.piercenet.com

Although there are many choices for bioconjugation methods to form DNA-protein conjugates, these methods frequently require mutually exclusive reaction conditions that are incompatible with each other, or not suitable for cellular conditions. In contrast, bioorthogonal conjugation methods can overcome this limitation. The term bioorthogonal chemistry refers to any chemical reaction that can occur inside of living systems without interfering with native biochemical processes. This group involves enzymes, which self-catalyze specific substrates that can be pre-modified on DNA, and more currently "click" chemistry, a concept that mimics nature to generate substances quickly and reliably by joining small modular units. For enzyme approaches, the proteins of interests (POI) have to be cloned with the enzymes before the catalytic reactions happen between the enzymes and modified DNA substrates. For convenience, several kits for cloning POI with the enzyme tags are commercially available. The first example is the IMPACT (Intein Mediated Purification with an Affinity Chitin-binding Tag) Kit (New England BioLabs). This is also known as "expressed protein ligation" (EPL). In this method, the POI is recombinant with a protein domain called INTEIN and a chitin binding (CBD) domain. CBD binds to chitin-modified beads or columns to purify the protein complex. The intein domain causes an acyl shift between the target protein and itself to form a thioester group which can be cleaved by adding a small molecule compound such as mercapto-ethane-sulfonic acid to release the target protein from the column. This step generates the C-terminal thioester of the POI, which is then ligated with cysteine-modified nucleic acid as described in Figure 1.5 a. The EPL method is advantageous over conventional cross-linking techniques because it allows DNA–

protein conjugates to be readily prepared with well-defined stoichiometric composition and regiospecific linkage.[72-77]

Another self-labeling protein that is adapted to widely use for protein-DNA conjugation is called the SNAP tag (New England BioLabs, Ipswich, MA). The SNAP protein is a 20 kDa mutant of the DNA repair protein O^6-alkylguanine-DNA alkyltransferase (hAGT), which can react with benzylguanine (BG) substrates to form a stable covalent thioether bond. SNAP tag was one of the methods used in the work; therefore, it will be discussed later in greater detail. Similarly, a sibling of the SNAP tag is the CLIP tag, also a mutant form of hAGT, which reacts specifically and rapidly with O2-benzylcytosine (BC) derivatives (Figure 1.5 b). The New England Biolabs website contains a list of publications using SNAP tag and CLIP tag with useful information about the systems and their applications. More recently, HaloTag Protein (Promega, Madison, WI) has been developed for bioorthogonal protein-DNA conjugation with the advantage of having many different HaloTag Ligand Building Blocks (Promega Corporation, Madison, WI) that can be modified with DNA using amine or thiol chemistry. Similar to the SNAP tag and CLIP tag, the HaloTag is a modified haloalkane dehalogenase which catalyzes conjugation specifically and covalently to chloroalkane derivatives (Figure 1.5 c).[78, 79]

In another approach, different from self-ligation proteins which lack turnover activity and remain linked to the products after the reaction, a new enzyme with true catalytic activity called sortase has been utilized to form covalent DNA-protein conjugates. Sortase is also a method used in this work, so it will be discussed in more detail in the next chapter.

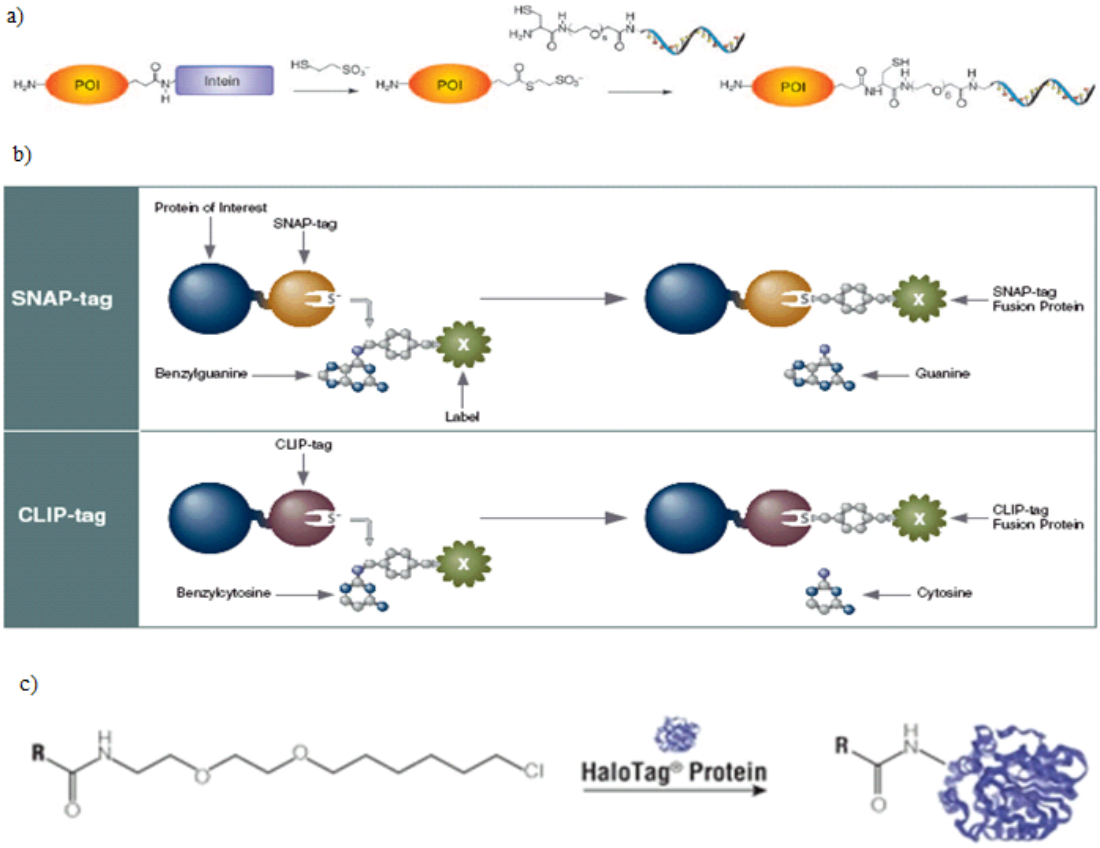

Figure 1.5. Mechanisms of self-labeling proteins. a) Expressed protein ligation system ("EPL"), b) SNAP tag, CLIP tag, and c) Halo tag. (Pictures a, b, c are obtained from reference [59], New England Biolabs and Promega websites, respectively.)

Recently, "click" chemistry with several types of reactions have emerged in the applications of biomedical researches.[80-84] Among the "click reactions", the copper(I)-catalyzed Huisgen 1,3-dipolar cycloaddition of azides and alkynes (CuAAC)[83, 85-87] has proven to be a versatile methods for the modification of synthetic DNA oligonucleotides. Currently copper-free method[88] is also widely used. Normally, for DNA-protein conjugation using "click" reactions, DNA oligonucleotides are modified with alkyne groups which are commercially available, and proteins are

modified with azide groups. However, in order to modify azide groups onto the proteins, azide-modified compounds (for example, sugars[89] and amino acids[90]) are incubated with cultured cells. Azido-sugars are metabolically incorporated into cell surface O-linked glycoproteins through the oligosaccharide biosynthesis pathway. For other proteins that are not glycoproteins, azide-modified amino acid analogs are fed to cultured cells and incorporated into proteins during active protein synthesis. These approaches, therefore, cannot generate a 1:1 molar ratio conjugation between DNA and protein, unlike several of the enzyme-based approaches. On the other hand, "click" chemistry has become very effective in producing short polypeptide-DNA conjugates[91-93] since it is simpler to directly modify the azide groups onto short polypeptides.

1.3. Protein Detection

Although there are a large number of tools for nucleic acid analysis, there are fewer tools for protein detection due to the complicated and varied physical and chemical properties of proteins. In this section, I will briefly introduce some common methods and materials used for protein detection as a general background for the development of the field. Traditionally, proteins are detected by enzyme-linked immunosorbent assay (ELISA) [94] or western blotting (WB)[95] techniques, which were developed in early 1970s and 1980s, respectively. For ELISA methods, a target protein is captured by an antibody then sandwiched with a second antibody that incorporates a catalytic, signal-generating entity. Nowadays, there are a wide variety of complete ELISA kits commercially available for measuring intracellular and

extracellular proteins using different types of detection signals including colorimetric, fluorescent, and chemiluminescent. To detect protein by WB, the protein targets are separated from the others by gel electrophoresis (1D or 2D) before being transferred to a membrane where they are detected by specific antibodies. The primary antibodies could be directly conjugated with fluorophores or recognized by secondary antibodies carrying enzymes or dyes to generate colorimeric, chemiluminescent, or fluorescent signals. This is an effective and useful method to detect and characterize specific proteins in a complex mixture of proteins. Similar to ELISA, many WB kits are commercially available with a variety of signal detection systems. Among the choices for detection signals, fluorescence-based detection strategies are increasingly used, with approximately 3,000 fluorescent probes available over a broad spectral range allowing simultaneous imaging of multiple components at the intercellular or intracellular levels.[96]

Adapting from the ELISA concept, high throughput protein planar and bead-based microarrays provide powerful multiplexed approaches to identify protein targets, or protein-protein interactions.[97-100] However, there are many challenges in protein microarray developments due to the structural diversity and complexity of proteins. Proteins are highly sensitive to the physiochemical properties of the chip support materials. Moreover, issues with low polarity, solubility, and incompatible surface chemistries promote the retention of proteins, cause denaturation, or result in improper folding leading to loss in biological activity [101-103]. To overcome these challenges, DNA microarrays which are more stable, easier to make, and are more well developed to build protein arrays using DNA protein binding domains[104, 105] or

DNA-protein conjugates[106-109] have been considered as an alternative approach (Figure 1.6 a). Furthermore, with the advantage of having two functional moieties in one molecule, DNA-protein conjugates were used to detect proteins by using polymerase chain reaction (PCR) technology to amplify the signal of the protein targets[50, 110-115]. The novel concept was introduced as immuno-PCR (iPCR) technique (Figure 1.6 b) by Sano *et al.* in 1992[48]. This target-based amplification strategy is much more sensitive, about 1,000-10,000 fold, than signal-based amplification methods such as ELISA. Later, instead of using PCR, the immuno-PCR technique was adapted to use another DNA amplification technique called rolling circle amplification (RCA) to visualize endogenous proteins on cells using an isothermal process (Figure 1.6 c).[49, 50] Recently, proximity ligation, a technique developed from ELISA and immuno-PCR concepts, which was introduced by Landegren *et al*. in 2002, are widely used for the detection of proteins with high sensitivity at zeptomole ($40 \times 10^{-21)}$ amount. [116-125] In this method, basically, the protein targets are sandwiched between two antibodies-DNA conjugates, enabling hybridization with a DNA probe for signal amplification by PCR due to their close proximity (Figure 1.6 d).

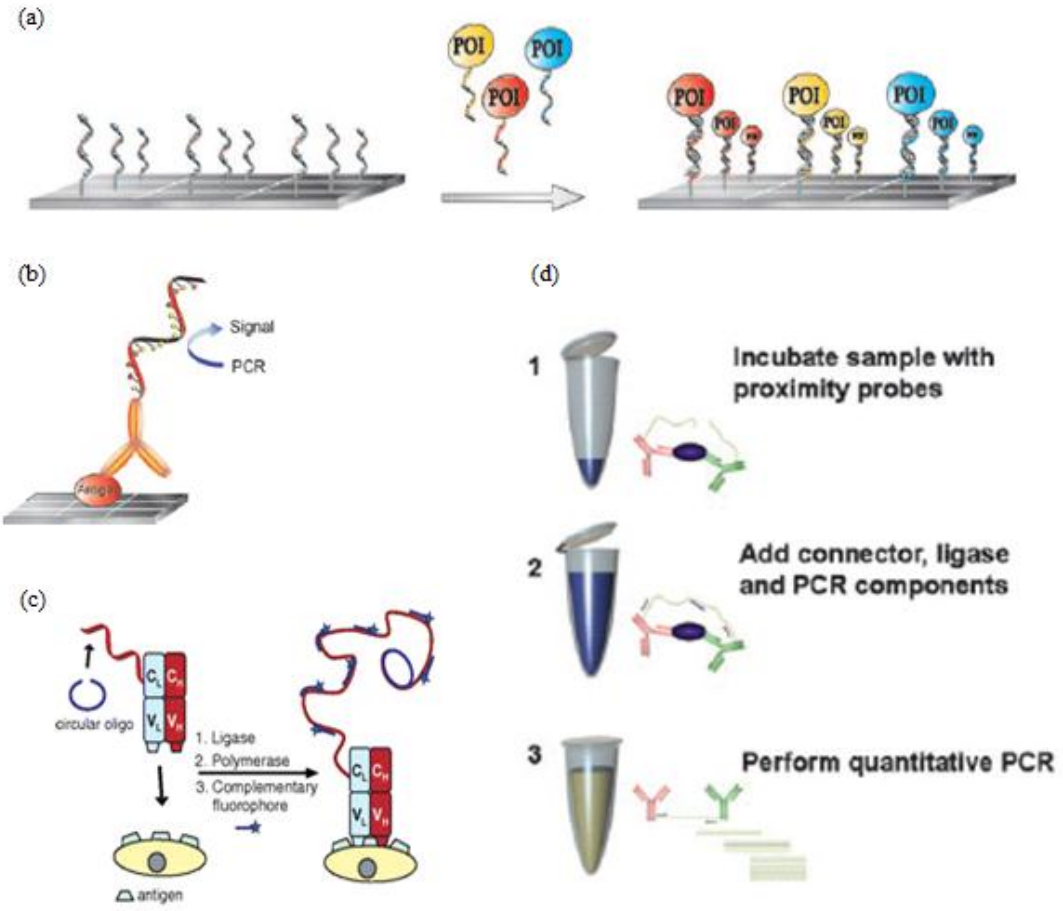

Figure 1.6. Application of DNA-protein conjugates in analytical systems. a) DNA-directed hybridization of protein arrays.[54] b) immuno-PCR by PCR amplification.[48] c) immuno-PCR by RCA amplification[50]. d) proximity ligation.[117]

Recently, with the emergence of nanotechnology, besides the development of DNA-protein hybrid materials in protein detection, new materials are used to develop novel assays for detecting proteins with higher sensitivity, specificity, and robustness (Table 1.3). Nanomaterials with unique and controllable size-dependent properties, tunable chemical compositions, and in certain cases chemically and physically robust structures[126, 127] has given rise to new platforms for protein detection. Among those materials, gold nanoparticles with high surface-to-volume ratios give the advantage that target-binding events are often more easily transduced into detectable signals.[128, 129] DNA-functionalized gold nanoparticles have been used to develop different protein detection approaches, including aptamers[130, 131], fluorescent[132, 133], chemiluminescent[134], and scanometric[135] strategies. Moreover, due to the unique optical and electronic properties of nanoparticles, surface plasmon resonance (SPR)-based[136-139], and Raman-spectroscopy-based[140, 141, 141] methods have been successfully developed to detect protein targets in label-free approaches. Besides gold nanoparticles, other nanomaterials such as carbon nanotubes[141, 142] and silicon nanowires[143] have been explored to provide new detection systems based on changes in electrical conductivity in the presence of protein targets.

Table 1.3. Detection of protein biomolecules.[128]

Tool or technique	Read-out	Illustration	Detection limit*	Molecules per drop (60 µl)	In clinical use
Colorimetry	Visual		150 pM	10^9	Yes
Carbon nanotubes	Electrical		100 pM	10^9	No
Chemi-luminescence	Luminescence		30 pM	10^9	Yes
ELISA	Luminescence		1–10 pM	10^7	Yes
Quantum dots	Fluorescence		500 fM	10^7	No
Silicon nanowires	Electrical		1 fM	10^4	No
Metal nano-particles (bio-barcode)	Scanometric and/or light scattering		30 aM	900	Yes
Immuno-PCR	Fluorescence		20 aM	700	Yes

*Detection limits are best-case examples from the literature and can vary substantially depending on the target and the assay conditions.

1.4. Protein Delivery

As important as early detection of diseases, delivering proteins and peptides as therapeutic modalities to treat human diseases is also essential and attracts a lot of attention from researchers and pharmaceutical companies. Many diseases occur from the overexpression or alterations in the functions of intracellular proteins. As a result, inhibiting those malfunctioned proteins or delivering their active forms to specific cells or organs in living organisms is an important goal for many medical applications, including cancer therapy, vaccination, regenerative medicine, treating loss-of-function genetic disease, and imaging.[144-147] However, all current protein drugs target only the surface of the cells to trigger signaling pathways to affect the real targets downstream,[144, 148] and therefore this is a relatively indirect way to correct the functioning of the cell. In order to achieve more direct responses from protein targets inside cells to obtain more efficient cures, protein intracellular delivery beyond surface delivery is essential. However, there are many issues related to delivery of proteins and peptides. Proteins have complicated high order structures, but poor physical, chemical, and biological stability. Physical (shear pressure), chemical (pH, temperature), or biological (enzyme digestion, immunogenicity) changes of their native structures could affect their biological activities. Moreover, unfavorable pharmacokinetics, pharmacodynamics, and permeability across biological membranes of protein drugs are also significant barriers for intracellular delivery of target proteins.

There are two basic focuses in protein delivery research: establishing an

effective delivery means and increasing the biological half-life of the protein targets. Most native proteins are membrane impermeable due to electrostatic repulsions; therefore, appropriate delivery vehicles are required to escort proteins into the cytosol. More importantly, the carriers also have to be able to release the proteins after entering the cytosol to avoid being degraded from proteolysis or trafficked through endomembrane compartments for clearance.[149] To date, many materials have been used to develop efficient carriers for protein intracellular delivery as summarized in Table 1.4, which includes peptides, peptide nucleic acid (PNA), lipids, polymers, carbon nanotubes, nanoparticles and even proteins. For more details on the current development of protein delivery, please read the following reviews.[145-147, 150-152]

The most commonly used approaches for intracellular protein delivery utilize the genetic fusion of the target protein to protein transduction domains (PTDs) or cell-penetrating peptides (CPPs), such as the HIV-1 transactivator of transcription (TAT) peptide, oligoarginines, and the *Drosophila* Antennapedia-derived penetratin peptide.[153-160] However, these methods have low efficiency in the escape of proteins from the endosome to the cytosol, leading to CPP-tagged cargoes sequestered in intracellular vesicles.[161-167] Alternately, lipid-based materials, especially liposomes, have been explored intensively for protein delivery since 1970s.[168-172] Liposomes are bilayered vesicles assembled from amphiphilic building blocks, such as lipids or phospholipids, which should not be confused with micelles composed of monolayers. Liposomes can adhere to plasma membranes and enter the cell via endocytosis or liposome-cell fusion[173]. Recently, several lipid-based reagents for protein delivery are commercially available; for examples, FuGENE®6 from Roche, BioPORTER® from

Sigma Aldrich, PULSin® from Pulsin, and Pro-Ject™ from Thermo Scientific.

Table 1.4. Summary of materials used for protein intracellular delivery.

Types of materials	Examples
Peptide-mediated materials	Protein to protein transduction domains (PTDs)[174-176] Cell penetrating peptides (CPPs) [153-160, 177]
Peptide nucleic acid (PNA)-based materials	PNA oligomer[178, 179]
Lipid-based materials	Liposomes[168-172] Commercial lipid-based reagents: BioPORTER™[180], PULSin[181] Solid-lipid nanoparticle[182, 183]
Polymeric materials	Polyionic complex (PIC) micelles[184-186] PEG, PEI, PLGA, etc.[187] {{1206 Shimoni,O. 2012}}[177] {{1206 Shimoni,O. 2012}}[187-192]
Inorganic materials	Carbon nanotubes[193, 194] Quantum dots[195-199] Gold nanoparticles[188, 200-202] Mesoporous silica nanoparticles[203-206] Magnetic nanoparticles[207-209]
Protein-mediated materials	Superpossitively charged protein[210] Engineering protein G[211] Virus-like nanoparticle[212]

With the advantage of being an extremely versatile class of materials, polymers have emerged to develop novel drug delivery systems. The selection and design of a polymer to give the desired chemical, interfacial, mechanical and biological functions is a challenging task and requires a thorough understanding of the

surface and bulk properties of the polymer.[213] To help with that, Angelova and Hunkeler have proposed a flow chart for rational selection of polymers for biomedical applications.[214] Although this flow chart is intended specifically for polymers, it can also provide insight for developing protein delivery systems using other materials. In addition, the interaction between polymers and proteins has been proven to increase the systemic circulation of protein drugs which is an important aspect of drug delivery.[146, 215] Many different strategies, such as direct conjugation via either chemical modifications[216-219], physical adsorption and electrostatic interactions[184-186], *in situ* polymerization[188, 220-223], emulsion-based[224-227] and layer-by-layer[228-230] encapsulations, can be used to incorporate target proteins with polymers. To date, various antibodies, cytokines, and growth factors have been PEGylated[231] with FDA approval for clinical use[232]. Besides PEG, many other polymers, which can be broadly classified as biodegradable or non-biodegradable[213], have been used to enhance the biological half-life of protein targets; for examples, poly(N-vinyl pyrrolidone) (PVPON)[187], non-degradable polymer matrices such as poly(lactide-co-glycolide) (PLGA)[189], PEI[190-192], PPAAc[233], methylenebisacrylamide or acid-degradable glycerol dimethacrylate (Figure 1.7)[188].

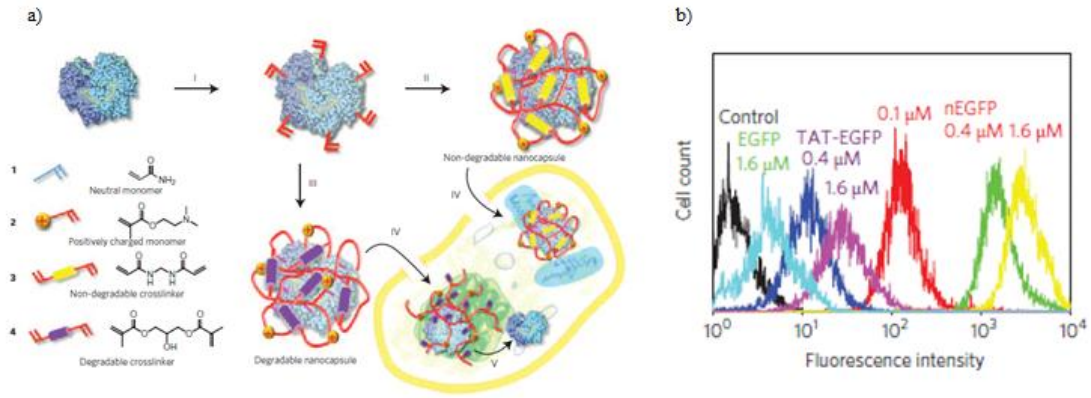

Figure 1.7. Single-protein nanocapsules for intracellular protein delivery.[188] a) Schematic showing the synthesis and cellular uptake of cationic single-protein nanocapsules with degradable and non-degradable polymeric shells. b) Fluorescence-assisted cell sorting of HeLa cells incubated with different concentrations of protein materials.

Recently, inorganic materials including carbon nanotubes[193, 194], quantum dots[195-199], gold[188, 200-202], silica[203-206], and magnetic particles[207-209] have also been explored for drug, gene, and protein delivery. The high surface area to volume ratio of these materials results in improved pharmacokinetics and biodistribution of the payload[234, 235]. Their size effects and toxicity on cell uptake have also been investigated to obtain a better understanding of the mechanism and rate of cell uptake, as well as to better characterize their ability to penetrate through tissue membranes[236-238]. In addition, taking advantage of molecular biology and protein engineering techniques, target proteins can be fused to engineered superpositively charged GFP protein, which were extensively mutated at their surface-exposed residues, as a delivery vehicle to penetrate cell membranes (Figure 1.8)[210]. Moreover, Lim et al. has

developed an engineered protein G system, containing cell penetration peptides and polyhistidine tag, in order to combine with Ni-NTA modified nanoparticles for the non-invasively delivery of IgG antibodies into cells.[211]

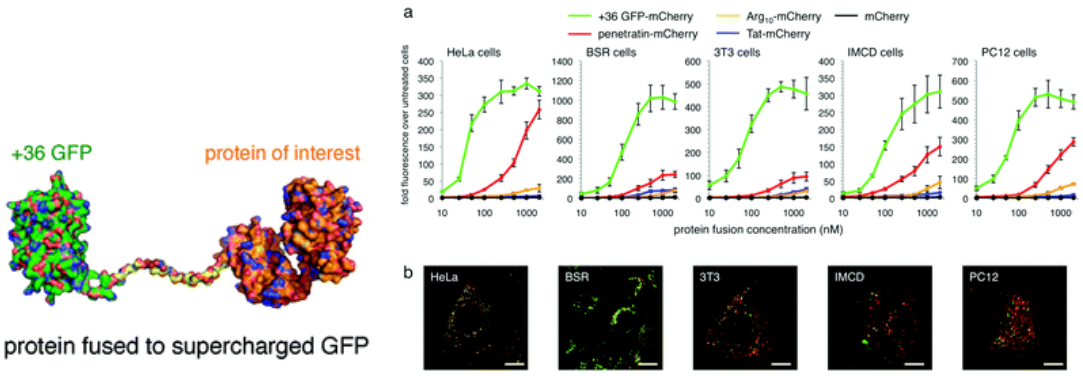

Figure 1.8. Comparison of mCherry delivery by +36 GFP, TAT, Arg_{10}, Penetratin. a) Flow cytometry of HeLa, BSR, 3T3, PC12, and IMCD cells incubated in the presence of specific concentrations of the protein targets. b) Confocal fluorescence microscopy of live cells incubated with 100 nM +36 GFP-mCherry for 4h at 37oC.[210]

1.5. Significance of this dissertation

Although DNA-protein hybrid materials have been developed for many applications as discussed above, there are still a lot of potential that has yet to be realized with this type of materials. In this work, a protein-DNA hybrid molecule was developed to serve as a universal adapter for interfacing between IgG antibodies and DNA nanotechnology. For the purposes of protein detection, DNA nanobarcodes were used as the reporters for an IgG-based protein detection system with potential for multiplexed detection. This system can be used as a versatile platform for protein detection due to the capability of detecting proteins in many systems, including bead-

based, membrane-based, and tissue-based. Furthermore, and for the first time, DNA-protein materials were used for intracellular delivery of proteins and IgG antibodies using branched DNA as the carrier. Combined with DNA transfection reagents, the DNA-assisted protein intracellular delivery (DAPID) system has greatly enhanced the efficiency of uptake. This could provide a new route for protein intracellular delivery with great efficiency. Furthermore, our system can be easily extended to deliver multiple proteins and other biomarkers, as well as moieties beyond proteins including but not limited to nanoparticles, lipids, and polymers, as long as they are conjugated onto branched DNA. We believe that this DNA-assisted protein intracellular delivery (DAPID) system will result in a paradigm shift in drug development and delivery.

References:

1. Nadrian C., S. Nucleic acid junctions and lattices. *J. Theor. Biol.* **99**, 237-247 (1982).

2. Seeman, N. C. DNA nanotechnology: novel DNA constructions. *Annu. Rev. Biophys. Biomol. Struct.* **27**, 225-248 (1998).

3. Seeman, N. C. DNA in a material world. *Nature* **421**, 427-431 (2003).

4. Fu, T. J. & Seeman, N. C. DNA double-crossover molecules. *Biochemistry* **32**, 3211-3220 (1993).

5. LaBean, T. H. *et al*. Construction, Analysis, Ligation, and Self-Assembly of DNA Triple Crossover Complexes. *J. Am. Chem. Soc.* **9**, 1848-1860 (2000).

6. Shen, Z., Yan, H., Wang, T. & Seeman, N. C. Paranemic Crossover DNA: A Generalized Holliday Structure with Applications in Nanotechnology. *J. Am. Chem. Soc.* **126**, 1666-1674 (2004).

7. Mao, C., Sun, W. & Seeman, N. C. Designed Two-Dimensional DNA Holliday Junction Arrays Visualized by Atomic Force Microscopy. *J. Am. Chem. Soc.* **23**, 5437-5443 (1999).

8. Yan, H., Park, S. H., Finkelstein, G., Reif, J. H. & LaBean, T. H. DNA-templated self-assembly of protein arrays and highly conductive nanowires. *Science* **301**, 1882-1884 (2003).

9. He, Y., Chen, Y., Liu, H., Ribbe, A. E. & Mao, C. Self-assembly of hexagonal DNA two-dimensional (2D) arrays. *J. Am. Chem. Soc.* **127**, 12202-12203 (2005).

10. Zhang, C. *et al*. Conformational flexibility facilitates self-assembly of complex DNA nanostructures. *Proc. Natl. Acad. Sci. U. S. A.* **105**, 10665-10669 (2008).

11. He, Y., Tian, Y., Ribbe, A. E. & Mao, C. Highly connected two-dimensional crystals of DNA six-point-stars. *J. Am. Chem. Soc.* **128**, 15978-15979 (2006).

12. Winfree, E., Liu, F., Wenzler, L. A. & Seeman, N. C. Design and self-assembly of two-dimensional DNA crystals. *Nature* **394**, 539-544 (1998).

13. Reishus, D., Shaw, B., Brun, Y., Chelyapov, N. & Adleman, L. Self-assembly of DNA double-double crossover complexes into high-density, doubly connected, planar structures. *J. Am. Chem. Soc.* **127**, 17590-17591 (2005).

14. Yan, H., Zhang, X., Shen, Z. & Seeman, N. C. A robust DNA mechanical device controlled by hybridization topology. *Nature* **415**, 62-65 (2002).

15. Simmel, F. C. Three-dimensional nanoconstruction with DNA. *Angew. Chem. Int. Ed Engl.* **47**, 5884-5887 (2008).

16. Zheng, J. *et al*. From molecular to macroscopic via the rational design of a self-assembled 3D DNA crystal. *Nature* **461**, 74-77 (2009).

17. He, Y. *et al*. Hierarchical self-assembly of DNA into symmetric supramolecular polyhedra. *Nature* **452**, 198-201 (2008).

18. Bath, J. & Turberfield, A. J. DNA nanomachines. *Nat. Nanotechnol* **2**, 275-284 (2007).

19. Niemeyer, C. M. & Adler, M. Nanomechanical devices based on DNA. *Angew. Chem. Int. Ed Engl.* **41**, 3779-3783 (2002).

20. Rothemund, P. W. Folding DNA to create nanoscale shapes and patterns. *Nature* **440**, 297-302 (2006).

21. Douglas, S. M. *et al*. Self-assembly of DNA into nanoscale three-dimensional shapes. *Nature* **459**, 414-418 (2009).

22. Dietz, H., Douglas, S. M. & Shih, W. M. Folding DNA into twisted and curved nanoscale shapes. *Science* **325**, 725-730 (2009).

23. Andersen, E. S. *et al*. Self-assembly of a nanoscale DNA box with a controllable lid. *Nature* **459**, 73-76 (2009).

24. Yang, D. *et al*. Novel DNA materials and their applications. *Wiley Interdisciplinary Reviews: Nanomedicine and Nanobiotechnology* **2**, 648-669 (2010).

25. Pinheiro, A. V., Han, D., Shih, W. M. & Yan, H. Challenges and opportunities for structural DNA nanotechnology. *Nat. Nanotechnol* **6**, 763-772 (2011).

26. Seeman, N. & Lukeman, P. Nucleic acid nanostructures: bottom-up control of geometry on the nanoscale. *Reports on Progress in Physics* **68**, 237 (2005).

27. Lin, C., Liu, Y., Rinker, S. & Yan, H. DNA tile based self-assembly: building complex nanoarchitectures. *Chemphyschem* **7**, 1641-1647 (2006).

28. Seeman, N. C. An overview of structural DNA nanotechnology. *Mol. Biotechnol.* **37**, 246-257 (2007).

29. Hamada, S. & Murata, S. Substrate-assisted assembly of interconnected single-duplex DNA nanostructures. *Angew. Chem. Int. Ed Engl.* **48**, 6820-6823 (2009).

30. Shih, W. M., Quispe, J. D. & Joyce, G. F. A 1.7-kilobase single-stranded DNA that folds into a nanoscale octahedron. *Nature* **427**, 618-621 (2004).

31. Dan, L. The road from biology to materials. *Materials Today* **6**, 38-43 (2003).

32. Nilsen, T. W., Grayzel, J. & Prensky, W. Dendritic Nucleic Acid Structures. *J. Theor. Biol.* **187**, 273-284 (1997).

33. Orentas, R. J., Rospkopf, S. J., Casper, J. T., Getts, R. C. & Nilsen, T. W. Detection of Epstein–Barr virus EBER sequence in post-transplant lymphoma patients with DNA dendrimers. *J. Virol. Methods* **77**, 153-163 (1999).

34. Li, Y. *et al*. Controlled assembly of dendrimer-like DNA. *Nat. Mater.* **3**, 38-42 (2004).

35. Um, S. H. *et al*. Enzyme-catalysed assembly of DNA hydrogel. *Nat. Mater.* **5**, 797-801 (2006).

36. Li, Y., Cu, Y. T. & Luo, D. Multiplexed detection of pathogen DNA with DNA-based fluorescence nanobarcodes. *Nat. Biotechnol.* **23**, 885-889 (2005).

37. Park, N. *et al*. High-yield cell-free protein production from P-gel. *Nat. Protoc.* **4**, 1759-1770 (2009).

38. Roh, Y. H. *et al*. Photocrosslinked DNA Nanospheres for Drug Delivery. *Macromolecular Rapid Communications* **31**, 1207-1211 (2010).

39. Lee, J. B. *et al*. Multifunctional nanoarchitectures from DNA-based ABC monomers. *Nat. Nanotechnol* **4**, 430-436 (2009).

40. Cheng, W. *et al*. Free-standing nanoparticle superlattice sheets controlled by DNA. *Nat. Mater.* **8**, 519-525 (2009).

41. Cheng, W., Campolongo, M. J., Tan, S. J. & Luo, D. Freestanding ultrathin nano-membranes via self-assembly. *Nano Today* **4**, 482-493 (2009).

42. Cheng, W., Park, N., Walter, M. T., Hartman, M. R. & Luo, D. Nanopatterning self-assembled nanoparticle superlattices by moulding microdroplets. *Nat. Nanotechnol* **3**, 682-690 (2008).

43. Jablonski, E., Moomaw, E. W., Tullis, R. H. & Ruth, J. L. Preparation of oligodeoxynucleotide-alkaline phosphatase conjugates and their use as hybridization probes. *Nucleic Acids Res.* **14**, 6115-6128 (1986).

44. Urdea, M. S. *et al*. A comparison of non-radioisotopic hybridization assay methods using fluorescent, chemiluminescent and enzyme labeled synthetic oligodeoxyribonucleotide probes. *Nucleic Acids Res.* **16**, 4937-4956 (1988).

45. Ghosh, S. S., Kao, P. M., McCue, A. W. & Chappelle, H. L. Use of maleimide-thiol coupling chemistry for efficient syntheses of oligonucleotide-enzyme conjugate hybridization probes. *Bioconjug. Chem.* **1**, 71-76 (1990).

46. Kynclova, E., Hartig, A. & Schalkhammer, T. Oligonucleotide labelled lipase as a new sensitive hybridization probe and its use in bio-assays and biosensors. *Journal of Molecular Recognition* **8**, 139-145 (1995).

47. Wang, Y., Stanzel, M., Gumbrecht, W., Humenik, M. & Sprinzl, M. Esterase 2-oligodeoxynucleotide conjugates as sensitive reporter for electrochemical detection of nucleic acid hybridization. *Biosensors and Bioelectronics* **22**, 1798-1806 (2007).

48. Sano, T., Smith, C. & Cantor, C. Immuno-PCR: very sensitive antigen detection by means of specific antibody-DNA conjugates. *Science* **258**, 120-122 (1992).

49. Akter, F., Mie, M. & Kobatake, E. Immuno-rolling circle amplification using a multibinding fusion protein. *Anal. Biochem.* **416**, 174-179 (2011).

50. Kazane, S. A. *et al*. Site-specific DNA-antibody conjugates for specific and sensitive immuno-PCR. *Proc. Natl. Acad. Sci. U. S. A.* **109**, 3731-3736 (2012).

51. Soderberg, O. *et al*. Direct observation of individual endogenous protein complexes in situ by proximity ligation. *Nat. Methods* **3**, 995-1000 (2006).

52. Niemeyer, C. M., Sano, T., Smith, C. L. & Cantor, C. R. Oligonucleotide-directed self-assembly of proteins: semisynthetic DNA--streptavidin hybrid molecules as connectors for the generation of macroscopic arrays and the construction of supramolecular bioconjugates. *Nucleic Acids Res.* **22**, 5530-5539 (1994).

53. Schroeder, H. *et al*. User configurable microfluidic device for multiplexed immunoassays based on DNA-directed assembly. *Anal. Chem.* **81**, 1275-1279 (2009).

54. Bano, F. *et al*. Toward multiprotein nanoarrays using nanografting and DNA directed immobilization of proteins. *Nano Lett.* **9**, 2614-2618 (2009).

55. Jung, Y., Lee, J. M., Jung, H. & Chung, B. H. Self-directed and self-oriented immobilization of antibody by protein G-DNA conjugate. *Anal. Chem.* **79**, 6534-6541 (2007).

56. Ng, J. K. *et al*. Spatially addressable protein array: ssDNA-directed assembly for antibody microarray. *Electrophoresis* **28**, 4638-4644 (2007).

57. Boozer, C., Ladd, J., Chen, S. & Jiang, S. DNA-directed protein immobilization for simultaneous detection of multiple analytes by surface plasmon resonance biosensor. *Anal. Chem.* **78**, 1515-1519 (2006).

58. Niemeyer, C. M. Functional devices from DNA and proteins. *Nano Today* **2**, 42-52 (2007).

59. Niemeyer, C. M. Semisynthetic DNA-protein conjugates for biosensing and nanofabrication. *Angew. Chem. Int. Ed Engl.* **49**, 1200-1216 (2010).

60. Niemeyer, C. M. The developments of semisynthetic DNA-protein conjugates. *Trends Biotechnol.* **20**, 395-401 (2002).

61. Niemeyer, C. M. Bioorganic applications of semisynthetic DNA-protein conjugates. *Chemistry* **7**, 3188-3195 (2001).

62. Singh, Y., Murat, P. & Defrancq, E. Recent developments in oligonucleotide conjugation. *Chem. Soc. Rev.* **39**, 2054-2070 (2010).

63. Green, N. M. in *Advances in protein chemistry* 85-133 (Elsevier, 1975).

64. Meredith, G. D., Wu, H. Y. & Allbritton, N. L. Targeted protein functionalization using His-tags. *Bioconjug. Chem.* **15**, 969-982 (2004).

65. Shimada, J. *et al*. Conjugation of DNA with protein using His-tag chemistry and its application to the aptamer-based detection system. *Biotechnol. Lett.* **30**, 2001-2006 (2008).

66. Shen, W., Zhong, H., Neff, D. & Norton, M. L. NTA directed protein nanopatterning on DNA Origami nanoconstructs. *J. Am. Chem. Soc.* **131**, 6660-6661 (2009).

67. Goodman, R. P. *et al*. A facile method for reversibly linking a recombinant protein to DNA. *Chembiochem* **10**, 1551-1557 (2009).

68. Bock, L. C., Griffin, L. C., Latham, J. A., Vermaas, E. H. & Toole, J. J. Selection of single-stranded DNA molecules that bind and inhibit human thrombin. *Nature* **355**, 564-566 (1992).

69. Famulok, M., Hartig, J. S. & Mayer, G. Functional aptamers and aptazymes in biotechnology, diagnostics, and therapy. *Chem. Rev.* **107**, 3715-3743 (2007).

70. Fruk, L., Kuo, C. H., Torres, E. & Niemeyer, C. M. Apoenzyme reconstitution as a chemical tool for structural enzymology and biotechnology. *Angew. Chem. Int. Ed Engl.* **48**, 1550-1574 (2009).

71. Fruk, L. & Niemeyer, C. M. Covalent hemin-DNA adducts for generating a novel class of artificial heme enzymes. *Angew. Chem. Int. Ed Engl.* **44**, 2603-2606 (2005).

72. Lovrinovic, M. *et al*. Synthesis of protein-nucleic acid conjugates by expressed protein ligation. *Chem. Commun. (Camb)* **(7)**, 822-823 (2003).

73. Takeda, S., Tsukiji, S. & Nagamune, T. Site-specific conjugation of oligonucleotides to the C-terminus of recombinant protein by expressed protein ligation. *Bioorg. Med. Chem. Lett.* **14**, 2407-2410 (2004).

74. Lovrinovic, M. & Niemeyer, C. M. Rapid synthesis of DNA-cysteine conjugates for expressed protein ligation. *Biochem. Biophys. Res. Commun.* **335**, 943-948 (2005).

75. Burbulis, I., Yamaguchi, K., Gordon, A., Carlson, R. & Brent, R. Using protein-DNA chimeras to detect and count small numbers of molecules. *Nat. Methods* **2**, 31-37 (2005).

76. Lovrinovic, M. & Niemeyer, C. M. Microtiter plate-based screening for the optimization of DNA-protein conjugate synthesis by means of expressed protein ligation. *Chembiochem* **8**, 61-67 (2007).

77. Takeda, S., Tsukiji, S., Ueda, H. & Nagamune, T. Covalent split protein fragment-DNA hybrids generated through N-terminus-specific modification of proteins by oligonucleotides. *Org. Biomol. Chem.* **6**, 2187-2194 (2008).

78. Los, G. V. & Wood, K. The HaloTag: a novel technology for cell imaging and protein analysis. *Methods Mol. Biol.* **356**, 195-208 (2007).

79. Los, G. V. *et al*. HaloTag: a novel protein labeling technology for cell imaging and protein analysis. *ACS Chem. Biol.* **3**, 373-382 (2008).

80. Nwe, K. & Brechbiel, M. W. Growing applications of "click chemistry" for bioconjugation in contemporary biomedical research. *Cancer Biother. Radiopharm.* **24**, 289-302 (2009).

81. Moses, J. E. & Moorhouse, A. D. The growing applications of click chemistry. *Chem. Soc. Rev.* **36**, 1249-1262 (2007).

82. Kolb, H. C. & Sharpless, K. B. The growing impact of click chemistry on drug discovery. *Drug Discov. Today* **8**, 1128-1137 (2003).

83. Lutz, J. F. & Nanotechnology for Life Science Research Group. 1,3-Dipolar Cycloadditions of Azides and Alkynes: a Universal Ligation Tool in Polymer and Materials Science. *Angew. Chem. Int. Ed Engl.* **46**, 1018-1025 (2007).

84. Lim, R. K. V. & Lin, Q. Bioorthogonal Chemistry: Recent Progress and Future Directions. *Chem. Commun.* **46**, 1589-1600 (2010).

85. Liang, L. & Astruc, D. The copper(I)-catalyzed alkyne-azide cycloaddition (CuAAC) “click” reaction and its applications. An overview. *Coord. Chem. Rev.* **255**, 2933-2945 (2011).

86. Gramlich, P. M., Wirges, C. T., Manetto, A. & Carell, T. Postsynthetic DNA modification through the copper-catalyzed azide-alkyne cycloaddition reaction. *Angew. Chem. Int. Ed Engl.* **47**, 8350-8358 (2008).

87. Spiteri, C. & Moses, J. E. Copper-catalyzed azide-alkyne cycloaddition: regioselective synthesis of 1,4,5-trisubstituted 1,2,3-triazoles. *Angew. Chem. Int. Ed Engl.* **49**, 31-33 (2010).

88. Gutsmiedl, K., Wirges, C. T., Ehmke, V. & Carell, T. Copper-free "click" modification of DNA via nitrile oxide-norbornene 1,3-dipolar cycloaddition. *Org. Lett.* **11**, 2405-2408 (2009).

89. Clark, P. M. *et al*. Direct in-gel fluorescence detection and cellular imaging of O-GlcNAc-modified proteins. *J. Am. Chem. Soc.* **130**, 11576-11577 (2008).

90. Dieterich, D. C., Link, A. J., Graumann, J., Tirrell, D. A. & Schuman, E. M. Selective identification of newly synthesized proteins in mammalian cells using bioorthogonal noncanonical amino acid tagging (BONCAT). *Proc. Natl. Acad. Sci. U. S. A.* **103**, 9482-9487 (2006).

91. Gogoi, K., Mane, M. V., Kunte, S. S. & Kumar, V. A. A versatile method for the preparation of conjugates of peptides with DNA/PNA/analog by employing chemo-selective click reaction in water. *Nucleic Acids Res.* **35**, e139 (2007).

92. Wenska, M. *et al*. An activated triple bond linker enables 'click' attachment of peptides to oligonucleotides on solid support. *Nucleic Acids Res.* **39**, 9047-9059 (2011).

93. Steunenberg, P., Wenska, M. & Stromberg, R. Conversion of Commercial Peptides into “Clickable” Derivatives for Labeling and Conjugate Synthesis. *Nature protocol exchange* (2010).

94. Engvall, E. & Perlmann, P. Enzyme-linked immunosorbent assay (ELISA). Quantitative assay of immunoglobulin G. *Immunochemistry* **8**, 871-874 (1971).

95. Burnette, W. N. “Western Blotting”: Electrophoretic transfer of proteins from sodium dodecyl sulfate-polyacrylamide gels to unmodified nitrocellulose and radiographic detection with antibody and radioiodinated protein A. *Anal. Biochem.* **112**, 195-203 (1981).

96. Lichtman, J. W. & Conchello, J. Fluorescence microscopy. *Nature methods* **2**, 910-219 (2010).

97. Hartmann, M., Roeraade, J., Stoll, D., Templin, M. F. & Joos, T. O. Protein microarrays for diagnostic assays. *Anal. Bioanal Chem.* **393**, 1407-1416 (2009).

98. Templin, M. F. *et al*. Protein microarray technology. *Drug Discov. Today* **7**, 815-822 (2002).

99. Hu, S., Xie, Z., Qian, J., Blackshaw, S. & Zhu, H. Functional protein microarray technology. *Wiley Interdisciplinary Reviews: Systems Biology and Medicine* **3**, 255-268 (2011).

100. Jun, B. H., Kang, H., Lee, Y. S. & Jeong, D. H. Fluorescence-based multiplex protein detection using optically encoded microbeads. *Molecules* **17**, 2474-2490 (2012).

101. Talapatra, A., Rouse, R. & Hardiman, G. Protein microarrays: challenges and promises. *Pharmacogenomics* **3**, 527-536 (2002).

102. Joos, T. & Bachmann, J. Protein microarrays: potentials and limitations. *Front. Biosci.* **14**, 4376-4385 (2009).

103. Stoll, D., Templin, M. F., Bachmann, J. & Joos, T. O. Protein microarrays: applications and future challenges. *Curr. Opin. Drug Discov. Devel.* **8**, 239-252 (2005).

104. MacBeath, G. & Schreiber, S. L. Printing proteins as microarrays for high-throughput function determination. *Science* **289**, 1760-1763 (2000).

105. Kaushansky, A. *et al*. Quantifying protein-protein interactions in high throughput using protein domain microarrays. *Nat. Protoc.* **5**, 773-790 (2010).

106. Jongsma, M. A. & Litjens, R. H. Self-assembling protein arrays on DNA chips by auto-labeling fusion proteins with a single DNA address. *Proteomics* **6**, 2650-2655 (2006).

107. Schweller, R. M., Constantinou, P. E., Frankel, N. W., Narayan, P. & Diehl, M. R. Design of DNA-conjugated polypeptide-based capture probes for the anchoring of proteins to DNA matrices. *Bioconjug. Chem.* **19**, 2304-2307 (2008).

108. Stoevesandt, O., Taussig, M. J. & He, M. Producing protein microarrays from DNA microarrays. *Methods Mol. Biol.* **785**, 265-276 (2011).

109. Wacker, R. & Niemeyer, C. M. DDI-microFIA--A readily configurable microarray-fluorescence immunoassay based on DNA-directed immobilization of proteins. *Chembiochem* **5**, 453-459 (2004).

110. Joerger, R. D., Truby, T. M., Hendrickson, E. R., Young, R. M. & Ebersole, R. C. Analyte detection with DNA-labeled antibodies and polymerase chain reaction. *Clin. Chem.* **41**, 1371-1377 (1995).

111. Ren, J. *et al*. Detection of circulating gastric carcinoma-associated antigen MG7-Ag in human sera using an established single determinant immuno-polymerase chain reaction technique. *Cancer* **88**, 280-285 (2000).

112. Wiltshire, S. *et al*. Detection of multiple allergen-specific IgEs on microarrays by immunoassay with rolling circle amplification. *Clin. Chem.* **46**, 1990-1993 (2000).

113. Morin, I., Askin, S. P. & Schaeffer, P. M. IgG-detection devices for the Tus-Ter-lock immuno-PCR diagnostic platform. *Analyst* **136**, 4815-4821 (2011).

114. Niemeyer, C. M., Adler, M. & Wacker, R. Detecting antigens by quantitative immuno-PCR. *Nat. Protoc.* **2**, 1918-1930 (2007).

115. Niemeyer, C. M., Adler, M. & Wacker, R. Immuno-PCR: high sensitivity detection of proteins by nucleic acid amplification. *Trends Biotechnol.* **23**, 208-216 (2005).

116. Fredriksson, S. *et al*. Protein detection using proximity-dependent DNA ligation assays. *Nat. Biotechnol.* **20**, 473-477 (2002).

117. Gullberg, M. *et al*. Cytokine detection by antibody-based proximity ligation. *Proc. Natl. Acad. Sci. U. S. A.* **101**, 8420-8424 (2004).

118. Soderberg, O. *et al*. Direct observation of individual endogenous protein complexes in situ by proximity ligation. *Nat. Methods* **3**, 995-1000 (2006).

119. Gustafsdottir, S. M. *et al*. Detection of individual microbial pathogens by proximity ligation. *Clin. Chem.* **52**, 1152-1160 (2006).

120. Schallmeiner, E. *et al*. Sensitive protein detection via triple-binder proximity ligation assays. *Nat. Methods* **4**, 135-137 (2007).

121. Gustafsdottir, S. M. *et al*. In vitro analysis of DNA-protein interactions by proximity ligation. *Proc. Natl. Acad. Sci. U. S. A.* **104**, 3067-3072 (2007).

122. Fredriksson, S. *et al*. Multiplexed protein detection by proximity ligation for cancer biomarker validation. *Nature methods* **4**, 327-329 (2007).

123. Soderberg, O. *et al*. Characterizing proteins and their interactions in cells and tissues using the in situ proximity ligation assay. *Methods* **45**, 227-232 (2008).

124. Darmanis, S. *et al*. Sensitive plasma protein analysis by microparticle-based proximity ligation assays. *Mol. Cell. Proteomics* **9**, 327-335 (2010).

125. Lundberg, M. *et al*. Multiplexed homogeneous proximity ligation assays for high-throughput protein biomarker research in serological material. *Mol. Cell. Proteomics* **10**, M110.004978 (2011).

126. Alivisatos, P. The use of nanocrystals in biological detection. *Nat. Biotechnol.* **22**, 47-52 (2004).

127. Rosi, N. L. & Mirkin, C. A. Nanostructures in biodiagnostics. *Chem. Rev.* **105**, 1547-1562 (2005).

128. Giljohann, D. A. & Mirkin, C. A. Drivers of biodiagnostic development. *Nature* **462**, 461-464 (2009).

129. Giljohann, D. *et al*. Gold nanoparticles for biology and medicine. *Angewandte Chemie (International ed.in English)* **49**, 3280-3294 (2010).

130. Chai, Y., Tian, D. & Cui, H. Electrochemiluminescence biosensor for the assay of small molecule and protein based on bifunctional aptamer and chemiluminescent functionalized gold nanoparticles. *Anal. Chim. Acta* **715**, 86-92 (2012).

131. Du, Y., Guo, S., Qin, H., Dong, S. & Wang, E. Target-induced conjunction of split aptamer as new chiral selector for oligopeptide on graphene-mesoporous silica-gold nanoparticle hybrids modified sensing platform. *Chem. Commun. (Camb)* **48**, 799-801 (2012).

132. You, C. C. *et al*. Detection and identification of proteins using nanoparticle-fluorescent polymer 'chemical nose' sensors. *Nat. Nanotechnol* **2**, 318-323 (2007).

133. De, M. *et al*. Sensing of proteins in human serum using conjugates of nanoparticles and green fluorescent protein. *Nat. Chem.* **1**, 461-465 (2009).

134. Wang, Z., Hu, J., Jin, Y., Yao, X. & Li, J. In situ amplified chemiluminescent detection of DNA and immunoassay of IgG using special-shaped gold nanoparticles as label. *Clin. Chem.* **52**, 1958-1961 (2006).

135. Taton, T. A., Mirkin, C. A. & Letsinger, R. L. Scanometric DNA array detection with nanoparticle probes. *Science* **289**, 1757-1760 (2000).

136. Kwon, M. J., Lee, J., Wark, A. W. & Lee, H. J. Nanoparticle-enhanced surface plasmon resonance detection of proteins at attomolar concentrations: comparing different nanoparticle shapes and sizes. *Anal. Chem.* **84**, 1702-1707 (2012).

137. Zhou, W. J., Halpern, A. R., Seefeld, T. H. & Corn, R. M. Near infrared surface plasmon resonance phase imaging and nanoparticle-enhanced surface plasmon resonance phase imaging for ultrasensitive protein and DNA biosensing with oligonucleotide and aptamer microarrays. *Anal. Chem.* **84**, 440-445 (2012).

138. Law, W. C., Yong, K. T., Baev, A. & Prasad, P. N. Sensitivity improved surface plasmon resonance biosensor for cancer biomarker detection based on plasmonic enhancement. *ACS Nano* **5**, 4858-4864 (2011).

139. Kim, S., Lee, J., Lee, S. J. & Lee, H. J. Ultra-sensitive detection of IgE using biofunctionalized nanoparticle-enhanced SPR. *Talanta* **81**, 1755-1759 (2010).

140. Li, T., Liu, D. & Wang, Z. Microarray-based Raman spectroscopic assay for kinase inhibition by gold nanoparticle probes. *Biosens. Bioelectron.* **24**, 3335-3339 (2009).

141. Li, T., Guo, L. & Wang, Z. Microarray based Raman spectroscopic detection with gold nanoparticle probes. *Biosens. Bioelectron.* **23**, 1125-1130 (2008).

142. Wang, J., Liu, G. & Jan, M. R. Ultrasensitive electrical biosensing of proteins and DNA: carbon-nanotube derived amplification of the recognition and transduction events. *J. Am. Chem. Soc.* **126**, 3010-3011 (2004).

143. Zheng, G., Patolsky, F., Cui, Y., Wang, W. U. & Lieber, C. M. Multiplexed electrical detection of cancer markers with nanowire sensor arrays. *Nat. Biotechnol.* **23**, 1294-1301 (2005).

144. Kelloff, G. J. & Sigman, C. C. Cancer biomarkers: selecting the right drug for the right patient. *Nat. Rev. Drug Discov.* **11**, 201-214 (2012).

145. Gu, Z., Biswas, A., Zhao, M. & Tang, Y. Tailoring nanocarriers for intracellular protein delivery. *Chem. Soc. Rev.* **40**, 3638-3655 (2011).

146. Brown, L. R. Commercial challenges of protein drug delivery. *Expert Opin. Drug Deliv.* **2**, 29-42 (2005).

147. Lu, Y., Yang, J. & Sega, E. Issues related to targeted delivery of proteins and peptides. *AAPS J.* **8**, E466-78 (2006).

148. Leader, B., Baca, Q. J. & Golan, D. E. Protein therapeutics: a summary and pharmacological classification. *Nat. Rev. Drug Discov.* **7**, 21-39 (2008).

149. Bareford, L. M. & Swaan, P. W. Endocytic mechanisms for targeted drug delivery. *Adv. Drug Deliv. Rev.* **59**, 748-758 (2007).

150. Jain, K. K. Drug delivery systems - an overview. *Methods Mol. Biol.* **437**, 1-50 (2008).

151. Goldberg, M., Langer, R. & Jia, X. Nanostructured materials for applications in drug delivery and tissue engineering. *J. Biomater. Sci. Polym. Ed.* **18**, 241-268 (2007).

152. Shi, Y. & Li, L. C. Current advances in sustained-release systems for parenteral drug delivery. *Expert Opin. Drug Deliv.* **2**, 1039-1058 (2005).

153. Gomez, J. A. *et al*. Cell-Penetrating Penta-Peptides (CPP5s): Measurement of Cell Entry and Protein-Transduction Activity. *Pharmaceuticals (Basel)* **3**, 3594-3613 (2010).

154. Zonin, E. *et al*. TAT-mediated aequorin transduction: an alternative approach for effective calcium measurements in plant cells. *Plant Cell Physiol.* **52**, 2225-2235 (2011).

155. Haas, A. K. *et al*. Human-protein-derived peptides for intracellular delivery of biomolecules. *Biochem. J.* **442**, 583-593 (2012).

156. Mussbach, F., Franke, M., Zoch, A., Schaefer, B. & Reissmann, S. Transduction of peptides and proteins into live cells by cell penetrating peptides. *J. Cell. Biochem.* **112**, 3824-3833 (2011).

157. Sawant, R. & Torchilin, V. Intracellular transduction using cell-penetrating peptides. *Mol. Biosyst* **6**, 628-640 (2010).

158. Patel, L. N., Zaro, J. L. & Shen, W. C. Cell penetrating peptides: intracellular pathways and pharmaceutical perspectives. *Pharm. Res.* **24**, 1977-1992 (2007).

159. Fonseca, S. B., Pereira, M. P. & Kelley, S. O. Recent advances in the use of cell-penetrating peptides for medical and biological applications. *Adv. Drug Deliv. Rev.* **61**, 953-964 (2009).

160. Heitz, F., Morris, M. C. & Divita, G. Twenty years of cell-penetrating peptides: from molecular mechanisms to therapeutics. *Br. J. Pharmacol.* **157**, 195-206 (2009).

161. Wu, R. P. *et al*. Cell-penetrating peptides as transporters for morpholino oligomers: effects of amino acid composition on intracellular delivery and cytotoxicity. *Nucleic Acids Res.* **35**, 5182-5191 (2007).

162. Green, I., Christison, R., Voyce, C. J., Bundell, K. R. & Lindsay, M. A. Protein transduction domains: are they delivering? *Trends Pharmacol. Sci.* **24**, 213-215 (2003).

163. Floren, A., Mager, I. & Langel, U. Uptake kinetics of cell-penetrating peptides. *Methods Mol. Biol.* **683**, 117-128 (2011).

164. Madani, F., Lindberg, S., Langel, U., Futaki, S. & Graslund, A. Mechanisms of cellular uptake of cell-penetrating peptides. *J. Biophys.* **2011**, 414729 (2011).

165. Bogoyevitch, M. A., Kendrick, T. S., Ng, D. C. & Barr, R. K. Taking the cell by stealth or storm? Protein transduction domains (PTDs) as versatile vectors for delivery. *DNA Cell Biol.* **21**, 879-894 (2002).

166. Green, I., Christison, R., Voyce, C. J., Bundell, K. R. & Lindsay, M. A. Protein transduction domains: are they delivering? *Trends Pharmacol. Sci.* **24**, 213-215 (2003).

167. Ross, M. F., Filipovska, A., Smith, R. A., Gait, M. J. & Murphy, M. P. Cell-penetrating peptides do not cross mitochondrial membranes even when conjugated to a

lipophilic cation: evidence against direct passage through phospholipid bilayers. *Biochem. J.* **383**, 457-468 (2004).

168. Paliwal, S. R., Paliwal, R., Agrawal, G. P. & Vyas, S. P. Liposomal nanomedicine for breast cancer therapy. *Nanomedicine (Lond)* **6**, 1085-1100 (2011).

169. Willis, L., Hayes, D.,Jr & Mansour, H. M. Therapeutic Liposomal Dry Powder Inhalation Aerosols for Targeted Lung Delivery. *Lung* (2012).

170. Iwase, Y. & Maitani, Y. Dual functional octreotide-modified liposomal irinotecan leads to high therapeutic efficacy for medullary thyroid carcinoma xenografts. *Cancer. Sci.* **103**, 310-316 (2012).

171. Chaudhury, A., Das, S., Bunte, R. M. & Chiu, G. N. Potent therapeutic activity of folate receptor-targeted liposomal carboplatin in the localized treatment of intraperitoneally grown human ovarian tumor xenograft. *Int. J. Nanomedicine* **7**, 739-751 (2012).

172. Bertrand, N., Bouvet, C., Moreau, P. & Leroux, J. C. Transmembrane pH-gradient liposomes to treat cardiovascular drug intoxication. *ACS Nano* **4**, 7552-7558 (2010).

173. Chou, L. Y., Ming, K. & Chan, W. C. Strategies for the intracellular delivery of nanoparticles. *Chem. Soc. Rev.* **40**, 233-245 (2011).

174. Beerens, A. M., Al Hadithy, A. F., Rots, M. G. & Haisma, H. J. Protein transduction domains and their utility in gene therapy. *Curr. Gene Ther.* **3**, 486-494 (2003).

175. Lundberg, M., Wikstrom, S. & Johansson, M. Cell surface adherence and endocytosis of protein transduction domains. *Mol. Ther.* **8**, 143-150 (2003).

176. Rapoport, M. & Lorberboum-Galski, H. TAT-based drug delivery system--new directions in protein delivery for new hopes? *Expert Opin. Drug Deliv.* **6**, 453-463 (2009).

177. Chugh, A., Eudes, F. & Shim, Y. S. Cell-penetrating peptides: Nanocarrier for macromolecule delivery in living cells. *IUBMB Life* **62**, 183-193 (2010).

178. Chinnery, P. F. *et al*. Peptide nucleic acid delivery to human mitochondria. *Gene Ther.* **6**, 1919-1928 (1999).

179. Koppelhus, U. *et al*. Cell-dependent differential cellular uptake of PNA, peptides, and PNA-peptide conjugates. *Antisense Nucleic Acid Drug Dev.* **12**, 51-63 (2002).

180. Zassler, B., Blasig, I. E. & Humpel, C. Protein delivery of caspase-3 induces cell death in malignant C6 glioma, primary astrocytes and immortalized and primary brain capillary endothelial cells. *J. Neurooncol.* **71**, 127-134 (2005).

181. Weill, C. O., Biri, S., Adib, A. & Erbacher, P. A practical approach for intracellular protein delivery. *Cytotechnology* **56**, 41-48 (2008).

182. Muller, R. H., Radtke, M. & Wissing, S. A. Solid lipid nanoparticles (SLN) and nanostructured lipid carriers (NLC) in cosmetic and dermatological preparations. *Adv. Drug Deliv. Rev.* **54 Suppl 1**, S131-55 (2002).

183. Almeida, A. J., Runge, S. & Müller, R. H. Peptide-loaded solid lipid nanoparticles (SLN): Influence of production parameters. *Int. J. Pharm.* **149**, 255-265 (1997).

184. Hwa Kim, S., Hoon Jeong, J., Joe, C. O. & Gwan Park, T. Folate receptor mediated intracellular protein delivery using PLL–PEG–FOL conjugate. *J. Controlled Release* **103**, 625-634 (2005).

185. Akagi, T., Wang, X., Uto, T., Baba, M. & Akashi, M. Protein direct delivery to dendritic cells using nanoparticles based on amphiphilic poly(amino acid) derivatives. *Biomaterials* **28**, 3427-3436 (2007).

186. Lee, Y. *et al*. Charge-conversional polyionic complex micelles-efficient nanocarriers for protein delivery into cytoplasm. *Angew. Chem. Int. Ed Engl.* **48**, 5309-5312 (2009).

187. Shimoni, O. *et al*. Macromolecule functionalization of disulfide-bonded polymer hydrogel capsules and cancer cell targeting. *ACS Nano* **6**, 1463-1472 (2012).

188. Yan, M., Du, J., Gu, Z. & Liang, M. A novel intracellular protein delivery platform based on single-protein nanocapsules. *Nature nanotechnology* **5**, 48-53 (2009).

189. Klose, D., Siepmann, F., Elkharraz, K. & Siepmann, J. PLGA-based drug delivery systems: importance of the type of drug and device geometry. *Int. J. Pharm.* **354**, 95-103 (2008).

190. Futami, J. *et al*. Intracellular delivery of proteins into mammalian living cells by polyethylenimine-cationization. *Journal of Bioscience and Bioengineering* **99**, 95-103 (2005).

191. Murata, H. *et al*. Intracellular delivery of glutathione S-transferase-fused proteins into mammalian cells by polyethylenimine-glutathione conjugates. *J. Biochem.* **144**, 447-455 (2008).

192. Kitazoe, M. *et al*. Protein transduction assisted by polyethylenimine-cationized carrier proteins. *J. Biochem.* **137**, 693-701 (2005).

193. Kam, N. W., Liu, Z. & Dai, H. Carbon nanotubes as intracellular transporters for proteins and DNA: an investigation of the uptake mechanism and pathway. *Angew. Chem. Int. Ed Engl.* **45**, 577-581 (2006).

194. Kam, N. W. & Dai, H. Carbon nanotubes as intracellular protein transporters: generality and biological functionality. *J. Am. Chem. Soc.* **127**, 6021-6026 (2005).

195. Liu, B. R. *et al*. Cellular internalization of quantum dots noncovalently conjugated with arginine-rich cell-penetrating peptides. *J. Nanosci Nanotechnol* **10**, 6534-6543 (2010).

196. Liu, B. R., Huang, Y. W., Chiang, H. J. & Lee, H. J. Cell-penetrating peptide-functionalized quantum dots for intracellular delivery. *J. Nanosci Nanotechnol* **10**, 7897-7905 (2010).

197. Zrazhevskiy, P., Sena, M. & Gao, X. Designing multifunctional quantum dots for bioimaging, detection, and drug delivery. *Chem. Soc. Rev.* **39**, 4326-4354 (2010).

198. Koshman, Y. E. *et al*. Delivery and visualization of proteins conjugated to quantum dots in cardiac myocytes. *J. Mol. Cell. Cardiol.* **45**, 853-856 (2008).

199. Medintz, I. L. *et al*. Intracellular delivery of quantum dot-protein cargos mediated by cell penetrating peptides. *Bioconjug. Chem.* **19**, 1785-1795 (2008).

200. Boisselier, E. & Astruc, D. Gold nanoparticles in nanomedicine: preparations, imaging, diagnostics, therapies and toxicity. *Chem. Soc. Rev.* **38**, 1759-1782 (2009).

201. Ghosh, P., Han, G., De, M., Kim, C. K. & Rotello, V. M. Gold nanoparticles in delivery applications. *Adv. Drug Deliv. Rev.* **60**, 1307-1315 (2008).

202. Huang, Y. *et al*. Co-administration of protein drugs with gold nanoparticles to enable percutaneous delivery. *Biomaterials* **31**, 9086-9091 (2010).

203. Bale, S. S. *et al*. Nanoparticle-mediated cytoplasmic delivery of proteins to target cellular machinery. *ACS Nano* **4**, 1493-1500 (2010).

204. Slowing, I., Trewyn, B. G. & Lin, V. S. Effect of surface functionalization of MCM-41-type mesoporous silica nanoparticles on the endocytosis by human cancer cells. *J. Am. Chem. Soc.* **128**, 14792-14793 (2006).

205. Slowing, I. I., Trewyn, B. G. & Lin, V. S. Mesoporous silica nanoparticles for intracellular delivery of membrane-impermeable proteins. *J. Am. Chem. Soc.* **129**, 8845-8849 (2007).

206. Vivero-Escoto, J. L., Slowing, I. I., Trewyn, B. G. & Lin, V. S. -. Mesoporous Silica Nanoparticles for Intracellular Controlled Drug Delivery. *Small* **6**, 1952-1967 (2010).

207. Chorny, M., Hood, E., Levy, R. J. & Muzykantov, V. R. Endothelial delivery of antioxidant enzymes loaded into non-polymeric magnetic nanoparticles. *J. Controlled Release* **146**, 144-151 (2010).

208. Laurent, S. *et al*. Magnetic iron oxide nanoparticles: synthesis, stabilization, vectorization, physicochemical characterizations, and biological applications. *Chem. Rev.* **108**, 2064-2110 (2008).

209. Gao, J., Gu, H. & Xu, B. Multifunctional magnetic nanoparticles: design, synthesis, and biomedical applications. *Acc. Chem. Res.* **42**, 1097-1107 (2009).

210. Cronican, J. J. *et al*. Potent delivery of functional proteins into Mammalian cells in vitro and in vivo using a supercharged protein. *ACS Chem. Biol.* **5**, 747-752 (2010).

211. Lim, Y. T., Cho, M. Y., Lee, J. M., Chung, S. J. & Chung, B. H. Simultaneous intracellular delivery of targeting antibodies and functional nanoparticles with engineered protein G system. *Biomaterials* **30**, 1197-1204 (2009).

212. Abbing, A. *et al*. Efficient intracellular delivery of a protein and a low molecular weight substance via recombinant polyomavirus-like particles. *J. Biol. Chem.* **279**, 27410-27421 (2004).

213. Pillai, O. & Panchagnula, R. Polymers in drug delivery. *Curr. Opin. Chem. Biol.* **5**, 447-451 (2001).

214. Angelova, N. & Hunkeler, D. Rationalizing the design of polymeric biomaterials. *Trends Biotechnol.* **17**, 409-421 (1999).

215. Diwan, M. & Park, T. G. Pegylation enhances protein stability during encapsulation in PLGA microspheres. *J. Controlled Release* **73**, 233-244 (2001).

216. Nochi, T. *et al*. Nanogel antigenic protein-delivery system for adjuvant-free intranasal vaccines. *Nat. Mater.* **9**, 572-578 (2010).

217. Lee, A. L. Z. *et al*. Efficient intracellular delivery of functional proteins using cationic polymer core/shell nanoparticles. *Biomaterials* **29**, 1224-1232 (2008).

218. Hasadsri, L., Kreuter, J., Hattori, H., Iwasaki, T. & George, J. M. Functional protein delivery into neurons using polymeric nanoparticles. *J. Biol. Chem.* **284**, 6972-6981 (2009).

219. Hu, Y. *et al*. Cytosolic delivery of membrane-impermeable molecules in dendritic cells using pH-responsive core-shell nanoparticles. *Nano Lett.* **7**, 3056-3064 (2007).

220. Du, J. *et al*. Quantum-dot-decorated robust transductable bioluminescent nanocapsules. *J. Am. Chem. Soc.* **132**, 12780-12781 (2010).

221. Gu, Z. *et al*. Protein nanocapsule weaved with enzymatically degradable polymeric network. *Nano Lett.* **9**, 4533-4538 (2009).

222. Biswas, A. *et al*. Endoprotease-mediated intracellular protein delivery using nanocapsules. *ACS Nano* **5**, 1385-1394 (2011).

223. Zhou, H. *et al*. Generation of induced pluripotent stem cells using recombinant proteins. *Cell. Stem Cell.* **4**, 381-384 (2009).

224. Murthy, N. *et al*. A macromolecular delivery vehicle for protein-based vaccines: acid-degradable protein-loaded microgels. *Proc. Natl. Acad. Sci. U. S. A.* **100**, 4995-5000 (2003).

225. Cohen, J. A. *et al*. T-cell activation by antigen-loaded pH-sensitive hydrogel particles in vivo: the effect of particle size. *Bioconjug. Chem.* **20**, 111-119 (2009).

226. Beaudette, T. T. *et al*. Chemoselective ligation in the functionalization of polysaccharide-based particles. *J. Am. Chem. Soc.* **131**, 10360-10361 (2009).

227. Bachelder, E. M. *et al*. Acid-degradable polyurethane particles for protein-based vaccines: biological evaluation and in vitro analysis of particle degradation products. *Mol. Pharm.* **5**, 876-884 (2008).

228. De Rose, R. *et al*. Binding, Internalization, and Antigen Presentation of Vaccine-Loaded Nanoengineered Capsules in Blood. *Adv Mater* **20**, 4698-4703 (2008).

229. Rivera-Gil, P., De Koker, S., De Geest, B. G. & Parak, W. J. Intracellular processing of proteins mediated by biodegradable polyelectrolyte capsules. *Nano Lett.* **9**, 4398-4402 (2009).

230. Shu, S., Zhang, X., Wu, Z., Wang, Z. & Li, C. Gradient cross-linked biodegradable polyelectrolyte nanocapsules for intracellular protein drug delivery. *Biomaterials* **31**, 6039-6049 (2010).

231. Roberts, M. J., Bentley, M. D. & Harris, J. M. Chemistry for peptide and protein PEGylation. *Adv. Drug Deliv. Rev.* **54**, 459-476 (2002).

232. Francesco M., V. in *PEGylated Protein Drugs: Basic Science and Clinical Applications* 297 (Birkhäuser Basel, 2009).

233. Lackey, C. A., Press, O. W., Hoffman, A. S. & Stayton, P. S. A biomimetic pH-responsive polymer directs endosomal release and intracellular delivery of an endocytosed antibody complex. *Bioconjug. Chem.* **13**, 996-1001 (2002).

234. Peer, D. *et al*. Nanocarriers as an emerging platform for cancer therapy. *Nat. Nanotechnol* **2**, 751-760 (2007).

235. Chou, L. Y., Ming, K. & Chan, W. C. Strategies for the intracellular delivery of nanoparticles. *Chem. Soc. Rev.* **40**, 233-245 (2011).

236. Lu, F., Wu, S. H., Hung, Y. & Mou, C. Y. Size effect on cell uptake in well-suspended, uniform mesoporous silica nanoparticles. *Small* **5**, 1408-1413 (2009).

237. Albanese, A. & Chan, W. C. Effect of gold nanoparticle aggregation on cell uptake and toxicity. *ACS Nano* **5**, 5478-5489 (2011).

238. Yue, T. & Zhang, X. Cooperative Effect in Receptor-Mediated Endocytosis of Multiple Nanoparticles. *ACS Nano* (2012).

CHAPTER 2: SYNTHESES OF DNA-PROTEIN CONJUGATES

2.1. Introduction

As mentioned previously, this dissertation focuses on the use of covalent conjugation methods to construct one-to-one molar ratio DNA-protein hybrids for controlling the stoichiometry and geometry of the proteins by DNA. Three different conjugation methods were explored: SNAP tag, sulfo-SMCC crosslinker, and sortase A. (Two other methods were tried without success: "express protein ligation" (EPL), and Michael addition chemistry between acrydite and thiol groups.) For all methods, a small protein called EZZ (16 kDa) was used to create a DNA-protein hybrid, a universal adapter which can interface with both a DNA molecule and an IgG antibody. EZZ protein is an engineered version of the native protein A from *Staphylococcus aureus* (SpA).[1] It contains two repeating Z domains which were engineered based on the B domain, and a short signal sequence from the E domain of the native protein A to help direct protein expression. Similar to native protein A, EZZ protein possesses many interesting properties. For example, it is stable over a broad range of pH (2-12) and in the presence of various detergents. It can bind reversibly to a large variety of IgGs via the Fc fragment (Table 2.1), and the IgG-EZZ complex can be dissociated under controlled conditions (pH 3.5-4.5) without apparent loss of activity. Some research groups have also used native protein A, or different engineered versions of it, with quantum dot[2] and magnetic nanoparticles[3, 4] for protein detection or labeling. However, none have taken advantage of DNA nanotechnology to enhance the capabilities and possibilities of using EZZ protein as a universal adapter for IgG

antibody-based detection and IgG antibody delivery systems. This chapter introduces how to conjugate the DNA-EZZ protein hybrid molecule. Later chapters will describe the applications of the DNA-protein hybrid molecules.

Table 2.1. Binding affinity of Protein A to antibodies.

	Strong binding	Weak binding	No binding
Species	Antibody Class	Antibody Class	Antibody Class
Human	Total IgG IgG1 IgG2 IgG4	IgG3 IgM IgA Fab ScFv	IgD
Mouse	Total IgG IgG_{2a} IgG2b IgG3	IgG_1	IgM
Rat	IgG2c	Total IgG IgG1	IgG2a IgG2b
Cow	IgG2	Total IgG IgG1	n/a
Goat	IgG2	Total IgG IgG1	n/a
Sheep	IgG2	Total IgG IgG1	n/a
Rabbit	Total IgG	n/a	n/a
Guinea Pig	Total IgG	n/a	n/a
Pig	Total IgG	n/a	n/a
Dog	Total IgG	n/a	n/a
Cat	Total IgG	n/a	n/a
Horse	n/a	Total IgG IgG(ab) IgG(c)	IgG(T)
Chicken	n/a	n/a	Total IgY

n/a: not available. [Source: Thermo Scientific Tech Tip #34]

One of the primary motivations for creating DNA-protein conjugates is to build artificial proteins out of different domains using DNA linkers instead of protein engineering. To achieve this, it is necessary to find a general method which can directly link DNA to the proteins of interest (POI) with an ability to control the stoichiometry and geometry of the proteins by DNA. As the first step, one protein must be able to be connected to one DNA molecule easily and efficiently.

SNAP tag was first developed and widely used for directly labeling proteins *in vivo* with small molecules or fluorophores for imaging.[5-9] [10]Later, it was also used to immobilize proteins on microarrays[11-14] and to form DNA-protein conjugates[5, 11, 15-17]. SNAP protein is a mutant of the DNA repair protein O^6-alkylguanine-DNA alkyltransferase (hAGT), which can react with O6-benzylguanine (BG) substrates to form a stable covalent thioether bond[5]. The catalytic activity of the SNAP protein is due to the active site residue Cys-145 which is activated through a charge relay involving His-146, Glu-172 and a Zn^{2+} ion.[18, 19] However, SNAP protein does not act as a true enzyme since it does not have catalytic turnover activity. Thus, one SNAP protein will catalyze one BG group to form a 1:1 ratio product. In order to generate DNA-protein conjugate using SNAP tag, the EZZ protein as the POI was cloned to C-terminal of SNAP protein. As described in Figure 2.1, BG-modified DNA as the substrate for SNAP protein, has to be obtained by maleimide-thiol reaction between BG and DNA molecules before it can be catalyzed by SNAP-EZZ protein to form EZZ-SNAP-DNA (ESD) conjugates.

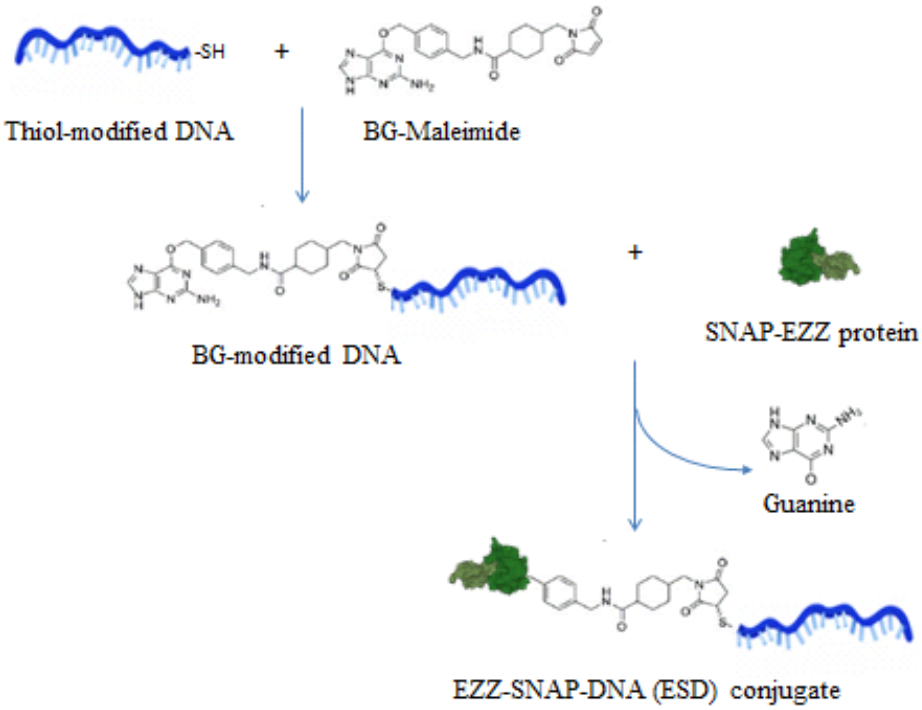

Figure 2.1. Scheme of forming DNA-SNAP-EZZ protein conjugate. Thiol-modified DNA reacted with BG-maleimide substrate to generate BG-modified DNA, which was catalyzed by SNAP protein in order to form SNAP-EZZ-DNA conjugate.

Although SNAP tag or other self-labeling protein-based methods such as the CLIP tag or the HaloTag are good and efficient methods, the large size of the SNAP protein (20 kDa) might interfere with the structure and function of the resulting hybrid. Therefore, we look for a general method that can directly link DNA to the POI without a bulky protein tag. As an attempt to achieve direct linkage, the hetero-bifunctional crosslinker sulfo-SMCC (Thermo Scientific, Bradfold, IL) was used to conjugate EZZ protein with DNA. Sulfo-SMCC contains NHS ester and maleimide

chemical groups which specifically react with amine and sulfhydryl groups that can be easily modified on DNA and proteins, respectively. As described in Figure 2.2, sulfo-SMCC reacted with amine-modified DNA to generate maleimide-activated DNA which easily formed a covalent link with the thiol groups from the cysteine amino acids of the protein. Normally, the thiol-maleimide reaction between protein and DNA could generate multiple DNA molecules per each protein depending on how many cysteine amino acids are present in the protein. However, the EZZ protein is a small protein which has no cysteine amino acids in its structure; therefore, it is the perfect candidate for taking advantage of this thiol reaction after adding a single cysteine residue at the C-terminus of the protein sequence.

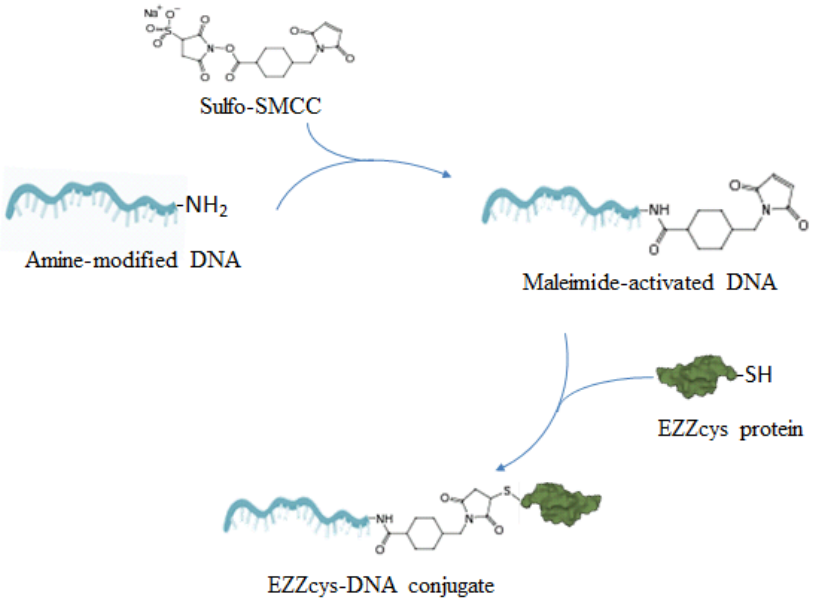

Figure 2.2. Scheme of forming EZZcys-DNA conjugate. Amine-modified DNA reacted with sulfo-SMCC to create maleimide-activated DNA product, which can easily react with thiol group from cysteine residue at C-terminal of EZZcys protein

This thiol coupling approach can be used to achieve direct linkage, but its generality is limited because it is rare to have a POI without any cysteine residues in its sequence. As a more broadly applicable method, *Staphylococcus aureus* Sortase Transpeptidase SrtA has been used. Several reviews detail the mechanisms of SrtA[20-23]. Basically, as shown in Figure 2.3, SrtA recognizes a specific LPXTG motif, where X could be any amino acid, and catalyzes a cleavage between threonine (T) and glycine (G) to form a thiolester acyl-enzyme target intermediate. The intermediate is then attacked by an amine group of the oligoglycine-modified probe to form a transpeptidation product between target protein and probe.[23] The amine group of glycine amino acid, as the nucleophile, donates an electron pair to form a chemical bond and plays an important role in the reaction. In fact, when an amine-modified oliugonucleotide is used, the yield of forming the DNA-protein conjugates by sortase is extremely low (data not shown). Moreover, the efficiency of the transpeptidation reaction also depends on the length of the oligoglycine, which is normally best between three and five glycines.[24] Since polyglycine is important for sortase reactions, in order to obtain a protein-DNA conjugate using this method, I first conjugated a pentaglycine (pG) peptide with DNA before it was used to react with the target protein, LPETG-tagged GFP. Figure 2.4 describes the strategy of forming GFP-DNA conjugate catalyzed by sortase A. First, sulfo SMCC was used to crosslink amine-modified DNA with the thiol group from the cysteine amino acid at the C-terminal of pG peptide. The amine group from pG-DNA conjugate then served as the nucleophile to attack the GFP-sortase intermediate to form a GFP-DNA conjugate.

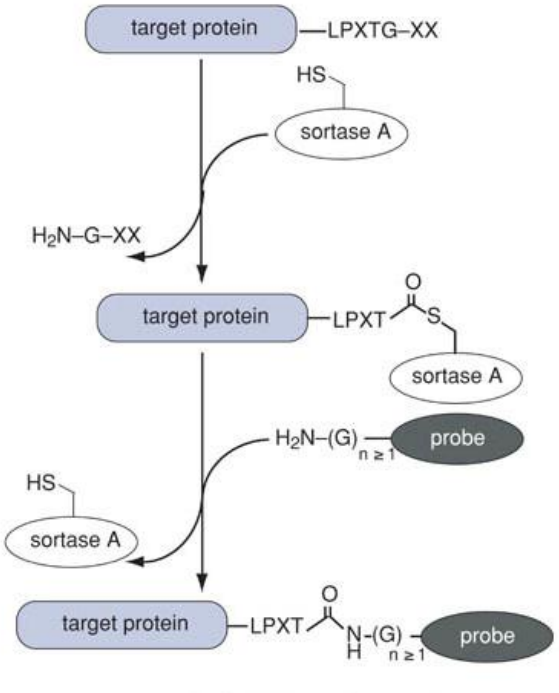

Figure 2.3. Sortase-mediated transpeptidation mechanism.[23]

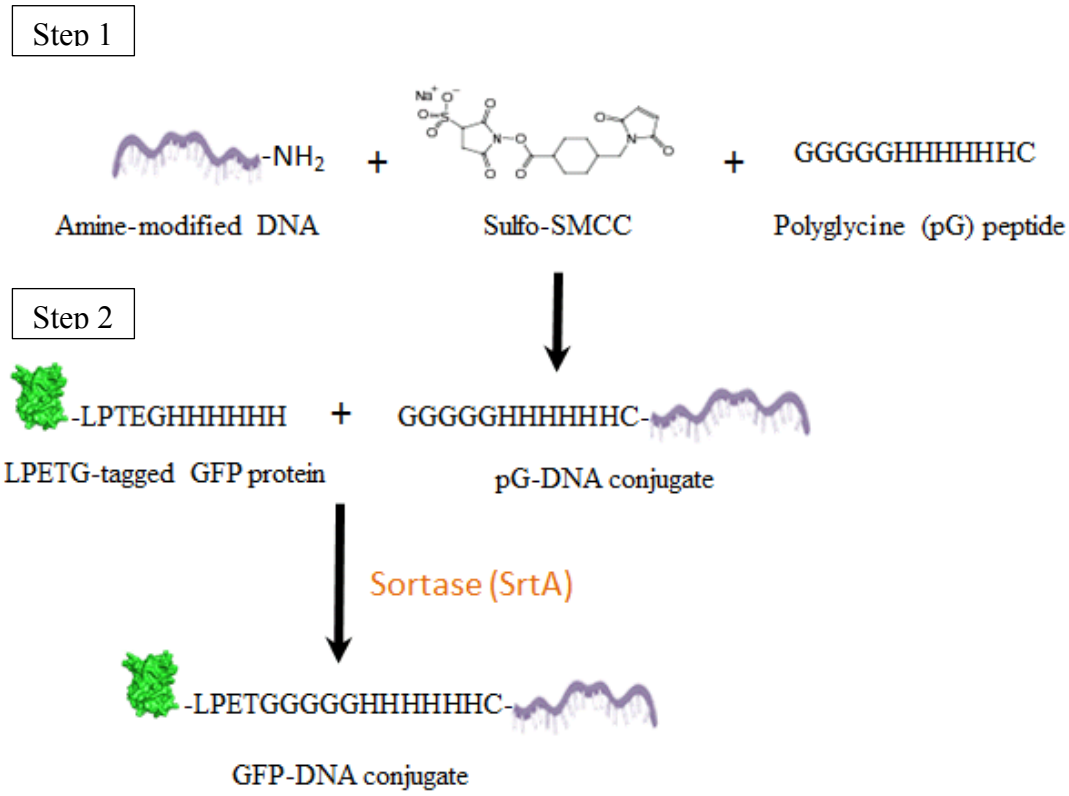

Figure 2.4. Scheme of forming GFP-DNA conjugate using sortase A. Step 1. Polyglycine (pG)-DNA conjugate was created by using sulfo-SCMM to crosslink thiol and amine groups between peptide and DNA, respectively. Step 2. Sortase reaction was performed to generate GFP-DNA conjugate.

2.2. Materials and methods

2.2.1. DNA and protein materials

All oligonucleotides (Table 2.2) were commercially synthesized with standard desalting by Integrated DNA Technologies (Coralville, Iowa). Without further purification, the oligonucleotides were dissolved in 1x TE buffer (10 mM Tris, pH=8.0, 1 mM ethylenediaminetetraacetic acid (EDTA)) with a final concentration of 100 μM.

Table 2.2. Summary of DNA materials

DNA	5'- modification	Sequence (from 5' to 3')
Linker 1	Thiol-modified	/5ThiolMC6/ TAC GTC AAC GTC GTC GAA TG
Linker 2	Amine-modified	/5AmMC6/ CGA GCT GCC ACA ACT CCA TC
Linker 3	Amine-modified	/5AmMC6/ TGC CAC AAC CAC CTC CGT AA

a. Cloning, expression and purification of SNAP-EZZ protein

The pSNAP-EZZ vector which encodes the SNAP-EZZ protein was created by combining EZZ protein from pEZZ18 Protein A Gene Fusion Vector (GE Healthcare) with SNAP protein from pSNAP-tag®(T7) vector (New England Biolabs, Ipswich, MA) at its C-terminus. In addition, a short peptide linker Gly-Gly-Gly-Ser (GGGS) was included to create flexibility between the SNAP and EZZ proteins, and a polyhistidine-tag (6xHis) was added to the C-terminus of the EZZ protein. The molecular weight of the SNAP-EZZ protein in this work is about 36 kDa, which is combined between 20 kDa and 16 kDa of SNAP and EZZ proteins, respectively.

BL21-AI™ One Shot® Chemically Competent E. coli (Invitrogen, Carlsbad, CA) cells transformed with the appropriate plasmid were grown overnight on LB (Luria Broth) plates containing 50mg/ml Ampicillin. Several colonies were selected to test the protein expression, and the best one was used for a 400 ml culture of bacteria in LB medium with 50mg/ml Ampicillin. The cells were grown at 37 °C until the OD_{600} reached approximately 0.7. Protein expression was induced by the addition of Arabinose to a final concentration of 20% (v/v). The cells were harvested by centrifugation after additional 6 hours with shaking. The cell pellet was resuspended and lysed in 1x BugBuster® Protein Extraction Reagent (Novagen, Madison, WI) (1:10 v/v). Cell debris was removed by centrifugation and the soluble part of the lysate was transferred into Poly-Prep® Chromatography Columns (Bio-Rad, Hercules, CA) which contained IgG Sepharose 6 Fast Flow (GE Healthcare, Pittsburgh, PA) according to the manufacturer's instructions to purify the SNAP-EZZ protein. The eluted protein was immediately dialyzed three times (two of two hours, and one overnight dialysis) in 10 mM PBS, pH=7.4, using a 3000 MWCO Slide-A-Lyzer ® Dialysis Cassette (Thermo Scientific, Bradfold, IL). The concentration of SNAP-EZZ protein was determined by the Micro BCA™ Protein Assay Kit (Thermo Scientific, Bradfold, IL) calibrated with bovin serum albumin (BSA) as reference protein. The protein was aliquoted into 1 ml of 150 μM tubes, which were then lyophilized and stored at -80˚C, and dissolved in de-ionized water prior to use.

b. Cloning, expression and purification of EZZcys protein

The EZZcys protein was created simply by adding a cysteine amino acid at the end of the C-terminus of EZZ protein, and cloned into a pET 18b(+) vector. Please

note that there is no 6xHis tag in this protein. The molecular weight of the EZZcys protein in this work is 16 kDa. The procedure for the expression and purification of EZZcys protein was similar to what was described above for the SNAP-EZZ protein. However, BL21-DE3 cells (Invitrogen, Carlsbag, CA) were used to transform the pET 18b(+) vector containing EZZcys protein instead of BL21-Ai, and the cells were cultured in LB medium with 50 mg/ml Kanamycin instead of Ampicillin. Also, isopropyl thioglucoside (IPTG) was added to a final concentration of 1 mM to induce the expression of EZZcys protein instead of Arabinose.

c. Expressions and purifications of LPETG-tagged GFP and Sortase A

Plasmids encoding for GFP and Sortase A proteins were received from other labs. Plasmid pHTT27 (Ton-That et al. Journal of Biological Chemistry 277 (2002) 7447-7452) encodes for hexahistidine-tagged recombinant Sortase A. Plasmid pLLC152 encodes for eGFP-LPETGG-HHHHHH (Chan et al. PLoS ONE 2 (2007) e1164). The incorporation of an additional glycine group following the LPXTG motif was shown to maximize the activity of sortase ligation (Pritz et al. J. Org Chem 72 (2007) 3909-3912; Tanaka et al. ChemBioChem 9 (2008) 802-807). The molecular weights of the sortase and GFP proteins used in this work are 22 and 29 kDa respectively.

BL21-DE3 cells transformed with the appropriate plasmid were grown overnight on LB plates containing ampicillin. A single colony from each plate was used to inoculate a small starter culture that was then used to inoculate 2 L of a nutrient-rich media which was grown at 37 °C until the OD_{600} reached approximately 0.7. Protein expression was induced by the addition of isopropyl thioglucoside (IPTG)

to a final concentration of 1 mM. After an additional 3 hours of shaking, the resulting bacterial mass was harvested and lysed. The cellular lysate was purified with a gravity-chromatography column containing Ni-NTA resin (Qiagen) according to the manufacturer's instructions. The column eluents were collected in 1 mL fractions and the most highly concentrated fractions were pooled. An overnight dialysis step was performed to remove low molecular weight compounds that were used to elute the protein from the column using a 3.5 kDa molecular weight cut-off Spectra/Por membrane (Spectrum Laboratories) and dialysis buffer (71 mM Tris-HCl pH 8.0, 214 mM NaCl). Glycerol was added to the dialysate product to a final concentration of 30% by volume and the resulting solution was divided into small aliquots that were stored at −20 °C. The purity and concentration of the final protein product was assessed by SDS-PAGE analysis and Bradford assay respectively.

2.2.2. Synthesis of EZZ-SNAP-DNA (ESD) conjugates by SNAP-tag

Thiol-modified DNA linker 1 (IDTDNA, Coralville, Iowa) (Table 2.2) was first reduced by tris(2-carboxyethyl)phosphine (TCEP) (Sigma, Ronkonkoma, NY) at 1:100 molar ratio at 25^{o}C for an hour. After the excess of TCEP was removed by Microcon Centrifugal Filter Devices YM-3 (Millipore Corp., Billerica, MA), thiol-modified DNA was reacted with BG-maleimide (New England Biolabs, Ipswich, MA) at 1:5 molar ratio in 10 mM Tris buffer, pH= 7.5 at 30^{o}C, overnight to form BG-modified DNA. The excess of BG-maleimide was removed again by using Microcon Centrifugal Filter Devices YM-3 (Millipore Corp., Billerica, MA) before BG-modified DNA was reacted with 50 μM of SNAP-EZZ protein at 5:1 molar ratio between DNA and protein. The reaction was incubated at room temperature, shaken at 900 rpm,

overnight, and the EZZ-SNAP-DNA product was confirmed by SDS-PAGE gel electrophoresis under denaturing conditions, and then purified by a Sephacryl S-200 HR gel filtration column at flow rate of 0.15 ml/min.

2.2.3. Synthesis of EZZcys-DNA conjugates by sulfo-SMCC

The scheme for the synthesis of EZZcys-DNA conjugate is shown in Figure 8. First, maleimide-activated DNA was prepared by using amine-modified DNA linker 3 (Table 2.2) with 10 mM sulfo-SMCC in 1x PBS buffer, pH 7.4 at 1:40 molar ratio at room temperature for 2 hours. The excess sulfo-SMCC was removed by Microcon centrifugal filter devices YM-3 (Millipore Corporation, Billerica, MA) with 2 times of washing with 400 µl of 1x PBS buffer, pH 7.4 following the company's instruction. The DNA solution was then run through Illustra Micro Spin G-25 columns (GE Healthcare, Pittsburgh, PA) to completely remove any trace of sulfo-SMCC left in the solution. It is important to completely remove sulfo-SMCC since it would otherwise reduce the yield of the reaction between maleimide and thiol groups (data not shown). The maleimide-modified DNA should be used to react with thiol-modified protein immediately, but can be stored at 4^{o}C for about two days to avoid losing the reaction specificity for sulfhydryl group by hydrolysis.

Second, EZZcys protein was reduced with tris(2-carboxyethyl)phosphine (TCEP) (Sigma, Ronkonkoma, NY) to break down the protein dimers formed by the cysteine-cysteine disulfide bond to give the active thiol group which reacts with maleimide group from DNA. EZZcys protein dissolved in 1x PBS buffer, pH 7.4 was mixed with TCEP at 1:100 molar ratios, and incubated at room temperature for 15 minutes. Free TCEP was removed from the protein by using Microcon centrifugal

filter devices YM-10 (Millipore Corporation, Billerica, MA) following the company's instruction and washed four times with 1x PBS buffer, pH. 7.4. The reduced EZZcys protein was reacted with maleimide-modified DNA immediately to avoid the reform of the protein dimers.

50 μM of EZZcys protein was mixed with maleimide-modified DNA at a 1:10 molar ratio, and shaken at 900 rpm, at room temperature for overnight. The product was confirmed by 4-20% SDS-PAGE gel electrophoresis under denaturing conditions, and purified by Sephacryl S-200 HR gel filtration column at flow rate of 0.15 ml/min.

2.2.4. Synthesis of GFP-DNA conjugates by Sortase A enzyme

The synthesis of DNA-GFP protein conjugate was performed in two steps. The first step involved the synthesis of polyglycine (pG)-DNA peptide conjugate to act as the amine nucleophile in the sortase reaction later. The second step is the sortase reaction between GFP and pG-DNA to form DNA-GFP protein conjugate.

a. Synthesis of polyglycine-DNA (pG-DNA) conjugate by sulfo-SMCC

Maleimide-activated DNA was first prepared by using amine-modified DNA linker 2 (Table 2.2) as described in the synthesis of EZZcys-DNA conjugate by sulfo-SMCC above. It was then reacted with polyglycine (pG) peptide (GGGGGHHHHHHC, MW=1.2 kDa) at 1:1 molar ratio at 4°C for overnight to form polyglycine-DNA (pG-DNA) conjugate after boiling at 95°C for 15 minutes immediately before the reaction. The pG-DNA product was confirmed by 3% agarose gel electrophoresis in 1x TAE buffer (40 mM Tris-acetate and 1 mM EDTA with a pH of 8.3), and purified by Bio-gel P30 gel filtration (Bio-Rad, Hercules, CA) to eliminate unreacted peptides, followed by purification using Ni-NTA (Qiagen, Valencia, CA)

columns to eliminate unreacted DNA.

b. Synthesis of GFP-DNA conjugates by Sortase A enzyme

5 μM of GFP protein and 5 μM of pG-DNA conjugates were added into a reaction buffer (50 mM Tris-HCl, pH 7.5, 150 mM NaCl, and 5 mM CaCl2) with 15 μM SrtA, and incubated at 37°C for overnight. The GFP-DNA product was confirmed by 4-20% SDS-PAGE gel electrophoresis under denaturing conditions.

2.3. Results

2.3.1. EZZ-SNAP-DNA (ESD) conjugates

ESD conjugates were synthesized by the catalysis of SNAP-EZZ protein to BG-modified DNA at 1:5 molar ratios between protein and DNA. The product was confirmed by 4-20% SDS-PAGE gel under denaturing conditions. The samples were added with SDS loading dye and heated at 95°C for 5 minutes and cooled down to room temperature before loading. The gel was run in Tris-Glycine SDS running buffer, at 250 volts, at room temperature for 30 minutes. The gel was first stained with GelRed dye, which specifically stained DNA products for about one hour. After imaging by UV exposure with Kodak Imaging Station 4000R, the gel was stained for a second time with Coomassie Brilliant Blue (CBB) R-250 staining solution for 10 minutes then de-stained overnight to visualize protein products. Figure 2.5 shows that ESD conjugates in lane 1 with higher molecular weight migrated slower than BG-modified DNA only in lane 2 and SNAP-EZZ protein only in lane 3.

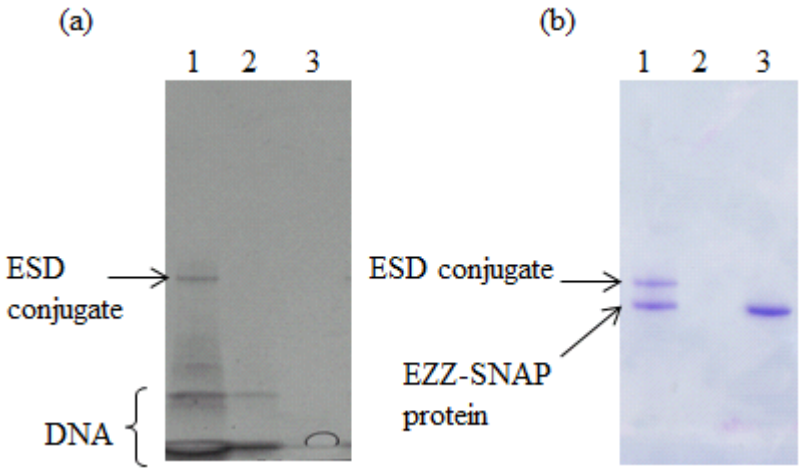

Figure 2.5. Confirmation of EZZ-SNAP-DNA (ESD) conjugates on 4-20% SDS-PAGE gel electrophoresis. The same gel was first stained with GelRed to visualize DNA products (a) and then stained with Coomassie Brilliant Blue (b) to visualize protein products. 1. ESD conjugates. 2. DNA only. 3. EZZ-SNAP protein only.

Furthermore, it was noticed that the mobility of DNA-SNAP-EZZ conjugates varied depending on the running conditions of PAGE gel electrophoresis. When run on SDS-PAGE gel electrophoresis under denaturing condition, ESD conjugates migrated slower than the individual components as shown in figures 2.5 and 2.6a. On the other hand, when run on native PAGE gel electrophoresis under non-denaturing conditions while there was no SDS in the gel and running buffer, DNA-SNAP-EZZ conjugates migrated faster than SNAP-EZZ protein itself (Figure 2.6b). This unexpected behavior could be due to the effects of charge and mass of the DNA-protein conjugate. In the SDS-PAGE case, since SDS is highly negatively- charged, it

cancels out the charge effects of the protein and DNA, which is also negatively charged. Thus, the mobility of DNA-SNAP-EZZ conjugate and SNAP-EZZ protein was purely dependent on the size of the molecule, and since the DNA-SNAP-EZZ conjugate was bigger, it ran slower, and remained closer to the wells of the gel. On the other hand, in native PAGE gel electrophoresis, there was no SDS involved, so the total net charge effect could play a more important role than the size effect in the mobility of DNA-SNAP-EZZ conjugate, compared to that of SNAP-EZZ protein only.

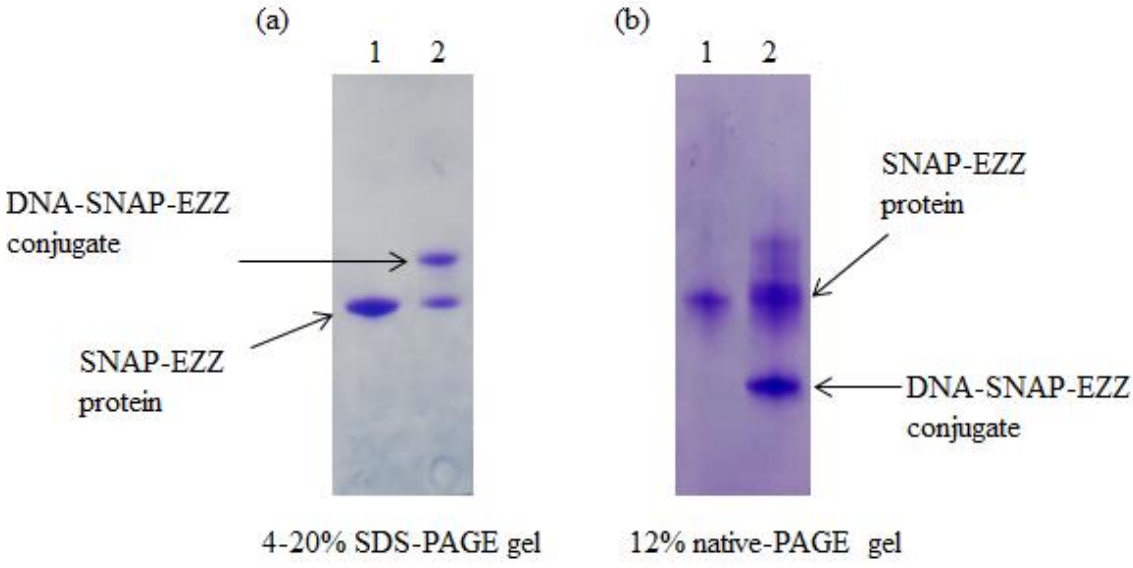

Figure 2.6. Mobility of EZZ-SNAP-DNA conjugates on 4-20% SDS-PAGE (A) and 15% native PAGE (B) gel electrophoresis. The gels were stained with CBB dye. Lanes 1. SNAP-EZZ protein only. Lanes 2. EZZ-SNAP-DNA conjugates.

2.3.2. EZZcys-DNA conjugates

EZZcys-DNA conjugates were synthesized by the reaction between thiol-modified EZZcys protein with maleimide-modified DNA at 1:10 molar ratios between protein and DNA. The product was confirmed by 4-20% SDS-PAGE gel under denaturing conditions. The samples were added with SDS loading dye and heated at 95°C for 5 minutes and cooled down to room temperature before loading. The gel was run in Tris-Glycine SDS running buffer, at 250 volts, at room temperature for 30 minutes. The gel was stained with Coomassie Brilliant Blue (CBB) R-250 staining solution for 10 minutes and de-stained overnight. Figure 2.7 shows that EZZcys-DNA conjugates in lane 2 with higher molecular weight migrated slower than the EZZcys protein only in lane 1.

Figure 2.7. Confirmation of EZZcys-DNA conjugates on 4-20% SDS-PAGE gel electrophoresis. 1. EZZcys protein only. 2. EZZcys-DNA conjugates.

2.3.3. GFP-DNA conjugates

Glycine-modified DNA (pG-DNA) conjugates were needed to serve as an amine nucleophile in sortase reactions for GFP-DNA conjugation. pG-DNA conjugates were obtained by a thiol-to-maleimide coupling reaction between thiol-modified polyglycine (pG) peptide and maleimide-modified DNA. The product was confirmed with 3% agarose gel electrophoresis in 1x TAE buffer (40 mM Tris-acetate and 1 mM EDTA with a pH of 8.3) at 120 volts for 50 minutes (Figure 2.8). The gel was stained with GelRed dye and imaged with the Kodak Imaging Station 4000R.

After pG-DNA was formed, it was reacted with LPETG-tagged GFP protein and sortase A enzyme. SrtA enzymes recognized the LPETG sequence on GFP protein and cleave it between T and G position to form an immediate GFP-sortase through a thiolester bond. The amine group at N-terminal of pG-DNA then acted as a nucleophile to attack the GFP-sortase intermediates and replace the thiolester bond with a peptide bond to form the GFP-DNA final products. First, different components were mixed to confirm that the final products were formed through SrtA enzymatic catalysis. In addition, the literature gives conflicting conditions for performing sortase reactions. Some reports have used very high concentrations of sortase (50 μM) [cite] while others recommended very low concentrations (50 nM – 1 μM) [cite]. Therefore, different molar ratios between enzymes, proteins and DNA were investigated to define the best reaction condition (Table 2.3) in this particular case. Figure 2.9 showed the results of forming GFP-DNA conjugates using the catalysis of the SrtA enzyme. SrtA, GFP and DNA were represented by “S”, “G”, and “D”, respectively. As expected, higher concentrations of SrtA enzymes gave higher yields. On the contrary, higher

concentrations of pG-DNA did not improve the coupling efficiency at all, in contrast to most of the literature, which recommends using three to five times more DNA than proteins. Unfortunately, due to the limit of pG-DNA amount available, I could not investigate the effects of using much higher excess of DNA vs. protein amounts, for example, five to ten fold excess. However, with the GSD4 condition (Table 2.3) which utilized 1:3:1 molar ratio between GFP:SrtA:DNA, the yield of GFP-DNA was obtained at about 50% yield based on protein, which is as high as literatures reported. Normally, the yield of sortase reactions between proteins and proteins or protein and small molecules would be higher (about 80%). However, DNA is much larger than small molecules, and highly negatively charged which might cause an internal ionic reaction between peptide backbone and phosphate backbone of DNA. Thus, this reduced the availability of the amine group of glycine for the ligation. After comparing the conditions in Table 2.3, I decided to choose the GSD4 condition as the standard for making GFP-DNA conjugates.

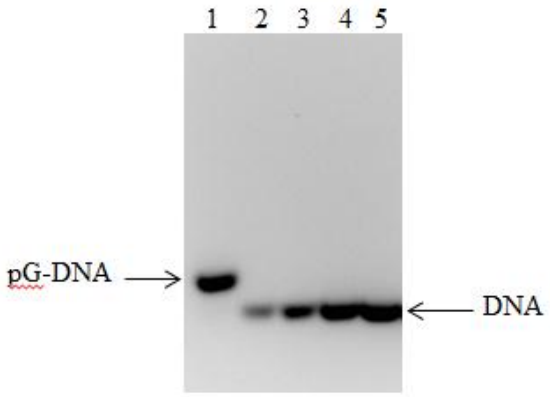

Figure 2.8. Confirmation of pG-DNA conjugates. 1. 140 pmol of peptide-DNA after Ni-NTA beads purification. 2-5. 40, 80, 160, and 240 pmol of DNA, respectively.

Table 2.3: Summary of sortase reaction conditions

Samples	S	D	G	GS	DS	GD	GSD1	GSD2	GSD3	GSD4
GFP (μM)			5	5		5	5	5	5	5
Sortase (μM)	5			5	5		1.7	5	5	15
pG-DNA (μM)		5			5	5	5	15	5	5
molar ratios	1	1	1	1:1	1:1	1:1	1:1/3:1	1:1:3	1:1:1	1:3:1

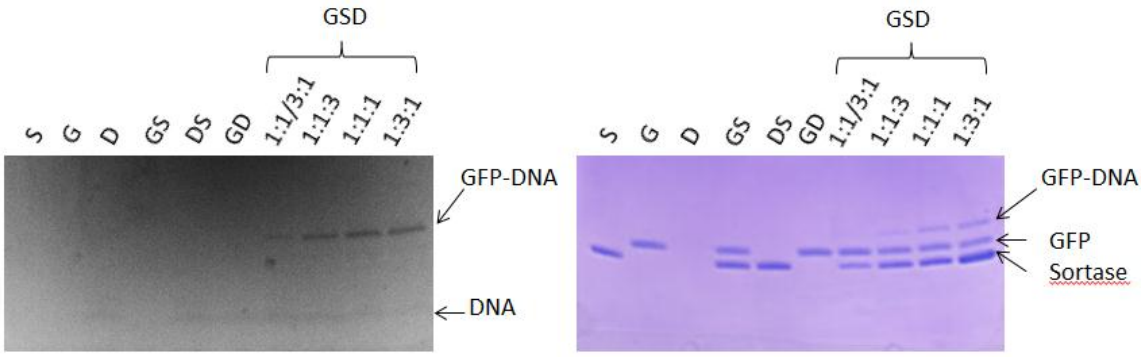

Figure 2.9. Synthesis of GFP-DNA conjugates using SrtA. All samples were boiled at 95°C for 5 minutes in SDS loading buffer before running 4-20% SDS-PAGE gel electrophoresis at 250 volts for 30 minutes. S. Sortase only. G. GFP only. D. pG-DNA only. GS. GFP + Srt A. DS. DNA + Srt A. GD. GFP + pG-DNA. GSD. GFP + Srt A + pG-DNA at different molar ratios. GFP-DNA conjugates with larger molecular weights would migrate slower on SDS-PAGE gel, compared to individual components. Higher concentrations of SrtA gave better yields of forming GFP-DNA conjugates while higher concentrations of pG-DNA did not substantially improve the yield.

2.4. Conclusions

In conclusion, three methods (utilizing the SNAP tag, sulfo-SMCC, and sortase A enzyme) were successfully used to obtain monovalent protein-DNA hybrid materials. The efficiency of conjugation was high, about 50% in the case of sortase, up to 80-90% in the case of SNAP tag and sulfo-SMCC. However, there are still many disadvantages for each method. For example, the SNAP tag method introduces a large tag (20kDa protein) beside the target proteins. Sulfo-SMCC only works for 1:1 conjugation when the target proteins do not contain cysteine amino acid in the sequences, which is very rare. Sortase A requires an additional conjugation step of pG-DNA products which is relatively low yield by now and requires further optimization. In addition, all of the described methods required multiple steps of modifications and purification of both proteins and DNA.

Unlike multivalent protein-DNA conjugation methods, which are more straightforward and involve fewer steps, monovalent conjugation methods face many challenges. The most significant disadvantage for all monovalent protein-DNA conjugation methods is probably the requirement for pre-modifications of the proteins and DNA. Proteins have to be re-cloned to add functional groups or tags, which is not always convenient or possible. DNA also needs to be modified with suitable functional groups to be able to react with proteins. Therefore, finding a simple (ideally single step) reaction for the protein-DNA conjugation is very desirable, but still a big challenge for chemists and biochemists. However, despite of these disadvantages, the current status of protein-DNA conjugation technology is still more than sufficient for creating exciting new protein-DNA hybrid materials with great potential, particularly

for the applications in protein detection and drug delivery.

References:

1. Nilsson, B. *et al*. A synthetic IgG-binding domain based on staphylococcal protein A. *Protein Eng.* **1**, 107-13.

2. Jin, T. *et al*. Antibody-protein A conjugated quantum dots for multiplexed imaging of surface receptors in living cells. *Mol. Biosyst* **6**, 2325-2331 (2010).

3. Mazzucchelli, S. *et al*. Single-domain protein A-engineered magnetic nanoparticles: toward a universal strategy to site-specific labeling of antibodies for targeted detection of tumor cells. *ACS Nano* **4**, 5693-5702 (2010).

4. Kuhara, M., Takeyama, H., Tanaka, T. & Matsunaga, T. Magnetic Cell Separation Using Antibody Binding with Protein A Expressed on Bacterial Magnetic Particles. *Anal. Chem.* **76**, 6207-6213 (2004).

5. Keppler, A. *et al*. A general method for the covalent labeling of fusion proteins with small molecules in vivo. *Nat. Biotechnol.* **21**, 86-89 (2003).

6. Keppler, A., Arrivoli, C., Sironi, L. & Ellenberg, J. Fluorophores for live cell imaging of AGT fusion proteins across the visible spectrum. *BioTechniques* **41**, 167-70, 172, 174-5 (2006).

7. Jansen, L. E., Black, B. E., Foltz, D. R. & Cleveland, D. W. Propagation of centromeric chromatin requires exit from mitosis. *J. Cell Biol.* **176**, 795-805 (2007).

8. Maurel, D. *et al*. Cell-surface protein-protein interaction analysis with time-resolved FRET and snap-tag technologies: application to GPCR oligomerization. *Nat. Methods* **5**, 561-567 (2008).

9. Carroll, C. W., Silva, M. C., Godek, K. M., Jansen, L. E. & Straight, A. F. Centromere assembly requires the direct recognition of CENP-A nucleosomes by CENP-N. *Nat. Cell Biol.* **11**, 896-902 (2009).

10. Hoskins, A. A. *et al*. Ordered and dynamic assembly of single spliceosomes. *Science* **331**, 1289-1295 (2011).

11. Jongsma, M. A. & Litjens, R. H. Self-assembling protein arrays on DNA chips by auto-labeling fusion proteins with a single DNA address. *Proteomics* **6**, 2650-2655 (2006).

12. Sielaff, I. *et al*. Protein function microarrays based on self-immobilizing and self-labeling fusion proteins. *Chembiochem* **7**, 194-202 (2006).

13. Kindermann, M., George, N., Johnsson, N. & Johnsson, K. Covalent and selective immobilization of fusion proteins. *J. Am. Chem. Soc.* **125**, 7810-7811 (2003).

14. Engin, S. *et al*. Benzylguanine thiol self-assembled monolayers for the immobilization of SNAP-tag proteins on microcontact-printed surface structures. *Langmuir* **26**, 6097-6101 (2010).

15. Meyer, R. & Niemeyer, C. M. Orthogonal protein decoration of DNA nanostructures. *Small* **7**, 3211-3218 (2011).

16. Sacca, B. *et al*. Orthogonal protein decoration of DNA origami. *Angew. Chem. Int. Ed Engl.* **49**, 9378-9383 (2010).

17. Johnsson, N. & Johnsson, K. Chemical tools for biomolecular imaging. *ACS Chem. Biol.* **2**, 31-38 (2007).

18. Tirat, A., Freuler, F., Stettler, T., Mayr, L. M. & Leder, L. Evaluation of two novel tag-based labelling technologies for site-specific modification of proteins. *Int. J. Biol. Macromol.* **39**, 66-76 (2006).

19. Daniels, D. S. *et al*. Active and alkylated human AGT structures: a novel zinc site, inhibitor and extrahelical base binding. *EMBO J.* **19**, 1719-1730 (2000).

20. Clancy, K. W., Melvin, J. A. & McCafferty, D. G. Sortase transpeptidases: insights into mechanism, substrate specificity, and inhibition. *Biopolymers* **94**, 385-396 (2010).

21. Huang, X. *et al*. Kinetic mechanism of Staphylococcus aureus sortase SrtA. *Biochemistry* **42**, 11307-11315 (2003).

22. Cossart, P. & Jonquières, R. Sortase, a universal target for therapeutic agents against Gram-positive bacteria? *Proceedings of the National Academy of Sciences* **97**, 5013-5015 (2000).

23. Popp, M. W., Antos, J. M. & Ploegh, H. L. Site-specific protein labeling via sortase-mediated transpeptidation. *Curr. Protoc. Protein Sci.* **Chapter 15**, Unit 15.3 (2009).

24. Marraffini, L. A., Dedent, A. C. & Schneewind, O. Sortases and the art of anchoring proteins to the envelopes of gram-positive bacteria. *Microbiol. Mol. Biol. Rev.* **70**, 192-221 (2006).

CHAPTER 3: CHARACTERIZATIONS OF PROTEIN-DNA CONJUGATE

3.1. Introduction

The main purpose of this chapter is to confirm that the protein and DNA are still functional after their conjugation. To confirm the DNA function, the DNA linker of the ESD conjugate was hybridized with its complementary sequence of the DNA nanobarcodes to form EZZ-SNAP-DNA (ESD) nanobarcodes. As discussed in the introduction chapter, DNA nanobarcodes have been developed in the previously-published works in our lab [1] and successfully used to detect DNA targets with a detection limit at 620 attomole. The barcodes were built based on the ratios of two fluorescent dyes, red and green colors which corresponds to Alexa 546 (Ex= 556 nm and Em= 573 nm) and Alexa 488 (Ex= 495 nm and Em= 519 nm) dyes, respectively, but is independent of the labeled positions. Therefore, the biggest advantage of this system is that it only requires green and red excitation and filter channels to resolve the differences between the DNA nanobarcodes. Theoretically, the coding capacity (C) of DL-DNA structures was determined by the number of colors (L) and the number of labeled positions (P) and was calculated by the formula, $C=(P+L-1)!/P!(L-1)!$. However, in this particular case when using only two (red and green), $C=(P+1)!/P!$. As a demonstration for multiplexed detection of proteins using DNA nanobarcodes in the next chapter, I only used the simplest barcode system which was built from just Y-shaped DNA and gave 3 different color ratios: R_2G_0, R_0G_2, and R_1G_1. Here, "R" represents the red dye, and "G" represents the green dye, and the number corresponds to the number of red and green dyes used in the nanobarcodes.

In addition, two methods were used to confirm the binding of EZZ protein to IgG antibodies. The first method was based on Streptavidin-coated polystyrene beads, and the fluorescence signal was detected from a fluorescence microscope. This bead-based format was also considered for its potential detection applications using ELISA, microarrays, or flow cytometer-based approaches. The second method was conducted on PVDF membrane as a dot blotting technique. This membrane-based format could potentially be used for 1D or 2D western blotting applications for the detection of proteins as well. Unfortunately, there were not enough signal generated from the conventional dot blotting method, using a blotting device such as the Bio-Dot Microfiltration Apparatus (BioRad, Hercules, CA), to be detected from a digital camera under UV exposure, unless a large amount of IgG antibodies and ESD nanobarcodes were used (at least 100 pmol). Therefore, in order to amplify the fluorescent signal and use a much lower volume (0.5-1 µl) and amount (0.5-1 pmol) of target, I designed a miniaturized, fast, and simple dot blot method which also reduced the time required for the blotting procedure to 5-10 minutes rather than three hours as in the conventional approach.

The combination of DNA nanobarcodes and different IgG binding generated a library of IgG nanobarcodes which were suitable for multiplexed protein detection. However, would the new configuration of IgG nanobarcodes affect the binding ability and efficiency of IgG antibodies due to steric hindrance of the ESD nanobarcodes? To answer that question, the IgG antibody competitive assay was conducted to prove that binding to ESD nanobarcodes did not affect the binding efficiency of IgG antibodies.

3.2. Materials and methods

3.2.1. DNA nanobarcodes formation

All oligonucleotides were commercially synthesized by Integrated DNA Technologies (Coralville, Iowa). Only fluorescent-labeled sequences were HPLC purified, and the rest were purified by standard desalting. Sequences from Table 3.1 were derived from previously published works.[1]Without further purification, the oligonucleotides were dissolved in TE buffer (10 mM Tris, pH=8.0, 1 mM ethylenediaminetetraacetic acid (EDTA)) with a final concentration of 100 μM. Y-DNA was synthesized by mixing the three oligonucleotide components Y_a, Y_b, and Y_c at a molar ratio of 1:1:1 in annealing buffer (10 mM Tris, pH 8.0, 1 mM EDTA, and 50 mM NaCl) with a final concentration of 10 μM for each oligonucleotide. The number of Y_a or Y_b with "R" and "G" defined the color ratios of the DNA nanobarcodes. For examples, R_1G_1-DNA nanobarcode could be formed with Y_{aR}, Y_{bG}, and Y_c_antilinker 1, or with Y_{aG}, Y_{bR}, and Y_c_antilinker 1; both would give the same outcome. The R_2G_0-DNA nanobarcode was formed with both Y_{aR} and Y_{bR}, and Yc_antilinker 1, and similarly, the R_0G_2 -DNA nanobarcode was formed with both Y_{aG} and Y_{bG}, and Yc_antilinker 1. The hybridization was performed with the annealing program shown in Table 3.2 using a thermo-cycler from Eppendorf AG (Hamburg, Germany).

3.2.2. DNA hybridization confirmation (ESD nanobarcodes formation)

The formation of ESD nanobarcodes was very simple, requiring only a single step of simple mixing. EZZ-SNAP-DNA (ESD) conjugate was mixed with R_2G_1-, R_0G_2-, R_1G_1-DNA nanobarcodes at a 1:1 molar ratio at room temperature for an hour

to form R_2G_0-, R_0G_2-, and R_1G_1-labeled ESD nanobarocodes. The products were confirmed with a 4-20% native PAGE gel, and purified by a Sephacryl S-200 HR gel filtration column at flow rate of 0.15 ml/min.

Table 3.1: Sequences of oligonucleotides for fluorescent-labeled Y-DNA

Name	Modification	Sequences (from 5' to 3')
Y_{aR}	5'-Alexa 546	TGGATCCGCATGACATTCGCCGTAAG
Y_{bR}	5'-Alexa 546	CTTACGGCGAATGACCGAATCAGCCT
Y_{aG}	5'-Alexa 488	TGGATCCGCATGACATTCGCCGTAAG
Y_{bG}	5'-Alexa 488	CTTACGGCGAATGACCGAATCAGCCT
Y_c_anti linker 1	None	AGGCTGATTCGGTTCATGCGGATCCACATT CGACGACGTTGACGTA

Table 3.2: Annealing program for Y-DNA formation

	Control	Block
	Lid=105^{o}C	
	Wait	Auto
Step 1:	95^{o}C	5 minutes
Step 2:	75^{o}C	2 minutes
Step 3:	60^{o}C	2 minutes
Step 4:	60 ^{o}C	30 seconds
	Temperature -0.5 ^{o}C	
Step 5:	go to step 4	repeat 80 times
Step 6:	Hold	4^{0C}

3.2.3. IgG binding confirmation

a. Bead-based confirmation

The IgG antibodies were biotinylated using the EZ-Link Sulfo-NHS-Biotin and Biotinylation Kits (Thermo Scientific, Rockford, IL) before immobilization onto 10 µm-size Streptavidin polystyrene beads (Bangs Laboratories, Inc., Fishers, IN). The IgG-immobilized beads were washed with 1x PBS, pH 7.4 three times before adding ESD nanobarcodes to 400 nM final concentration. The beads were gently rotated at room temperature for two hours, and washed with 1x PBS, pH 7.4 three times again before taking the images with the Olympus BX61 fluorescence microscope.

b. Membrane-based confirmation

The Low Fluorescence PVDF Transfer Membrane (Thermo Scientific, Rockford, IL) was cut approximately to 0.5 inch x 2.0 inch in size. Each dot was wet with 10 µl of methanol before spotting with 0.5 µl of 60 fmol of IgG antibody, using 10 µl round gel tips (USA Scientific, Ocala, FL) to obtain 250 µm diameter dots. The membrane was wet with 200 µl of methanol again before blocking with 500 µl of 5% skim milk in TBST blocking buffer (50 mM Tris-HCl, pH 7.4, 150 mM NaCl, and 0.005% Tween 20) in a 5ml clear glass dram vial for 5 minutes. ESD nanobarcodes were added into the samples to 50 nM final concentration. The membrane was incubated at room temperature for 4-6 hours before washing with TBST blocking buffer 3 times, and imaged with an Olympus BX61 fluorescence microscope after drying.

3.2.4. IgG antibody competitive assay

6His-tagged sortase protein was used as the antigen, and anti-His IgG antibody (mouse, monoclonal IgG antibody) without labeling was used as the competitor of the R_2G_0- labeled anti-His IgG nanobarcode in the assay. The samples were compared by looking at the fluorescence intensity of the antigen dots in dot blotting format as described above. The experiment was set up as follows: Three sets of samples were prepared, and each set of samples contained 4 dots of 1 pmol antigen and 2 dots of 1 pmol GAPDH protein as controls. Set 1 was labeled with 2.5 pmol of normal anti-His IgG (no label), set 2 was labeled with 2.5 pmol of R_2G_0-labeled anti-His IgG (red label), and set 3 was labeled with 2.5 pmol of R_2G_0- labeled anti-His IgG and 2.5 pmol of anti-His IgG together. These samples were incubated at room temperature for 6 hours before washing and imaging with an Olympus BX61 fluorescence microscope after drying.

3.3. Results

3.3.1. DNA nanobarcodes

Figure 1 shows a schematic drawing of the R_1G_1_DNA nanobarcode, which contains one red dye and one green dye on two arms of the Y-DNA, while 2R0G_ and 0R2G_Y-DNA would have two red or two green dyes on the Y-DNA, respectively. The third arm of the Y-DNA contains a 20-nt sticky end, which is complementary to the ssDNA sequence of DNA-protein conjugate.

Fluorescent-labeled Y-DNA samples were confirmed by 3% agarose gel (SeaKem® LE Agarose, Lonza, Rockland, ME) in Tris-acetate-EDTA (TEA) buffer

(40 mM Tris, 20 mM Acetic Acid, and 1 mM EDTA, pH 8.0, Biorad, Hercules, CA) at 120 volts at room temperature for 50 minutes. The images were taken by a Kodak Imaging Station 4000R (Kodak, Rochester, NY) with red and green filters, and processed with ImageJ to obtain the overlay images. Figure 3.2 shows the Y-DNA nanobarcodes (lane 3-5) were fully formed with three strands of oligonucleotides compared to a partial Y-DNA with two strands (lane 2) and one strand of oligonucleotide (lane 1). Lane 3-4 also showed the clear distinction of colors from three nanobarcodes, which were comprised of two red, one red and one green, and two green dyes, respectively.

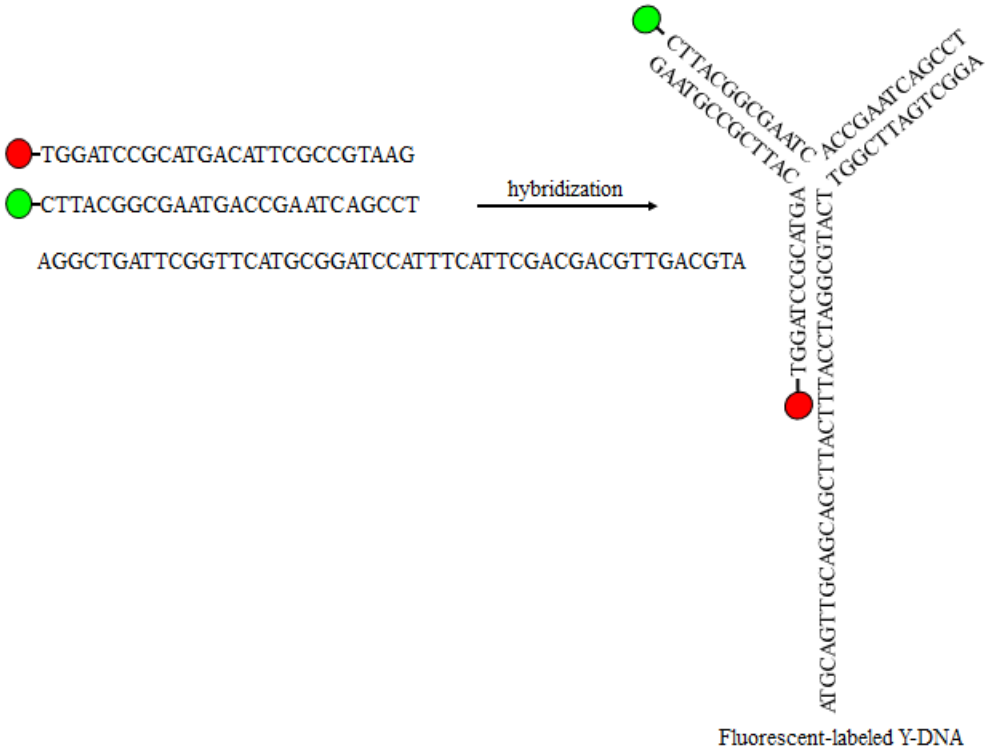

Figure 3.1. Schematic drawing of R_1G_1-Y-DNA anti linker 1, which contained one red dye from the Ya strand, one green dye from the Yb strand, and a complimentary sequence to protein-DNA conjugate from the Yc strand.

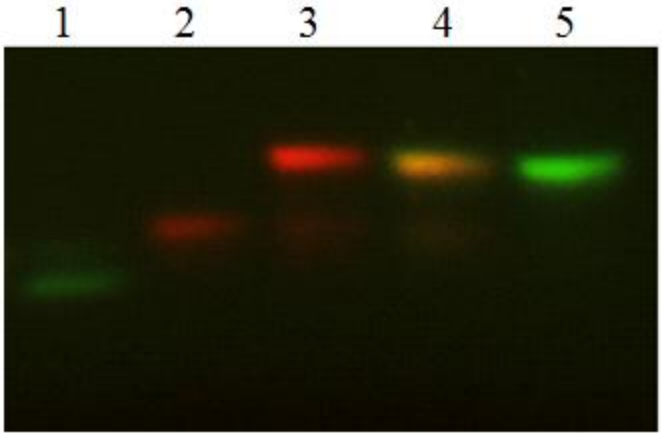

Figure 3.2. Gel images of fluorescent-labeled DNA nanobarcodes. 1. Y_{aG}. 2. Partial Y with Y_{aR} and Y_c. 3-5. R_2G_0-, R_1G_1-, and R_0G_2-DNA nanobarcodes, respectively.

3.3.2. Protein nanobarcodes formation

ESD nanobarcodes were formed by mixing ESD conjugates with different Y-DNA nanobarcodes at 1:1 molar ratio, and incubated at room temperature for about one hour. The products were confirmed with 4-20% native PAGE gel (Biorad, Hercules, CA) in 1x Tris/Glycine running buffer (25 mM Tris, 192 mM Glycine, pH 8.3) with 250 volts at room temperature for 60 minutes. Prior to staining, the gel was imaged by a Kodak Imaging Station 4000R (Kodak, Rochester, NY) with both red and green filters to capture only fluorescent-labeled products. It was then stained with GelRed dye (Biotium Inc., Hayward, CA) for one hour, and imaged again with Kodak Imaging Station 4000R to further visualize ESD conjugates and other DNA products such as DNA nanobarcodes and ESD nanobarcodes. Finally, the same gel was stained with Coomassie Brilliant Blue (CBB) R-250 staining solution for 10 minutes and de-

stained overnight to visualize the protein products, and the image was scanned with a DR-4010C Canon scanner.

Figure 3.3 confirms the formation of ESD nanobarcodes. Gels A, B, C correspond to the same gel but were imaged after staining with different dyes. Gel A was imaged before any staining, so only fluorescence-labeled products such as DNA nanobarcodes (lane 3, 4), and ESD nanobarcodes (lane 5-7) could be visualized. Gel B was stained with GelRed, a DNA staining dye, so any products containing DNA could be visualized, including the ESD conjugate (lane 2), the DNA nanobarcodes (lane 3, 4) and the ESD nanobarcodes (lane 5-7). At this point, it is clear that the ESD nanobarcodes were formed through the hybridization of the DNA linker with the R_2G_0-DNA nanobarcode. When mixing only the SNAP-EZZ protein and DNA nanobarcodes in lane 4, there were no shifted products as in lane 4-7 since there was no DNA linker in the SNAP-EZZ protein to bind with the R_2G_0-DNA nanobarcode in the mixture.

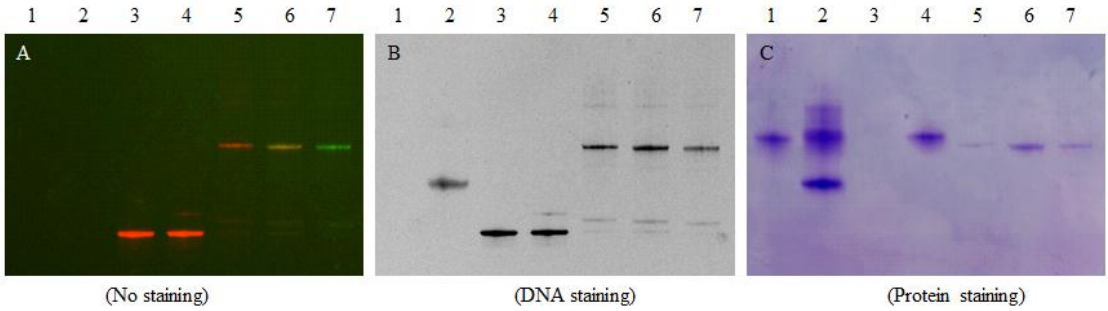

Figure 3.3. Characterization of ESD nanobarcodes on 4-20% native PAGE gel electrophoresis. 1. SNAP-EZZ protein. 2. ESD conjugate. 3. R_2G_0-DNA nanobarcode. 4. SNAP-EZZ protein with R_2G_0-DNA nanobarcode. 5-7. R_2G_0-, R_1G_1-, and R_0G_2-labeled ESD nanobarcodes, respectively.

3.3.3. IgG binding confirmation (IgG nanobarcodes detection)

After the ESD nanobarcodes were formed, they were used to confirm the ability to bind to IgG antibodies of EZZ domain. If after the conjugation, the EZZ protein had lost its function and could no longer bind to IgG antibodies, the ESD nanobarcodes would be useless. Therefore, this is an important characterization step since protein is normally less stable than DNA physically and chemically. The confirmation of IgG binding of ESD nanobarcodes was carried out by both bead-based and dot blotting-based protocols. The IgG antibodies used in this work were mostly rabbit polyclonal antibodies or carefully chosen from other species to have a strong binding affinity to EZZ protein, according to Table 2.1. Three rabbit polyclonal IgG antibodies, anti-Insulin IgG, anti-Glucagon IgG, and anti-PDX-1 IgG, were confirmed with ESD nanobarcodes on microbeads and PVDF membrane. As negative controls, mouse monoclonal anti-p53 IgG antibody, isotype IgG_1 antibody, and goat polyclonal anti-PDX-1 IgG antibody, which all have weak bindings to protein A, were used. The beads or dots were imaged with the Olympus BX61 fluorescence microscope with the same exposure time, and images were processed by ImageJ software with the same min-max value setting for all images.

- **Beads-based confirmation**

Figure 3.4 shows the results of ESD nanobarcodes binding to different IgG antibodies. Figure 3.4A illustrates the scheme of the bead-based IgG binding experiments. Biotinylated-IgG antibodies were immobilized onto 10 μm streptavidin beads, incubated with DNA nanobarcodes for 4-6 hours, washed to remove unbound DNA nanobarcodes, and imaged with the Olympus BX61 fluorescence microscope

using the 20x objective for both red and green channels. The images were processed with ImageJ software to obtain the overlay images. Figures 3.4B, 3.4C, and 3.4D show the strong binding of R_2G_0-, R_1G_1-, and R_0G_2-ESD nanobarcodes to rabbit polyclonal anti-glucagon, anti-PDX-1, and anti-insulin IgG antibodies, respectively. Mouse, monoclonal anti-p53 IgG antibody, subtype IgG1a have weak binding affinity to protein A; therefore, there was almost no fluorescence signal on the beads of figure 3.4E, compared to those of figure 3.4C which have the same R_1G_1-ESD nanobarcodes used. This result shows that EZZ protein from ESD nanobarcodes was fully functional, and was able to bind to IgG antibodies strongly and specifically.

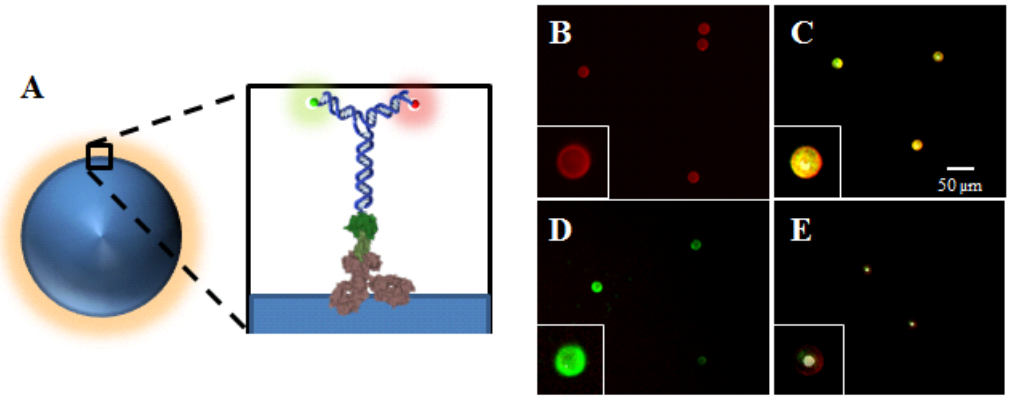

Figure 3.4. IgG nanobarcodes confirmation by beads. (A) Scheme illustrating microbead ratiometric color labeling. Beads were tagged with IgG antibodies then labeled with ESD nanobarcodes. (B) Anti-glucagon IgG was labeled with R_2G_0-ESD nanobarcode. (C) Anti-PDX-1 IgG was labeled with R_1G_1-ESD nanobarcode. (D) Anti-insulin IgG was labeled with R_0G_2-ESD nanobarcode. (E) Anti-p53 IgG1, which has weak binding to EZZ protein, was labeled with R_1G_1-ESD nanobarcodes as a negative control. The insets show magnified views of the beads.

❖ **Membrane-based (dot blotting) confirmation**

The IgG binding ability of ESD nanobarcodes was also confirmed using a dot blotting format. This also served to confirm that the fluorescence signals could be detected on PVDF membrane for protein detection applications later. Dots containing 60 fmol of different IgG antibodies were spotted onto a PVDF membrane, and incubated with different ESD nanobarcodes separately at 50 nM final concentration as described in scheme A of Figure 3.5. Figures 3.5B, 3.5C, and 3.5D are the images of dots showing the strong binding of anti-glucagon IgG labeled with R_2G_0-ESD nanobarcodes, anti-PDX-1 IgG labeled with R_1G_1-ESD nanobarcodes, and anti-insulin IgG labeled with R_0G_2-ESD nanobarcodes, respectively. Figure 3.5E and 3.5F are negative control samples of the weak binding between goat polyclonal anti-PDX-1 IgG with R_0G_2-ESD nanobarcode, and mouse monoclonal anti-p53 IgG, subtype IgG1a with R_2G_0-ESD nanobarcodes, respectively.

3.3.4. IgG antibody competitive assay

To further investigate the binding affinity of IgG nanobarcodes, an antibody competitive assay was conducted to check whether the binding efficiency of IgG antibodies were reduced or inhibited by the steric hindrance effects of ESD nanobarcodes or not. One pmol of His-tagged sortase protein and GAPDH protein was deposited on PVDF membrane as the targets and negative controls, respectively. The target proteins were separately incubated without fluorescence labeling (Figure 3.6A), with fluorescence labeling (Figure 3.6B), and with both (Figure 3.6C) antibodies in different vials to compare the binding ability and efficiency. GAPDH proteins (Figure

3.6D) were included in each strip to confirm that the fluorescence signals were only specific to the target proteins.

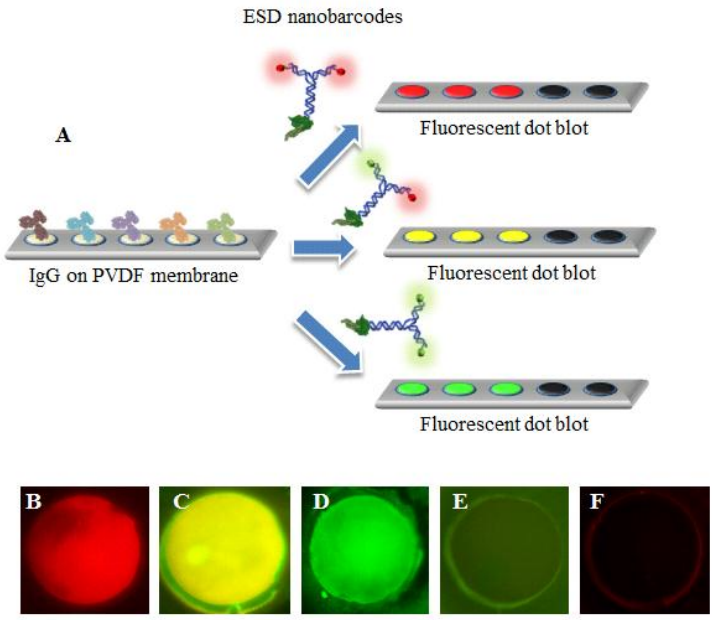

Figure 3.5. IgG nanobarcodes were confirmed by dot blotting. (A) Scheme illustrating dot blotting ratiometric color labeling. 60 fmol of IgG was dotted onto PVDF membrane then labeled with ESD nanobarodes. (B) Anti-glucagon IgG labeled with R_2G_0-ESD nanobarcode. (C) Anti-PDX-1 IgG labeled with R_1G_1-ESD nanobarcode. (D) Anti-insulin IgG labeled with R_0G_2-ESD nanobarcode. (E-F) Goat polyclonal anti-PDX-1 IgG and mouse monoclonal anti-p53 subtype IgG_1 labeled with R_0G_2- and R_2G_0-ESD nanobarcodes as negative controls, which have weak binding to EZZ protein,. The size of each dot is around 250 μm.

As a result, the control dots (D) and dots labeled with anti-His IgG (A) did not give any fluorescence signals, while the dots with fluorescence-labeled IgG antibodies (C and D) gave strong signals. The mean of fluorescence intensity was measured by ImageJ to quantify differences in the binding efficiency (Table 3.3). If binding to ESD nanobarcodes altered the binding ability of IgG antibodies, the fluorescence intensity in dot D would be less than that in dot C since R_2G_0-labeled IgG was competing with non-labeled IgG antibodies. However, the fluorescence intensity was similar in these cases, which indicated that IgG nanobarcodes still retained their original strong binding efficiency to target proteins at 10 nM concentration after the conjugation.

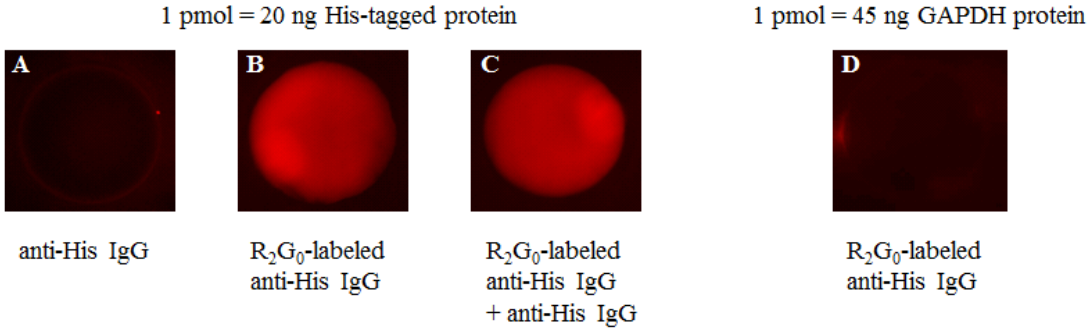

Figure 3.6. IgG competitive assay to confirm the binding efficiency of ESD nanobarcodes to IgG antibody. (A) His-tagged proteins were labeled with anti-His IgG antibodies. (B) His-tagged proteins were labeled with R_2G_0-anti-His IgG nanobarcodes. (C) His-tagged proteins were labeled with both anti-His IgG and R_2G_0-anti-His IgG nanobarcodes. (D) GAPDH proteins were labeled with R_2G_0-anti-His IgG nanobarcodes.

Table 3.3. Mean of fluorescence intensity for IgG competitive assay.

Dot	**Antigen**	**IgG labeling**	**Mean of fluorescence intensity**
A	His-tagged protein	anti-His IgG antibodies	200
B	His-tagged protein	R_2G_0-anti-His IgG nanobarcodes	2500
C	His-tagged protein	Both anti-His IgG antibodies and R_2G_0-anti-His IgG nanobarcodes	2700
D	GAPDH protein	R_2G_0-anti-His IgG nanobarcodes	200

3.4. Conclusions

The ESD conjugate could be used as a universal adapter for interfacing between the DNA and IgG antibody worlds since it has the ability to hybridize to R_2G_0-, R_1G_1-, and R_0G_2-DNA nanobarcodes and bind to IgG antibodies to generate a variety of fluorescence-labeled IgG nanobarcodes. The generation of a IgG nanobarcodes library, through a convenient and rapid process that involves only simple mixing, gives us the freedom to select suitable labels for detecting multiple targets simultaneously.

References

1. Li, Y. *et al*. Controlled assembly of dendrimer-like DNA. *Nat. Mater.* **3**, 38-42 (2004).

Chapter 4: APPLICATION 1 - Multiplexed Protein Detection

4.1. Introduction

As mentioned in the previous chapters, protein detection is one of the main applications of DNA-protein hybrid materials due to the advantages of having both DNA and protein moieties on one molecule. In this chapter, ESD conjugate, which was described in chapter 2 and 3, will serve as a universal adapter to interface between DNA nanobarcodes and IgG antibody to generate a IgG-based DNA nanobarcodes (IgG nanobarcodes) for multiplexed protein detection. In this approach, EZZ protein from ESD conjugate interacted with IgG antibodies as probes, and DNA nanobarcodes was used as the reporters, as illustrated in Figure 4.1. The IgG nanobarcodes can be generated through the hybridization process just by simply mixing all the components together at 1:1:1 molar ratio between DNA nanobarcodes, ESD conjugate, and IgG antibodies. This generated a library of IgG nanobarcodes suitable for multiplexed protein detection with the freedom of choosing the color labels rather than relying on the limited prelabeled primary IgG antibodies available on the market. Similar to using prelabeled primary antibody in protein labeling or detection, using IgG nanobarcodes to detect proteins requires fewer steps in staining and washing procedures, which is more convenient, and time efficient. Moreover, the IgG nanobarcode system can be used as a versatile platform for multiplexed protein detection in several different systems including microbead-based assay, dot-blotting, western blotting, and immunofluorescence.

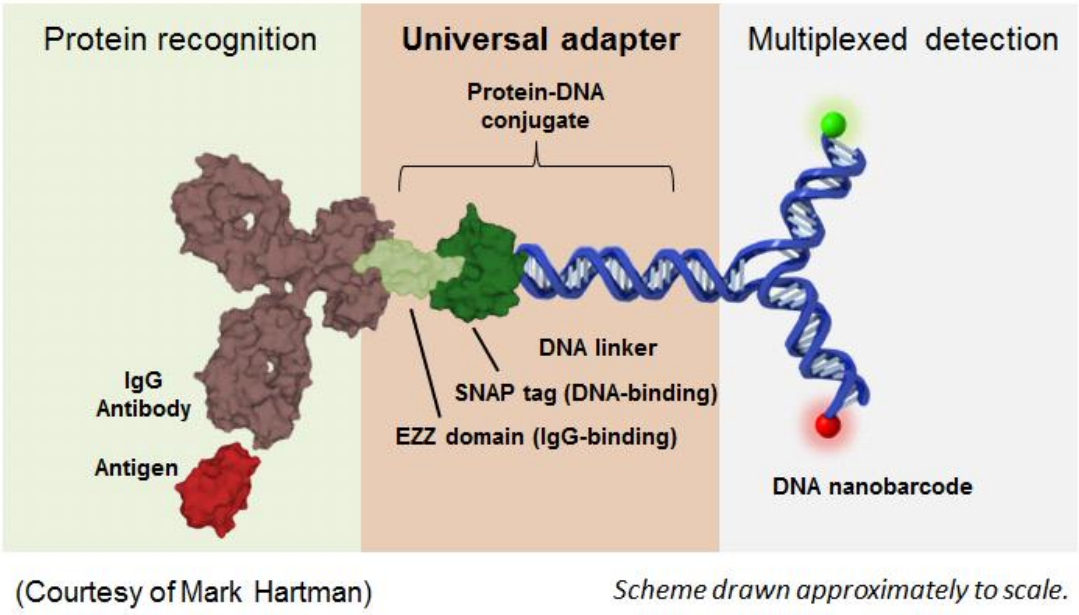

Figure 4.1. Scheme illustrating the generation of IgG nanobarcodes as a versatile platform for protein detection. The ESD conjugate served as a universal adapter for interfacing with a variety of both IgG antibodies and DNA nanobarcodes to generate a library of fluorescence-labled IgG antibodies for multiplexed protein detection.

4.2. Materials and Methods

4.2.1. Bead-based protein detection

First, the biotinylated-anti linker 1 oligonucleotide, which was complimentary to the DNA linker on the ESD conjugate, was deposited on 10 µm streptavidin polystyrene (PS) beads at a 10:1 molar ratio between the oligonucleotide and the binding capacity of the beads. The beads were rotated gently at room temperature for 30 min, and washed three times with TBST buffer (50 mM Tris-HCl, pH 7.4, 150 mM NaCl, and 0.005% Tween 20) after centrifuging at 1200 rcf for one minute to remove the free biotinylated-oligonucleotide. Second, the ESD conjugate was hybridized to anti linker 1-immobilized PS beads at a 1:1 molar ratio, and the beads were rotated gently at room temperature for one hour. Next, without washing, the anti-His IgG antibody was added to the ESD-modified beads at a 1:3 molar ratio between IgG antibody and ESD conjugate, and the beads were rotated gently at room temperature for overnight. The anti-His IgG-modified beads, after washing three times with TBST buffer, served as the capture probes for any protein targets containing a 6xHistidine tag.

For pure protein detection, for example GFP and Drosophila heat shock factor (HSF) proteins, 3 µl of 0.2 µM anti-His beads were incubated with a 0.5 µM final concentration of the protein targets. The samples were rotated gently at room temperature for 6 hours before washing three times with TBST buffer after centrifuging at 1200 rcf for one minute. For protein detection from lysate, for example Renilla Luciferase (RL) protein, 3 µl of 0.2 µM anti-His beads was incubated with 1 µl of 5 mg/ml lysate. The sample was rotated gently at room temperature for overnight

before washing five times with TBST buffer at the same conditions as above. For multiplexed protein detection, 3 µl of GFP, HSF, and RL beads were prepared separately as above and mixed together before labeling with three specific IgG nanobarcodes.

After the unbound targets were washed out with TBST buffer, corresponding specific fluorescent-labeled IgG nanobarcodes was added to the target beads at a 400 nM final concentration. R_2G_0-labeled anti GFP antibody, R_0G_2-labeled anti HSF antibody, and R_1G_1-labeled anti RL antibody were used to label GFP, HSF and RL targets, respectively. Note that with the flexibility of generating IgG nanobarcodes, we can use any fluorescence labels for any target by just mixing the IgG antibody with the desired ESD nanobarcode color ratio. After incubation for 6 hours, the samples were again washed three times with TBST buffer after centrifuging at 1200 rcf for one minute to remove the unbound labels. The samples were concentrated to 3 µl of beads which was used for imaging with the Olympus BX61 fluorescence microscope using the 20x objective.

4.2.2. Dot blotting

Similar to the dot blotting protocol described in the previous chapter, the Low Fluorescence PVDF Transfer Membrane (Thermo Scientific, Rockford, IL) was cut approximately to 0.5 inch x 2.0 inch in size, and wet with 10 µl of methanol before adding 0.5 - 1 µl of 0.5 – 1 pmol of protein target to each spot, using 10 µl round gel tips (USA Scientific, Ocala, FL) to obtain dots with 250 µm diameter. The membrane was wet with 200 µl of methanol before blocking with 500 µl of 5% skim milk in TBST blocking buffer (50 mM Tris-HCl, pH 7.4, 150 mM NaCl, and 0.005% Tween

20) in a 5ml clear glass dram vial for 5 minutes. Premixed IgG nanobarcodes (at 1:1 molar ratio between IgG antibodies and ESD nanobarcodes) were added to the samples at 20 nM final concentrations. For multiplexed protein detection, all IgG nanobarcodes were added to the samples at the same time. After 6 hours of incubation, the membranes were washed with TBST blocking buffer 3 times, and imaged with Olympus BX61 fluorescence microscope using the 10x objective after drying.

4.2.3. Western blotting (WB)

Protein samples (GFP and HSF proteins) were boiled at 95°C for 5 minutes before being loaded into a 4-20% Mini-PROTEAN TGX™ Precast gel (BioRad, Hercule, CA) and run with 1x SDS running buffer (250 mM Tris base, 192 mM Glycine, 0.1% SDS, pH 8.3) at 250 volts for 30 minutes. Protein samples on gel were transferred onto a low fluorescence PVDF membrane following a standard protocol for western blotting at 120V for 40 min. A prestained SeeBlue Plus 2 protein ladder (Invitrogen, Carlsbad, CA) was used as a marker to ensure proteins were transferred properly to the PVDF membrane. The membrane was then blocked with 15 ml of blocking buffer including 5% skim milk in TBST buffer (50 mM Tris-HCl, pH 7.4, 150 mM NaCl, and 0.005% Tween 20) for 5 minutes at room temperature. About 30 pmol of anti GFP IgG-DNA linker 1 (a mixture of anti GFP IgG + ESD conjugate at a 1:1 molar ratio) and 30 pmol of anti HSF-DNA linker 3 (a mixture of anti HSF IgG + EZZcys-DNA linker 3 at 1:1 molar ratio) were added into the blocking buffer. The membrane was incubated at room temperature for overnight. After washing three times with TBST buffer for 3 minutes, 5 µl of 1 µM of anti-linker 1-modified quantum dots 605 (red) and 5 µl of 1 µM anti-linker 3-modified quantum dots 525 (green) were

added into the TBST buffer to hybridize with the DNA linkers 1 and 3 of the IgG antibodies. The samples were incubated at room temperature for 1-2 hours before washing three times with TBST buffer again. The membrane was dried completely before being imaged with the Kodak Imaging Station 4000R with red and green filters, and the images were processed with ImageJ software.

4.2.4. Immunofluorescence

The pancreas tissues of sacrificed mice were fixed in 4% paraformaldehyde overnight and washed three times with 1x PBS buffer, pH 7.4 and soaked in 70% ethanol. The fixed tissues were then dissected. After deparaffinization, fixed tissue slides were steamed in 0.01M citrate buffer. After washing in 0.01M PBS (pH 7.2), 50 µl of blocking solution (1 mg/ml of salmon sperm single strand DNA (sssDNA) and 10% normal blocking rabbit serum in 5% BSA) was applied for one hour at room temperature in a humid chamber. Premixed IgG nanobarcodes were prepared by adding IgG antibodies with ESD nanobarcodes at 1:1 molar ratios, and incubating at room temperature overnight. Rabbit polyclonal anti-insulin, anti-glucagon, and anti-PDX-1 IgG antibodies (Santa Cruz Biotechnology, Santa Cruz, CA) were used in this work. One pmol of the corresponding IgG nanobarcodes was added to the samples in 50 µl of blocking buffer, and incubated in a humid chamber overnight at room temperature. After washing for three times in 1x PBS, the samples were mounted with ProLong® Gold antifade reagent (Invitrogen, Carlsbad, CA). Specimens were examined using the appropriate excitation wavelength for each fluorophore, and the images were taken with the Olympus BX61 fluorescence microscope using the 20x or 40x objectives.

4.3. Results

4.3.1. Multiplexed bead-based detection

Using a concept similar to ELISA, two different IgG antibodies, which recognized two different binding sites of an antigen, were used to detect a target protein. In this work, I used anti-His IgG antibody (Abcam, Cambridge, MA) as the first IgG antibody for all antigens, and chose the second IgG antibody specifically for each target protein. Figure 4.2A describes the general scheme of the bead-based protein detection strategy. Anti-His IgG-immobilized PS beads were used to bind protein targets before a second fluorescence-labeled IgG antibody (a complex of IgG antibody and ESD nanobarcodes) was added to label the beads. Anti-His IgG-immobilized PS beads were generated by mixing the ESD conjugate with DNA-modified PS beads (to form ESD beads) before they were bound to anti-His IgG antibody. Unlike direct biotinylated-IgG deposition on PS beads, using ESD beads enabled the generation of bead-based IgG antibodies with lower non-specific binding. EZZ protein specifically binds to the Fc region of IgG antibodies which prevented the non-specific binding between the first IgG antibodies and the unbound ESD nanobarcodes. As a result, in the absence of targets (Figure 4.2E), there was no fluorescence detected from the beads. When the targets were available, fluorescent beads were detected, either individually (Figures 4.2B-D) or together (Figure 4.2F).

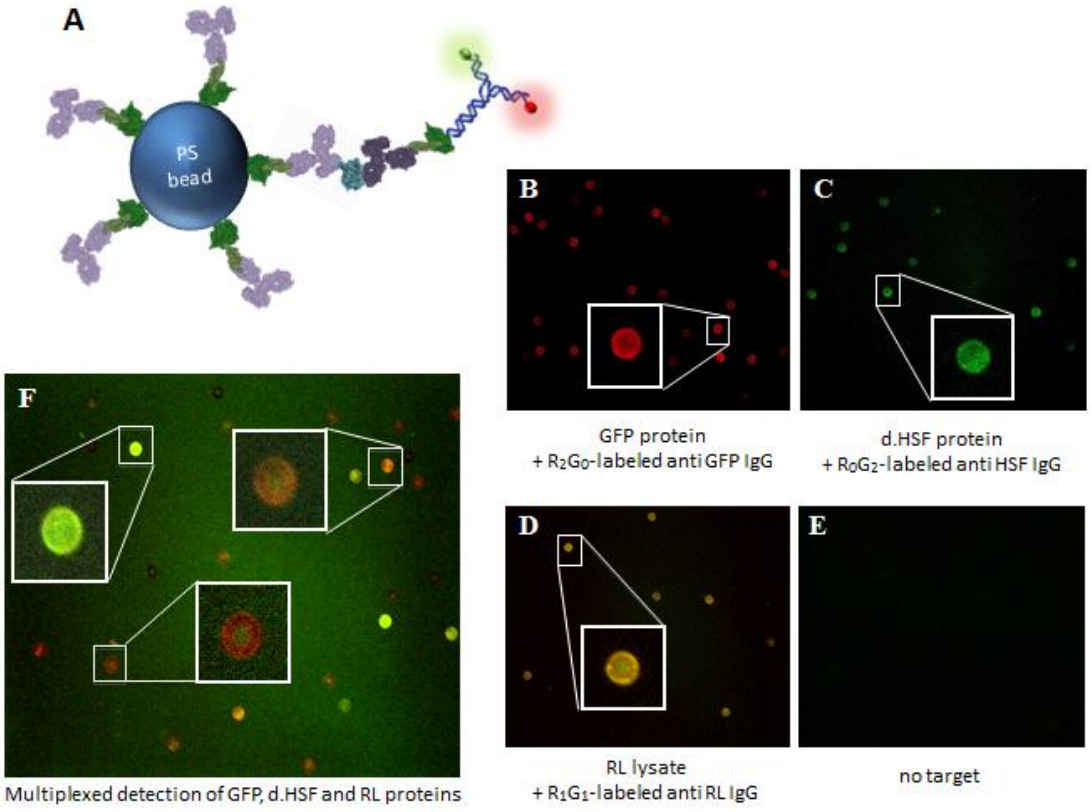

Figure 4.2. Multiplexed bead-based protein detection. (A) Scheme illustrating antigen detection using microbead labeling. Polysterene beads were tagged with the first IgG antibody which captured the antigen and then sandwiched with the second IgG nanobarcodes. (B) GFP protein target labeled with R_2G_0-labeled anti-GFP IgG antibody. (C) Drosophila heat shock factor (HSF) protein target labeled with R_0G_2-labeled anti-HSF IgG antibody. (D) Renilla Luciferase (RL) protein target labeled with R_1G_1-labeled anti-RL IgG antibody. (E) No target labeled with all three IgG antibodies used in samples B-D. (F) GFP, HSF, and RL protein targets labeled with R_2G_0-labeled anti-GFP, R_0G_2-labeled anti-HSF, and R_1G_1-labeled anti-RL IgG antibodies, respectively.

4.3.2. Multiplexed protein detection using a dot blotting technique

GFP, RL and HSF proteins were again used as the targets for dot blotting protein detection with IgG nanobarcodes. Different amount of target proteins, varying from 0.25 – 2 pmol, was spotted on low fluorescence PVDF membrane to give 250 µm protein dots. 20 nM of IgG nanobarcodes were used to detect the proteins on the membrane. For single protein detection (Figure 4.3), the minimum fluorescence signal that could be detected ranged from 0.25 pmol (for GFP and HSF proteins) to 0.5 pmol (for RL protein) amount of protein targets, corresponding to 7.5-20 ng of proteins. Sortase proteins were included as negative controls to confirm the specificity of the detection. The differences in sensitivity were due to the differences in binding affinity and efficiency between different antigens and antibodies; this was clearer in the multiplexed detection of proteins when all targets were present on the same membrane (Figure 4.4A), and incubated with all IgG nanobarcodes at the same time. The dots were imaged with the Olympus BX61 fluorescence microscope using the 10x objective with the same exposure times. Overlay images were prepared using ImageJ software with consistent brightness and contrast display settings. As shown in Figure 4.4, GFP showed much stronger binding and higher sensitivity compared to HSF and RL proteins. The signal was saturated at the 0.5 pmol amount of GFP protein while it was much weaker in the cases of 2 pmol of RL and 1 pmol of HSF proteins. Regardless of the big difference in fluorescence intensity of different targets, it is clear that multiple proteins could be detected simultaneously using this membrane-based system with IgG nanobarcode complexes.

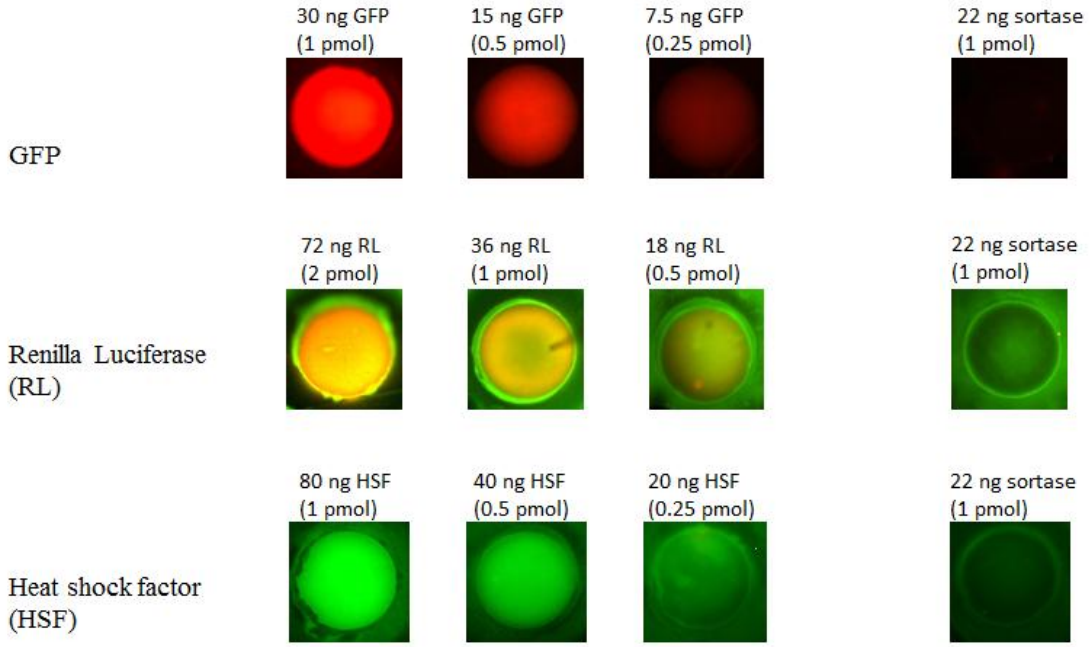

Figure 4.3. Protein detection using the dot blotting technique. The dot size is about 250 μm. Overlay images of the dots were achieved from the Olympus BX61 fluorescence microscope with the 10x objective using red, green channels. From top to bottom row, GFP protein was labeled with R_2G_0-labeled anti GFP IgG, RL protein was labeled with R_1G_1-labeled anti RL IgG, and HSF protein was labeled with R_0G_2-labeled anti HSF IgG antibodies. Sortase protein was used as negative controls. Different amounts of proteins were used to determine the limit of the detection. Depending on the binding affinity and efficiency, the detection limit was as low as 0.25 pmol (GFP and HSF proteins) or 0.5 pmol (RL protein), corresponding to 7.5-20 ng of proteins.

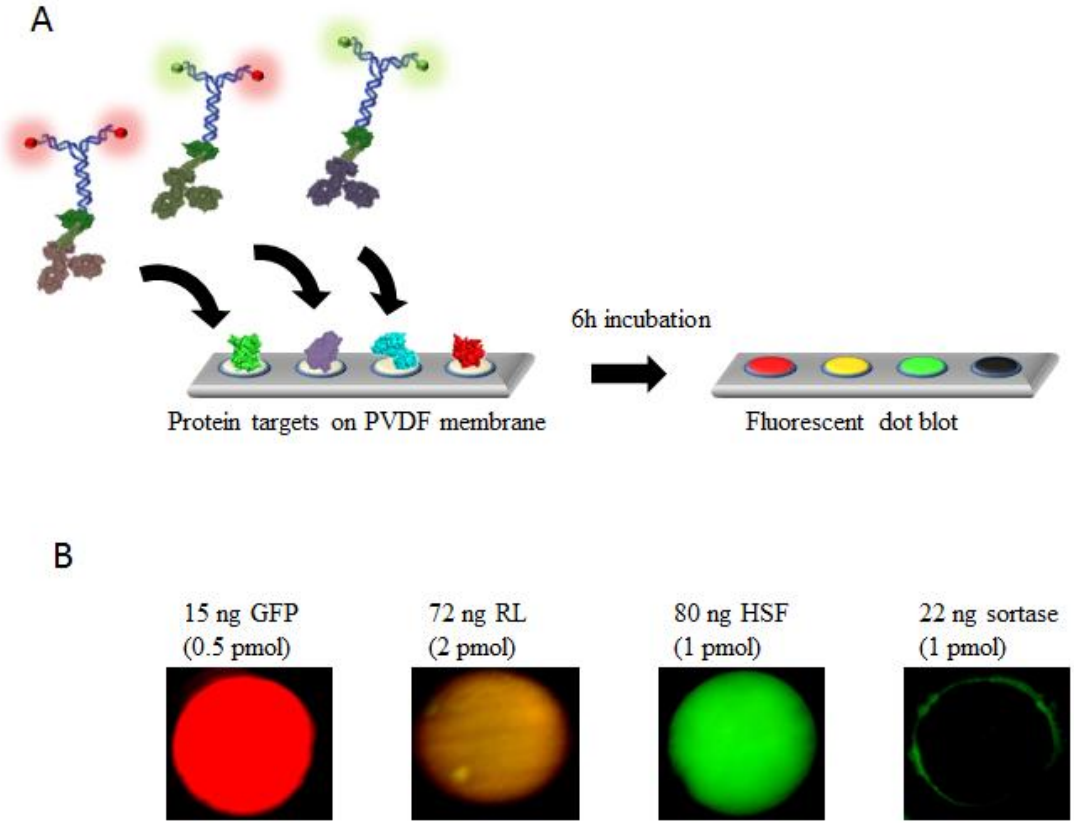

Figure 4.3. Multiplexed protein detection using the dot blotting technique. Each dot size is about 250 μm. A. Scheme illustrating the multiplexed protein detection. Different protein targets were spotted on the PVDF membrane and incubated with fluorescence-labeled IgG nanobarcodes to generate specific signals. B. Overlay images of the dots were achieved from the Olympus BX61 fluorescence microscope with the 10x objective using red, green channels. From left to right, GFP protein was labeled with R_2G_0-labeled anti GFP IgG, RL protein was labeled with R_1G_1-labeled anti RL IgG, HSF protein labeled was with R_0G_2-labeled anti HSF IgG antibodies, and sortase protein (which had no binding to the IgG antibodies) was used as a negative control.

4.3.3. Western Blotting (WB) detection

Although the dot blotting (DB) technique is fast, easy and simple to detect proteins, it requires pure proteins as the targets and is unable to detect a protein from a mixture of other proteins or from protein lysates. In contrast, WBhas the advantage of pre-separation of proteins on a PAGE gel before the proteins are transferred to a PVDF membrane, which helps to overcome this limit of the DB technique. In particular, using a 2D gel technique, the protein separation is even better due to the inclusion of a secondary separation based on the total number of charges of the proteins, in addition to the initial separation based on molecular weight differences. Thus, each protein will exist on the PVDF membrane as a single band for 1D-WB or a unique dot for 2D-WB.

Unfortunately, the fluorescence-labeled IgG nanobarcodes could not generate enough signal to be detected by the optical camera at the large scale typical for WB bands (about 0.5 cm x 0.1 cm)with low amounts of target (less than 50 pmol protein target, data not shown). Therefore, WB requires a much stronger signal to replace the fluorescence dyes of the IgG nanobarcodes in order to achieve more sensitive detection. Luckily, quantum dots are available with about 10 times stronger fluorescence intensity than fluorophores, and these quantum dots can be modified with DNA through the streptavidin-biotin interaction. Hence, a new strategy was developed for the detection of proteins using the WB technique, as described in Figure 4.4A. Proteins were transferred to a low fluorescence PVDF membrane and incubated with IgG-ESD conjugate. The unbound IgG was washed, and then DNA-immobilized quantum dots were added to specifically hybridize with the DNA linkers on the bound

IgG-ESD conjugate.

For the first attempt at using QDs for WB detection (Figure 4.4B), I used GFP and HSF as the targets which were labeled with QD 605 (red) and QD 525 (green), respectively. Although there are many types of quantum dots (QDs) available with a variety of emission spectra, I used two quantum dots (QD 525 and QD 605), with similar emission characteristics as Alexa 488 and Alexa 546 dyes, respectively, for WB detection due to the limited excitation and emission filters that were available. This emphasizes the simplicity of the DNA nanobarcode concept which requires only red and green dyes and filters to generate different color ratios for many distinct signals. Although it is not trivial and also requires a lot of purification steps, it is possible to create the monovalent quantum dots which contain a single DNA oligonucleotide per dot. These single DNA-modified quantum dots could be used as single dyes to replace the fluorescent dyes in the DNA nanobarcode system, mimicking the nanobarcode concept to generate a much more sensitive detection system. However, quantum dots are quite large, about 15 nm in size, which is a little bit bigger than Y-DNA (about 12 nm). Thus, replacing the fluorophores, small molecules of 20-100 atoms, with quantum dots would generate relatively giant complexes. This could introduce steric hindrance and reduce the binding efficiency of IgG antibodies to the protein targets, thus effectively reducing the sensitivity of the detection method. Therefore, the approach of replacing fluorophores with QDs to generate DNA nanobarcodes may not be a better alternative. However, for the WB application in particular, two different quantum dots could be sufficient to differentiate three, or more protein targets if we also consider the differences in sizes as an

indication for the target specificity.

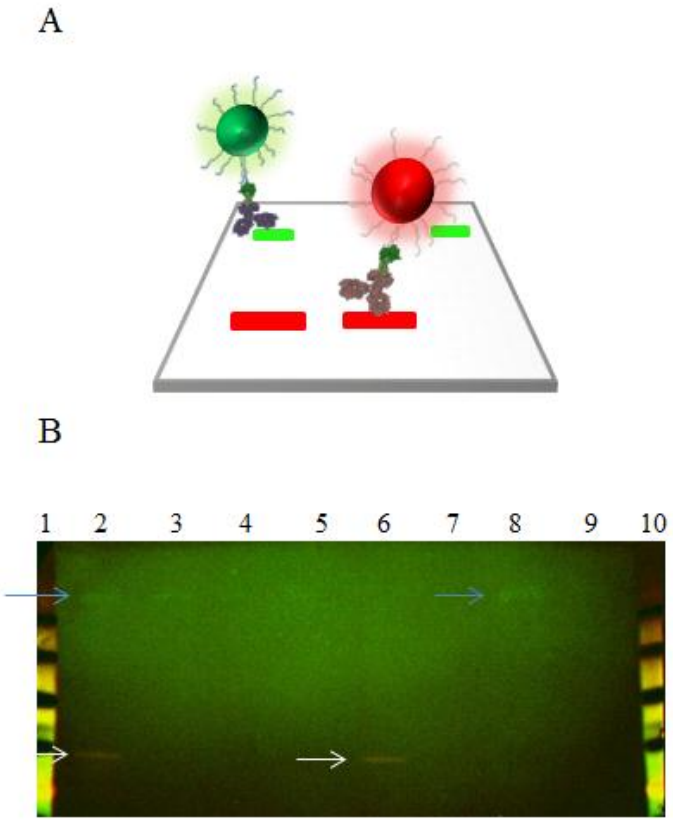

Figure 4.4. Multiplexed Western blotting. A. Scheme illustrating the strategy of using quantum dots (QDs) for western blotting (WB) detection. Protein samples were separated on PAGE gel before transferred to PVDF membrane which was incubated with IgG-ESD conjugate before DNA-immobilized QDs were added to generate signals. B. HSF, and GFP protein detection by QD 525 and QD 605, respectively. 1 and 10 are prestained SeeBlue Plus 2 protein ladders. 2-5. HSF and GFP proteins detection at 5, 2, 1, and 0.5 pmol, respectively. 6-7. GFP protein detection at 5 and 1 pmol, respectively. 8-9. HSF protein detection at 5 and 1 pmol, respectively.

4.3.4. Immunofluorescence

To further demonstrate the versatility of IgG nanobarcode system, immunofluorescence staining of the islets of mouse pancreas tissues was performed, using Insulin, Glucagon, and PDX-1 proteins as the protein targets. Insulin proteins are found in the beta cells, while glucagon proteins are located in the alpha cells surrounding the islets, and PDX-1 proteins are only present in the nuclei of the islets. Thus, this is an excellent system for demonstrating the multiplexed staining ability of IgG nanobarcodes. As shown in Figure 4.6, Insulin proteins were beautifully stained with three different R_2G_0-, R_1G_1-, and R_0G_2-labeled IgG nanobarcodes at 20 nM concentrations in one step. However, for Glucagon and PDX-1 protein targets, the staining efficiency was lower than for Insulin proteins, as shown in Figure 4.7 A and B. This is likely due to the lower specificity and binding efficiency of anti Glucagon and anti PDX-1 compared to anti Insulin IgG antibodies. To test this hypothesis, and also to explore an alternative approach, quantum dots were used as the labels instead of using the fluorescence-labeled DNA nanobarcodes. With the power of the confocal microscope, at least three or four different quantum dots with distinct excitation and emission wavelengths can be detected together. Three different quantum dots, QD 655 (red), QD 605 (orange) and QD 525 (green), were used to replace the R_2G_0-, R_1G_1-, and R_0G_2- DNA barcodes, respectively, to test if we could obtain improved signals. In addition, two different approaches were used, termed "one-step" and "two-step" approaches. For the one-step approach, DNA-immobilized QDs were hybridized directly to IgG-ESD conjugates before staining the samples. For the two-step approach, IgG-ESD conjugates were first incubated with the samples, and then the

unbound IgG was washed before it was labeled with DNA-immobilized QDs (similar to the WB protocol above). However, either with one-step or two-step approaches, only Insulin proteins were successfully labeled while Glucagon and PDX-1 did not give any signals at all. With the limit of IgG antibodies available due to the low efficiency of anti PDX-1 IgG antibody, we could only demonstrate the multiplexed immunofluorescence staining process with R_2G_0-labeled anti Glucagon IgG antibody and R_0G_2-labeled anti Insulin IgG antibody nanobarcodes together as shown in Figure 4.7 C. Clearly, Glucagon was stained with red fluorescence signal surrounding the islet, and Insulin was stained with green fluorescence signals inside the islet, which proved that our IgG nanobarcode system could be used for multiplexed immunofluorescence efficiently and specifically. These results confirmed that the IgG nanobarcode system can become a powerful, but simple and convenient tool not only for immunofluorescence staining, but also any IgG antibody-based detection system.

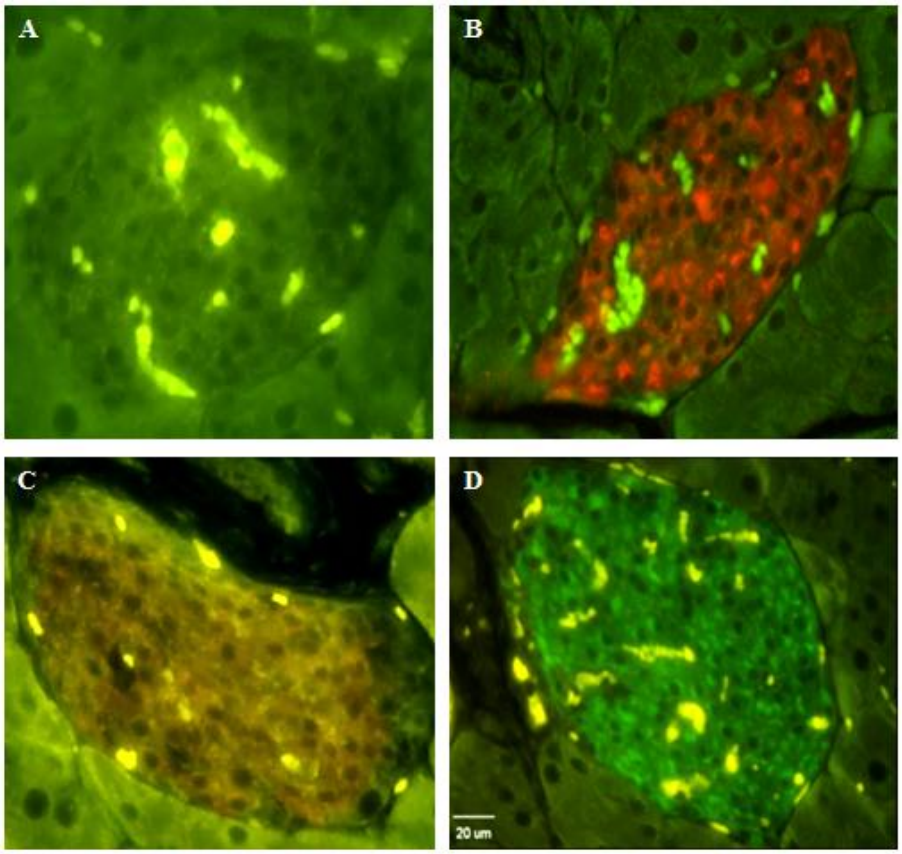

Figure 4.6. Immunofluorescence staining of mouse pancreas islets. A. Autofluorescence of a blank tissue without staining. B-D. Insulin-expressed islets stained with R_2G_0-, R_1G_1-, and R_0G_2-labeled anti Insulin IgG nanobarcodes, respectively.

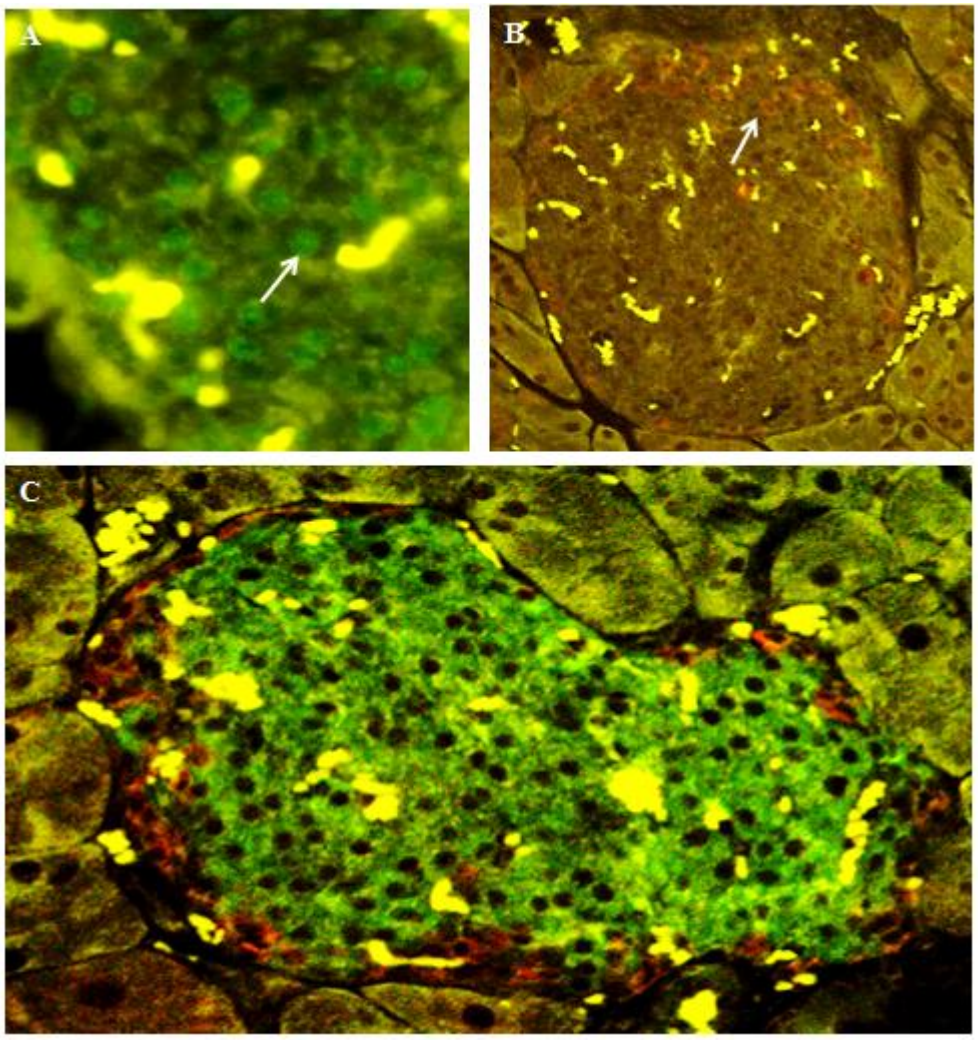

Figure 4.7. Immunofluorescence staining of mouse pancreas islets. A. PDX-1-expressed islet stained with R_0G_2-labeled anti PDX-1 IgG antibody nanobarcode. White arrows showed the representative green fluorescence signals inside the nuclei where PDX-1 proteins are located. B. Glucagon-expressed islet stained with R_2G_0-labeled anti Glucagaon IgG antibody nanobarcode. White arrows showed the representative red fluorescence signals from alpha cells surrounding the islets where glucagon proteins are expressed. C. Glucagon and Insulin-expressed islet stained with R_2G_0-labeled anti Glucagon IgG antibody (red) and R_0G_2-labeled anti Insulin IgG

antibody (green) nanobarcodes, simultaneously.

4.4. Conclusions

EZZ-SNAP-DNA conjugate was successfully developed as the universal adapter for interfacing both IgG antibody and DNA moieties, such as DNA nanobarcodes, or quantum dots, to generate a versatile IgG-based protein detection system which can be used in different systems; for example, bead-based assays, dot blotting, western blotting and immunofluorescence. Moreover, the system can be generated easily by simply mixing the components together without any chemical reactions involved. In particular, using ESD conjugate and DNA nanobarcodes to prelabel IgG antibodies, this helps avoidundesirable interspecies cross-activity between primary and secondary antibody pairs so that IgG antibodies from same species can be used together. This is a big advantage in multiplexed protein detection due to the limited availability of primary antibodies from different species. Also, the procedure requires fewer preparation steps, which is convenient and time efficient. However, since EZZ protein was engineered based on native protein A of *Staphylococcus aureus*, there are still IgG antibodies from some species that it cannot bind, especially from rat, goat, and sheep. However, with most of the IgG antibodies available from human, mouse, and rabbit, it is more than enough to choose appropriate IgG antibodies to perform multiplexed protein detection with this system. Furthermore, if necessary, EZZ protein can be easily replaced by protein G or protein A/G, which can bind to all IgG antibodies available, with the same concept.

Notably, although this work has focused on the use of DNA nanobarcodes, the DNA linker in this system is not limited to nanobarcodes but can be expanded to any

DNA-modified materials, such as quantum dots, nanoparticles, carbon nanotubes, etc. Therefore, the IgG based protein detection system is not limited to only fluorescence-based protein detection system, but is also applicable to other label-free methods, such as plasmon surface resonance based or Raman-spectroscopy-based methods, by utilizing the optical and electrical properties of nanoparticles and other materials. In conclusion, DNA-protein hybrid materials, as demonstrated here with the ESD conjugate, are a powerful platform for protein detection with the potential for high multiplexed capacity. However, in addition to these applications in protein detection, DNA-protein materials will also open a new direction as nanocarriers for protein delivery, as will be discussed in the next chapter.

Chapter 5: APPLICATION 2 - DNA-assisted Protein Intracellular Delivery System (DAPID system)

5.1. Introduction

Many diseases occur from alterations in the functions or overexpression of intracellular proteins. As a result, inhibiting those malfunctioned proteins or delivering their active forms to specific cells is an important goal for many medical applications, including cancer therapy, vaccination, regenerative medicine, and treating loss-of-function genetic diseases.[1-4] However, all current protein drugs target only the surface of the cells to trigger signaling pathways to affect the real targets downstream;[4, 5] and therefore, this is a relatively indirect way to correct the functioning of the cells. In order to achieve more direct responses from protein targets inside cells, protein intracellular delivery beyond surface delivery is essential.

Protein intracellular delivery has been intensively explored with many materials such as: cell penetrating peptide, proteins, peptide nucleic acid, lipids, polymers, and carbon nanotubes, quantum dots, and nanoparticles. However, no work has been done on the use of DNA for protein intracellular delivery, despite the excellent advantages offered by DNA such as controllability of size and structure, ability to interface with other chemical and biological groups, and its natural biocompatibility. DNA materials with the appropriate size, such as DNA spheres from photocrosslinker-modified building blocks, have shown the ability to enter the cells without DNA transfection reagents.[6-8] Hence, I would like to investigate the capability

of branched DNA that was previously developed in our lab, such as Y-DNA (Y) and G1 generation of DL-DNA (G1), as potential nanocarriers for protein intracellular delivery.

The original designs of Y-DNA and DL-DNA were such that each Y building block was linked to the previous ones in the same plane, and therefore, the structures were "flat" or 2D, which could be disadvantageous for cellular uptake. Therefore, I developed a different approach to form highly branched DNA scaffolds (e.g. D1 structure) using the hybridization of long palindromic sticky ends, instead of the ligation of short non-palindromic sticky ends in case of DL-DNA. The new approach could be able to generate "3D" DNA scaffolds due to the additional 10 nucleotide sticky ends at the 3'-end of the Y-based oligonucleotides, which "turned" each building block to different angles out of the plane of the previous Y-shaped structure. Also, there was no modification required to achieve this highly branched scaffold, unlike the phosphorylation modification required for DL-DNA, or the photocrosslinkable groups required for ABC monomers or DNA nanospheres. Moreover, this approach was more convenient, faster, and resulted in higher yield and tunable sizes of higher structures of DNA scaffolds, compared to the well-designed DL-DNA structures. However, the structures of the new DNA scaffolds were less precisely defined, and the sizes were not uniform.

First, different structures of branched DNA were investigated for cellular uptake before being selected as the carriers for proteins and IgG antibodies delivery, including Y, G1, D1, and others. The uptake efficiency was high with almost 100% of gated cells, whose contain positive fluorescence signals compare to negative controls

when analyzed with flow cytometry reader. However, we obtained only weak fluorescence signals from cells using confocal microscopy. To resolve this contradiction between flow cytometry and microscopy, we needed to find a way to increase uptake efficiency in order to see the fluorescence signals from microscope images. Since DNA was designed as the carrier to deliver proteins and IgG antibodies, we decided to use commercially available DNA transfection reagents to boost the uptake efficiency. As expected, these DNA transfection reagents, which have been developed to efficiently deliver genes and siRNA inside cells for more than 50 years, greatly enhanced the DNA-protein and DNA-IgG antibody intracellular uptake. For the first time, DNA transfection reagents were used to deliver proteins (Figure 5.1). This could provide a new route for protein intracellular delivery with great efficiency. Furthermore, our system can be easily extended to deliver multiple proteins and other biomarkers, as well as moieties beyond proteins including but not limited to nanoparticles, lipids, and polymers, as long as they are conjugated onto branched DNA. We believe that this DNA-assisted protein intracellular delivery (DAPID) system will result in a paradigm shift in drug development and delivery.

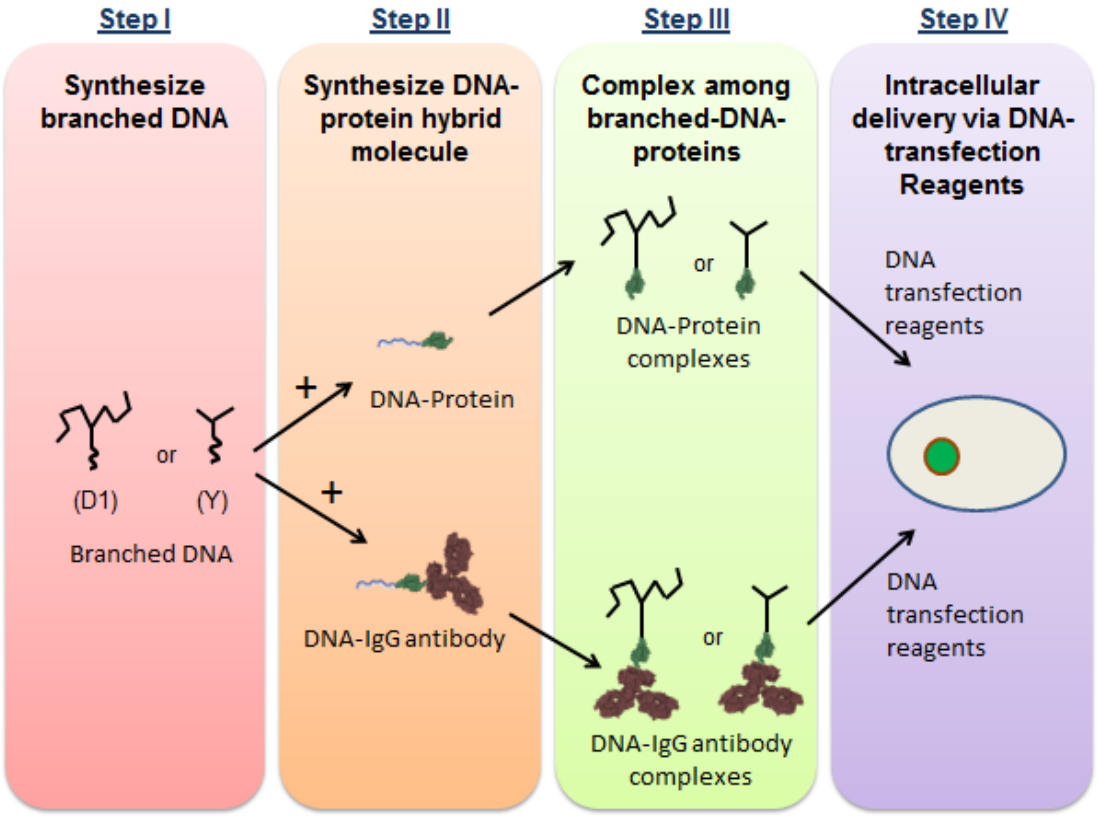

(IgG antibody serves as a special example for proteins)

Figure 5.1. Scheme illustrating DNA-assisted protein intracellular delivery system (DAPID system). Branched DNA structures (for examples, D1, or Y) were hybridized with DNA-protein hybrid molecules to serve as the nanocarriers for protein and IgG antibody intracellular delivery. Also, using DNA transfection reagents greatly enhanced the efficiency of protein and IgG antibody intracellular uptake.

5.2. Materials and methods

5.2.1. Alexa488-labeled DNA materials formation

All oligonucleotides were commercially synthesized by Integrated DNA Technologies (Coralville, Iowa). The sequences with modifications were HPLC purified, and the ones without modifications were standard desalting. Without further purification, the oligonucleotides were dissolved in TE buffer (10 mM Tris, pH=8.0, 1 mM ethylenediaminetetraacetic acid (EDTA)) with a final concentration of 100 μM.

a. Alexa488-labeled Y-DNA (Y) formation:

Y-DNA was annealed using the program showed in Table 3.2 of chapter 3. Three oligonucleotide components Y_a, Y_{bG}, $Y_{c\_anti\ linker\ 3}$ (Table 5.1) were mixed at a molar ratio of 1:1:1 in the annealing buffer (10 mM Tris, pH 8.0, 1 mM EDTA, and 50 mM NaCl) with a final concentration of 10 μM for each oligonucleotide. The product was confirmed with 3% agarose gel electrophoresis.

Table 5.1: Sequences of oligonucleotides for Y-DNA (Y)

Name	Modification	Sequences (from 5' to 3')
Y_a	None	TGGATCCGCATGACATTCGCCGTAAG
Y_{bG}	5'-Alexa488	CTTACGGCGAATGACCGAATCAGCCT
$Y_{c\_anti\text{-}linker\ 3}$	None	AGGCTGATTCGGTTCATGCGGATCCATT ACGGAGGTGGTTGTGGCA

b. Alexa488-labeled DL-DNA (G1) formation:

G1 generation of DL-DNA included four different Y-DNA which were modified from previously published works.[9] The sequences were shown in Table 5.2. Individual Y was formed at 10 µM final concentration with the same protocol as above. After that, T4 ligase enzyme was used at 0.1 U/µl concentration to link these Y together at 1:1:1:1 molar ratio to form G1 structure. The ligation reaction was conducted at room temperature for overnight. The product was confirmed with 3% agarose gel electrophoresis.

Table 5.2: Sequences of oligonucleotides for DL-DNA (G1)

	Name	Modification	Sequences (from 5' to 3')
Y1	Y_{1a}	None	TGGATCCGCATGACATTCGCCGTAAG
	Y_{1b}	5'- Phosphorylation	TGACCTTACGGCGAATGACCGAATCAGCCT
	$Y_{c\_anti\text{-}linker\ 3}$	None	AGGCTGATTCGGTTCATGCGGATCCATTACG GAGGTGGTTGTGGCA
Y2	Y_{2a}	5'- Phosphorylation	GCAATGGATCCGCATGACATTCGCCGTAAG
	Y_{2b}	None	CTTACGGCGAATGACCGAATCAGCCT
	Y_{2c}	None	AGGCTGATTCGGTTCATGCGGATCCA
Y3	Y_{3a}	5'- Phosphorylation	ATCGTGGATCCGCATGACATTCGCCGTAAG
	Y_{bG}	5'-Alexa488	CTTACGGCGAATGACCGAATCAGCCT
	Y_{3c}	None	AGGCTGATTCGGTTCATGCGGATCCA
Y4	Y_{4a}	5'- Phosphorylation	GTCATGGATCCGCATGACATTCGCCGTAAG
	Y_{4b}	5'- Phosphorylation	CGATCTTACGGCGAATGACCGAATCAGCCT
	Y_{4c}	5'- Phosphorylation	TTGCAGGCTGATTCGGTTCATGCGGATCCA

c. Other Alexa488-labeled DNA scaffolds formation

DNA scaffolds with different sizes were formed by mixing the three oligonucleotide components Y_{aG-10}, Y_{b-10}, and $Y_{c\_anti\ linker\ 3}$ (Table 5.3) at different molar ratios as described in Table 5.4 with the same protocol of forming Y-DNA. The products were confirmed with 2% agarose gel electrophoresis.

Table 5.3: Sequences of oligonucleotides for DNA scaffold

Name	Modification	Sequences (from 5' to 3')
Y_{aG-10}	5'-Alexa488	TGGATCCGCATGACATTCGCCGTAAGCGGACGTCCG
Y_{b-10}	None	CTTACGGCGAATGACCGAATCAGCCTCGGACGTCCG
Y_{c-10}	None	AGGCTGATTCGGTTCATGCGGATCCACGGACGTCCG
$Y_{c\_anti-linker\ 3}$	None	AGGCTGATTCGGTTCATGCGGATCCATTACGGAGGT GGTTGTGGCA

Table 5.4: Different conditions of DNA scaffolds. 1 molar ratio is equal to 20 μM final concentration. Alexa488 dye is represented by "G" in YaG-10 sequence.

Sample	Molar ratios			
	Y_{aG-10}	Y_{b-10}	Y_{c-10}	$Y_{c\_anti-linker\ 3}$
D1	1	1	0	1
D2	1	1	1	0
D3	1	1	0.5	0.5
D4	1	1	0.75	0.25
D5	1	1	0.25	0.75
D6	1	1	1	0.25
D7	1	1	1	0.5
D8	1	1	1	1

5.2.2. Cellular Uptake Protocol for DNA materials

100,000 cells were plated into each well of 24-well plate with 250 ul Dulbecco's Modified Eagle Medium (DMEM) (Cellgro, Mediatech, Inc., Manassas, VA), and incubated at 37°C for overnight. The next morning, the full medium was removed and replaced with 150 µl of Opti-MEM medium (Invitrogen, Grand Island, NY). Different DNA samples were added into each well at 50 nM and 200 nM final concentrations depending on the experiment designs. The samples were incubated at 37°C for about 6 hours, and then trypsinized with 170 µl of 0.2% trypsin EDTA (Cellgro, Mediatech, Inc., Manassas, VA) for two minutes at 37°C. 340 µl of full medium was then added to inhibit the trypsinization, and the cells were transferred into 0.5 ml eppendorf tubes, and centrifuged at 3000 rpm for 5 min. The supernatants were removed and the cells were resuspended in 250 µl PBS for flow cytometry analysis immediately.

5.2.3. DNA-protein complexes

EZZcys-DNA conjugates were incubated with Alexa488-labeled DNA materials (Y and D1 only) in 1x PBS buffer, pH 7.4 at 1:1 molar ratio for one hour at room temperature to form DNA-protein complexes. The DNA-protein materials were delivered into cells and analyzed with flow cytometer following the cellular uptake protocol for DNA materials as above. DNA-protein samples were also run on 2% agarose gel to double check the hybridization efficiency between EZZcys-DNA conjugates with Y and D1 materials.

5.2.4. DNA-IgG antibody complexes

EZZcys-DNA conjugates were first incubated with normal rabbit FITC-labeled IgG antibodies (Santa Cruz, Inc., Santa Cruz, CA) at 1:1 molar ratio in 1x PBS buffer, pH 7.4 at room temperature for overnight to form single stranded (ss) DNA-IgG antibody. In order to generate different DNA-IgG antibody materials, DNA materials, having complimentary sticky ends but without Alexa488 dyes, were added with ssDNA-IgG antibody at 1:1 molar ratio. For examples, double stranded (ds) DNA – IgG antibody, Y-IgG antibody, and D1-IgG antibody were formed by adding a complimentary oligonucleotide, Y, and D1 to ssDNA-IgG antibody, respectively. The DNA-IgG antibody materials were delivered into cells using a DNA transfection reagent, Lipofectamine-2000 (Invitrogen, Carlsbad, CA), and the samples were analyzed with flow cytometer as described below.

5.2.5. Cellular Uptake Protocol of DNA-IgG antibody complexes with Lipofectamine-2000

100,000 cells were plated into each well of 24-well plate with 250 µl Dulbecco's Modified Eagle Medium (DMEM) (Cellgro, Mediatech, Inc., Manassas, VA), and incubated at 37°C for overnight. The next morning, the full medium was removed and replaced with 150 µl of Opti-MEM medium (Invitrogen, Grand Island, NY). DNA-IgG antibody complexes were premixed separately with Lipofectamine-2000 as following before adding to cells. The appropriate volume of Lipofectamine-2000 (for examples, 0.5, 1.0, or 1.5 µl) was dissolved into 50 µl Opti-MEM medium and incubated at room temperature for 5 minute. At the meantime, appropriate amounts of DNA-IgG antibody samples were diluted into 50 µl Opti-MEM medium

before mixed with 50 µl of diluted Lipofectamine-2000 for 20 minutes at room temperature before the mixtures were added into cells. The samples were incubated at 37^0C for about 5 hours, and then trypsinized with 170 µl of 0.2% trypsin EDTA (Cellgro, Mediatech, Inc., Manassas, VA) for two minutes at 37°C. 340 µl of full medium was then added to inhibit the trypsinization, and the cells were transferred into 0.5 ml eppendorf tubes, and centrifuged at 3000 rpm for 5 min. The supernatants were removed and the cells were resuspended in 250 µl PBS for flow cytometry analysis immediately.

5.2.6. Fluorescence or Confocal microscope imaging

50,000 cells were prepared with 10 nM of different DNA-IgG antibody complexes in 8-well chamber slide (Thermo Fisher Scientific, NY) with 150 µl of full DMEM medium according to the protocol for intracellular uptake with Lipofectamine-2000. After incubated at 37°C for 5 hours, the cells were gently washed with 1x PBS buffer, pH 7.4 for two times at room temperature before the supernatants were removed completely. 200 µl of 4% paraformaldehyde was added, and the samples were incubated at room temperature for 30 – 45 minutes. The samples were then incubated to wash with 300 µl of 1x PBS buffer for two times for 5 minutes. The supernatants were removed and the cells were soaked with 200 µl of TBP solution (0.1% Triton X-100, 10 mg/ml BSA, and 1X PBS buffer, pH 7.4) at room temperature for 10 minutes. TBP solution was removed and the cells were washed again with 1x PBS buffer for 5 minutes before stained with 200 µl of 250 nM of DAPI solution. The samples were protected from light and incubated at room temperature for 5 minutes before washed with 300 µl of 1x PBS buffer for 10 minutes. PBS buffer was removed, and the wells and silicon surrounding were removed from the glass slide chamber. Anti-fade reagent was added before the samples were sealed with the cover glass slide. Cell images were taken by

the Olympus BX61 fluorescence microscope with appropriate exposure times. Images of Zstack series from Zeiss 510 confocal microscope was obtained to prove that the DNA-IgG antibody complexes were truly inside the cells.

5.3. Results

5.3.1. Alexa488-labeled DNA materials

DNA materials with well-defined structures such as Y-DNA and G1 DL-DNA as well as undefined structures such as DNA scaffolds were used to test the capability of getting inside the cells before being used as the carriers for protein delivery. Figure 5.2a shows the relative size comparison of oligo (lane 1), Y-DNA (Y) (lane 2-3), DNA scaffold (D1) (lane 4-7), and DL-DNA (G1) (lane 8). Based on the sizes of Y and G1 structures which are about 10 nm and 15 nm, respectively, we can assume that the sizes of D1 structures are also the same based on the similar mobility on gel. Moreover, several structures of DNA scaffolds (Figure 5.2b) were also formed with different ratios of oligonucleotide components as described on table c) to test whether the sizes would affect the uptake efficiency. For DNA scaffolds formation, when three 10 base non-palindromic sticky ends were used together (D2 structure), the network would expand easily to form very big structures. This behavior is similar to that of DNA hydrogels (data not shown). Thus, the product was mostly stuck in the well of the gel. When adding Yc_anti linker 3, which acted as a stopper to the polymerization of DNA scaffold, the structures got smaller depending on the total number of sticky ends available in the mixture. D1 with only two sticky ends used formed the smallest structure of DNA scaffold. However, although the average size could be controlled, the polydispersity was very high; more investigation and optimization may be needed

in order to reduce this variation.

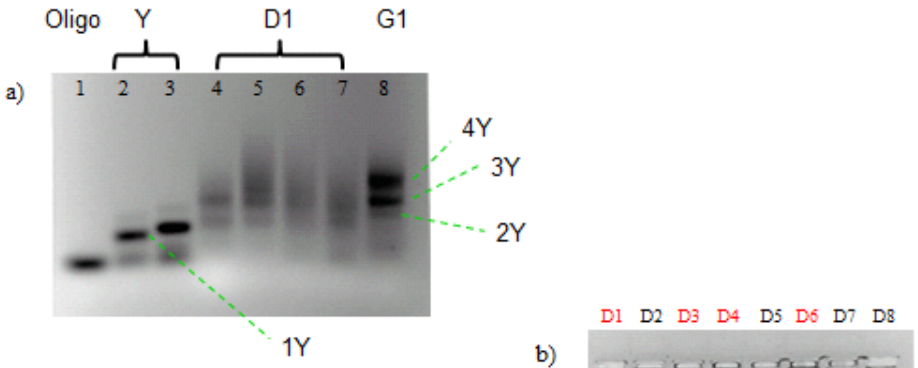

c)

Sample	Molar ratios			
	YaG-10	Yb-10	Yc-10	Yc_anti-linker 3
D1	1	1	0	1
D2	1	1	1	0
D3	1	1	0.5	0.5
D4	1	1	0.75	0.25
D5	1	1	0.25	0.75
D6	1	1	1	0.25
D7	1	1	1	0.5
D8	1	1	1	1

Figure 5.2. Relative size comparison of different DNA materials on agarose gel. DNA samples contained Alexa488 dye, so the images were taken directly without staining using a green filter. a) 3% agarose gel electrophoresis. 1. Oligonucleotide. 2. Y-DNA with one anti-linker overhang. 3. Y-DNA with two anti-linker overhang. 4-7. DNA scaffolds (D1 structure) at 1, 20, 50, and 75 µM concentrations, respectively. 8. G1 generation of DL-DNA. b) 2% agarose gel electrophoresis. D1-D8. DNA scaffold structures with different sizes were formed based on the molar ratios of oligonucleotide components as described in table c. D1 condition with only two 10 base non-palindromic sticky ends gave the smallest structure, while D2 condition with three sticky ends gave the largest one. In addition, for an estimation of sizes of DNA scaffolds, D1 sample on gel b is the same as D1 sample (lane 5) on gel a.

5.3.2. Intracellular uptake of DNA materials

DNA materials, including oligo, Y, G1, and some DNA scaffold structures (D1, D3, D4 and D6) as the representatives of different structures at different sizes were first tested for cellular uptake before considered as the carriers for proteins or IgG antibody delivery. 100,000 HeLa cells were spread in each well of 24-well plate and incubated overnight before Alexa488-labeled DNA materials were added and incubated for 6 hours at 37^{o}C. Samples were washed, resuspended in 200 µl of 1x PBS, pH 7.4, and analyzed with BD Biosciences LSR II flow cytometry analyzer, and the data was analyzed by FACSDiva Software, version 6.1.1 as described in Figure 5.3. 30,000 cells were used to be analyzed to define the uptake efficiency. Single cells were selected, and a gate of positive fluorescence signals was set up between cell only and other samples. The numbers of cells with positive fluorescence signal were divided to the number of singlets (single cells) to give % of gated cells (blue circle) which are normally used in many publications as the delivery efficiency. However, this information did not take into account of duplets, clusters of cells, differentiated cells, and especially dead cells which could be caused by materials triggering the apotosis cycle. Therefore, instead of using % of gated cells to reflect the efficiency of delivery, the numbers of cells containing positive signals were divided to 30,000 cells as the total cells analyzed to get the % uptake (red circle), which would more accurately reflect the true uptake efficiency. Moreover, it was important to look at the mean value of fluorescence intensity from singlets (green circle) since it reflected the average numbers of molecules getting inside the cells as a parameter to measure the efficiency of uptake. The amount of material that could be delivered inside the cells

depends on the material. Therefore, it is necessary to use both % uptake and mean of fluorescence intensity (FITC-A mean) to calculate the efficiency of intracellular delivery or uptake which is described in the formula, total fluorescence intensity (total F.I.) = % uptake x FITC mean.

The uptake efficiency of different materials, including single stranded (ss) DNA, Y, G1, and four different DNA scaffolds (D1, D3, D4 and D6) was investigated before they were selected as the nanocarriers for protein intracellular delivery (Figure 5.4). Surprisingly, ssDNA had a high uptake at high concentration (200 nM), but it reduced dramatically at lower concentration (50 nM). This high concentration dependence suggested that the ssDNA uptake happened nonspecifically. Besides, the higher generations of DNA structures with bigger sizes, such as G1, D3, D4, and D6 showed lower uptake efficiency, unexpectedly, compared to Y and D1 structures. Unlike silica nanoparticles, which showed the best uptake at 50 nm size[10], DNA structures seemed to be uptaken better at smaller sizes, around 10 – 20 nm instead. Y and D1 structures, therefore, were chosen to be used to delivery proteins for the next step.

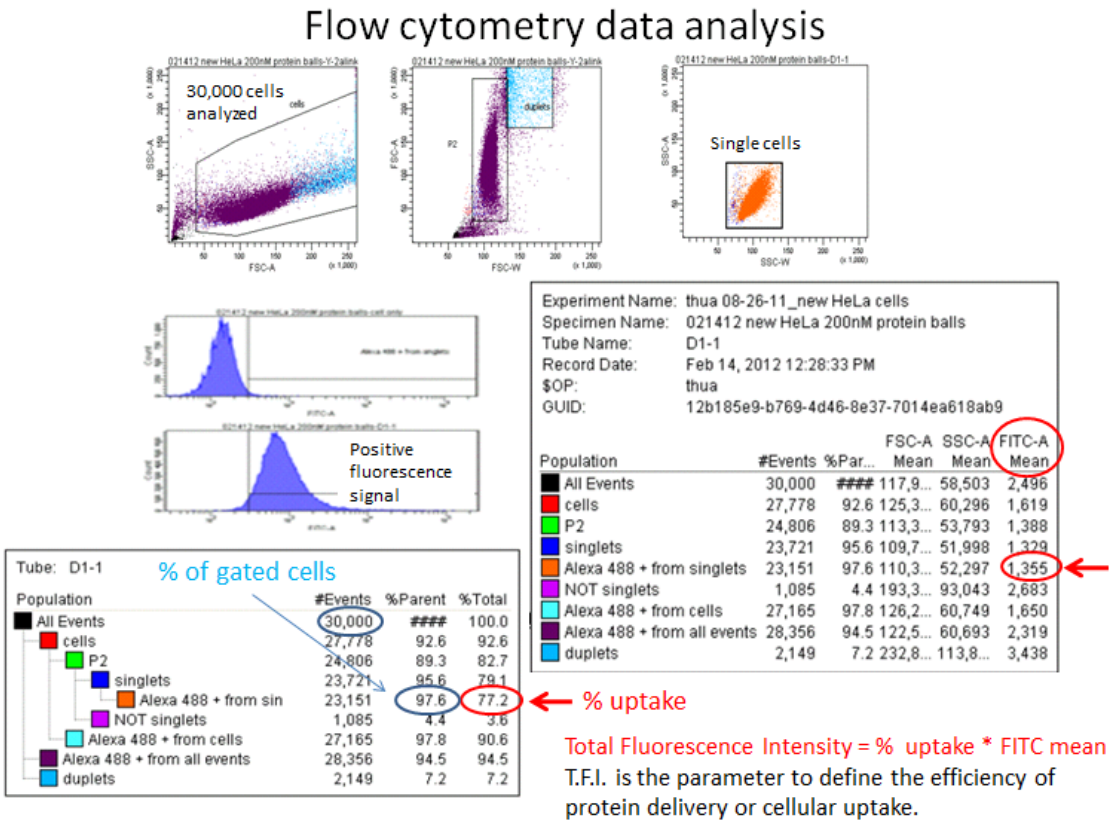

Figure 5.3. Flow cytometry analysis. 30,000 cells were analyzed, and positive fluorescence signals were collected from single cell population. The number of cells with positive signals was divided to total number of cells analyzed to get % uptake (red circle). Total fluorescence intensity was calculated by multiplying % uptake with fluorescence mean value (green circle) to define the efficiency of intracellular delivery or uptake efficiency.

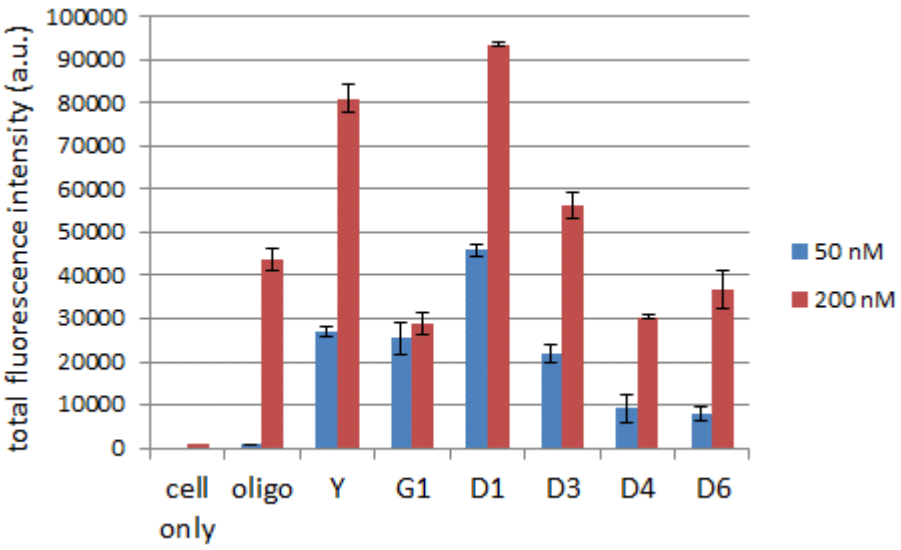

Figure 5.4. Intracellular uptake efficiency of different DNA materials. Total fluorescence intensity indicated the uptake efficiency. Single stranded DNA (oligo) had strong nonspecific uptake at high concentration (200 nM), but dramatically reduced at lower concentration (50 nM). Higher generations of DNA structures (G1, D3, D4, and D6) with larger sizes had lower uptake efficiency, compared to Y and D1 structures (which is around 10 – 20 nm size). Y and D1 which showed the best uptake among the samples were chosen to test their ability to carry proteins inside the cells. Error bars were calculated from 5 repeated separate experiments for cell only, oligo, Y, G1, and D1 samples, but only 2 repeated separate experiments for D3, D4, and D6 samples.

5.3.3. Intracellular uptake of DNA-protein complexes

Alexa488-labeled Y and D1 DNA materials were used to delivery EZZ protein inside HeLa cells. DNA-protein conjugates were incubated with Alexa488-labeled DNA materials (Y and D1 only) at 1:1 molar ratio form DNA-protein complexes for intracellular uptake. Flow cytometry analysis was performed to define the uptake efficiency. The incorporation of EZZ protein onto Y and D1 structures was confirmed by 2% agarose gel electrophoresis as well.

As shown in Figure 5.5 a, almost 100% of EZZcys-DNA conjugates were hybridized to Y and D1 structures, based on the amount of left over Y or D1 in the samples (lanes 2 and 4). Moreover, as a preliminary test, EZZ-SNAP-DNA conjugate was also used together with EZZcys-DNA conjugate to form a DNA-protein complex of one Y and two proteins (lane 3). The purpose of this sample was to see if multiple proteins could be delivered inside the cells using branched DNA structures. Although the incorporation efficiency of two proteins onto one Y was not as good as one protein and one Y, it still showed that we were able to form a two (or three) protein-DNA complex for multiplexed protein detection. Moreover, higher sequence specificity of different sticky ends of Y or branched structures could be designed in order to get higher hybridization efficiency of multiple DNA-protein conjugates with branched DNA.

Protein-DNA complexes were then delivered into HeLa cells for 6 hours at 37oC before analyzed with flow cytometry reader, similar to the procedures described for the intracellular uptake of DNA materials above. The images on the left hand of Figure 5.5 b showed the flow cytometry data of some representative samples, for

examples of cell only, Y-EZZ and D1-EZZ samples at 200 nM concentrations. Clearly, the protein-DNA complexes were uptaken by cells to give a clear shift when compared with cell only sample. For the quantitative data analysis, total fluorescence intensity (T.F.I.) was calculated and graphed as shown in the chart on the right-hand side. Based on T.F.I. value, the uptake of DNA-protein complexes (about 45,000-50,000 a.u.) was about half of that of DNA only (about 80,000 - 90,000 a.u.) although the % of gated cells appeared to be almost 100%. This indicated that the number of DNA-complexes getting inside the cells was about half that of DNA only so that FITC-A mean value reduced half. This is expected since the incorporation of protein onto DNA should have introduced some charge effects that interfered with the intracellular uptake efficiency. In addition, the bigger sizes of the DNA-protein complexes could have affected the uptake efficiency since we have known that cells did not uptake well the bigger DNA structures (such as G1, D3, D4, and D6) as concluded above.

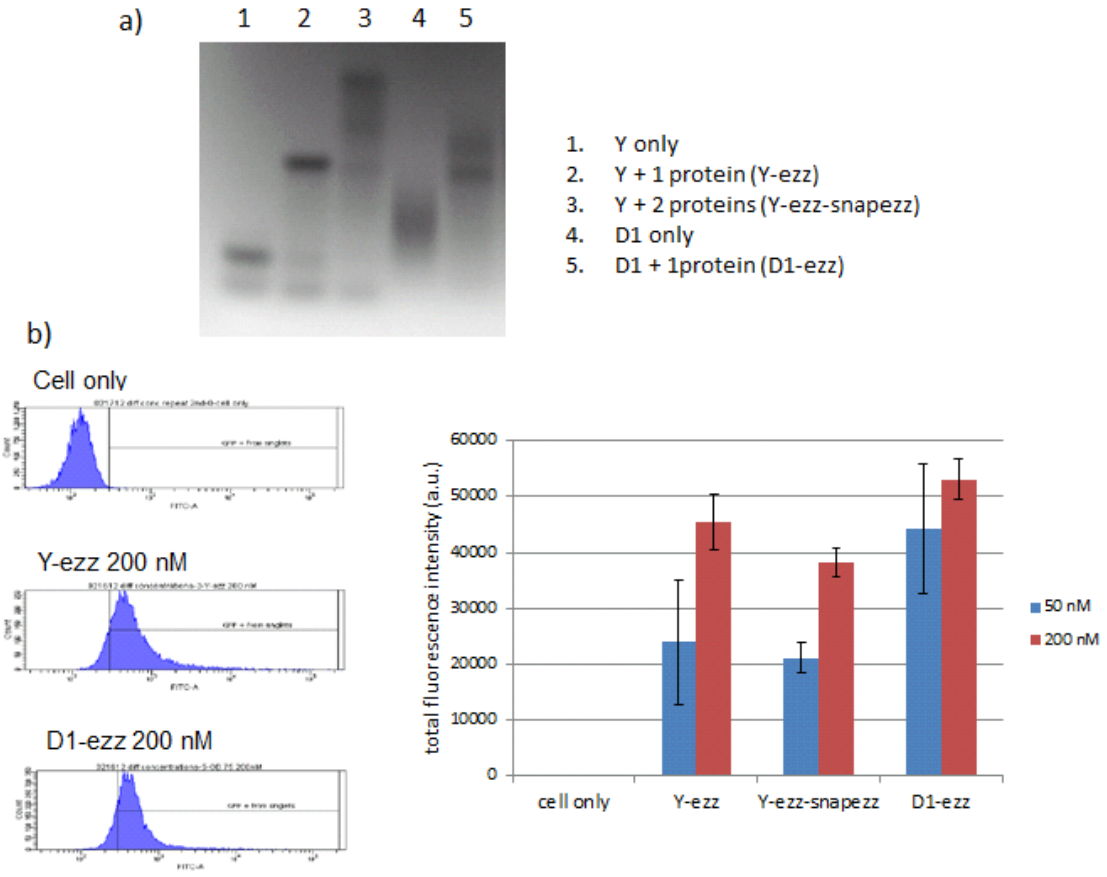

Figure 5.5. Intracellular uptake of DNA-protein complexes. a) confirmation of DNA-protein complexes on 2% agarose gel. 1. Y DNA only. 2. Y + EZZcys-DNA conjugate. 3. Y + EZZcys-DNA and EZZ-SNAP-DNA conjugates. 4. D1 DNA only. 5. D1 + EZZcys-DNA conjugate. b) on the left side, flow cytometry data on % of gated cells of some representative samples. The % of cells with positive fluorescence signals appeared to be almost 100%. However, the total fluorescence intensity was about only half, which indicated that the number of DNA-protein complexes getting inside the cells reduced half, when compared to that of DNA uptake only.

5.3.4. Intracellular uptake of DNA-IgG antibody complexes with Lipofectamine-2000

Although flow cytometry data showed a clear shift in fluorescence signals between cells with and without DNA-protein complexes, we were unable to obtain fluorescence microscope images with strong fluorescence signals to confirm the results. In order to enhance the uptake efficiency of DNA-IgG antibody, Lipofectamine-2000, a DNA transfection reagent, was used. Different DNA-IgG antibody materials were generated by mixing FITC-labeled IgG antibodies with EZZcys-DNA conjugate and DNA materials (oligonucleotide, Y, and G1) at 1:1:1 molar ratios. The DNA-IgG antibody materials were delivered into cells and analyzed with a flow cytometry reader to compare the efficiency of protein intracellular delivery. Besides, instead of using Alexa488-labeled DNA to generate fluorescence signals for flow cytometry analysis, the fluorescence signals now will be read directly from FITC dye of IgG antibodies. This helps to avoid the problem of getting positive signals from DNA materials getting inside the cells, but without proteins or IgG antibodies due to the low hybridization yield between DNA and DNA-IgG antibody products. The intensity of fluorescence signals in this case will truly reflect the number of IgG antibodies existed inside the cells so that it can be used to directly compare the uptake efficiency among the samples.

First, different amounts of Lipofectamine-2000 were used to define the best efficiency since one of the problems of using DNA transfection reagent is that it can kill a lot of cells if overused, which will affected the overall efficiency of uptake. Three different volumes, 0.5, 1, and 1.5 µl of Lipofectamine-2000 were used to test

the uptake efficiency of Y-IgG and D1-IgG samples at 10 and 50 nM. Cells only with DNA samples, but with the same amount of Lipofectamine-2000 were used as negative controls. Also, samples without Lipofectamine-2000 were used to compare the uptake efficiency. As expected, the uptake efficiency of the samples with Lipofectamine-2000 was much higher compared to that without Lipofectamine-2000, and it reduced with less amount of Lipofectamine-2000 used (Figure 5.6).

Since Lipofectamine-2000 greatly enhanced the intracellular uptake efficiency, we wondered if branched DNA would have any advantage over linear DNA since DNA transfection reagents were developed for genes (linear DNA), and siRNA (linear RNA). Therefore, we used the best uptake condition above, which is at 50 nM materials with 1.5 µl of Lipofectamine, to test the efficiency of different materials, including, cell only, IgG only, single stranded (ss) DNA-IgG, double stranded (ds) DNA-IgG, Y-IgG, and D1-IgG (Figure 5.7). The same set of samples but without Lipofectamine was used as controls. Clearly, Lipofectamine overpowered the uptake. Also, branched DNA (Y and D1) have shown much better yield compared to linear DNA (ss and ds). This could be due to branched DNA having more accessibility to Lipofectamine, a cationic lipid, which could enable the transfection complexes between Lipofectamine and branched DNA to enter the cells through endocytosis more efficiently.

As mentioned before, Lipofectamine could be toxic to the cells, so the MTT cell viability assay was conducted to determine the toxicity of Lipofectamine as well as that of DNA-protein hybrid molecules. The samples were prepared at 50 nM of materials with or without 1.5 µl at 37^{o}C for 5h. The same samples without

Lipofectamine were used as controls, and the data was normalized to cell only without Lipofectamine. As shown in Figure 5.8, Lipofectamine itself at 1.5 μl was not toxic to cells, and DNA-protein hybrid materials also showed low cytotoxicity.

Furthermore, fluorescence microscope images (Figure 5.9) were obtained to confirm the flow cytometry data that DNA-protein materials were delivered to cells with high efficiency. Moreover, z-stack series of confocal microscope images were also confirmed that the materials were actually delivered inside the cells (data not shown). In addition, endocytosis mechanism of cellular uptake for branched DNA-protein materials with Lipofectamine-2000 was confirmed with samples prepared at 37^{o}C and 4^{o}C (Figure 5.10).

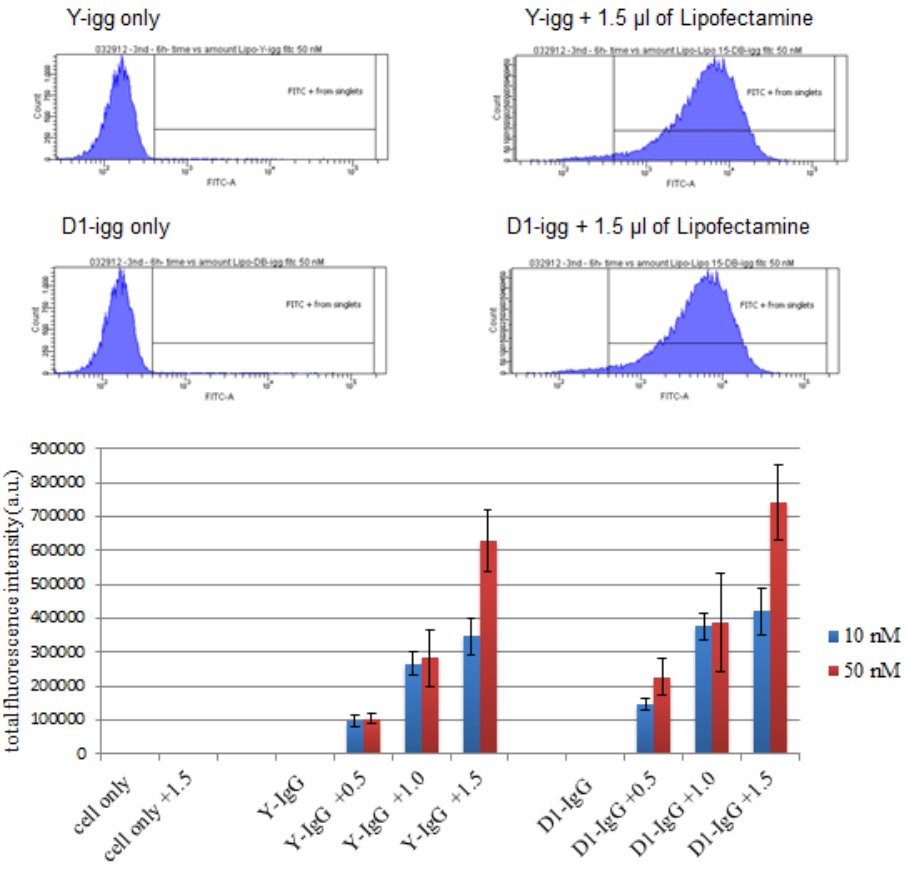

Figure 5.6. Effects of Lipofectamine-2000 on branched DNA-IgG antibody intracellular delivery. Y-IgG and D1-IgG samples were delivered inside the cells for 5h at 37^{o}C. +0.5, +1.0, +1.5 indicated the volume of Lipofectamine-2000 used in the samples. The upper graphs showed some representative flow cytometry data of Y-IgG and D1-IgG without and with 1.5 µl of Lipofectamine, which showed a strong effect of Lipofectamine in the cellular uptake. The chart below showed different efficiency of cellular uptake depending on the amount of Lipofectamine used. Clearly, the uptake efficiency was greatly enhanced with Lipofectamine. In addition, the effects are stronger and different between 10 and 50 nM concentrations when more volume of Lipofectamine was used (+1.5 µl). The error bars were obtained from 3 separate experiments.

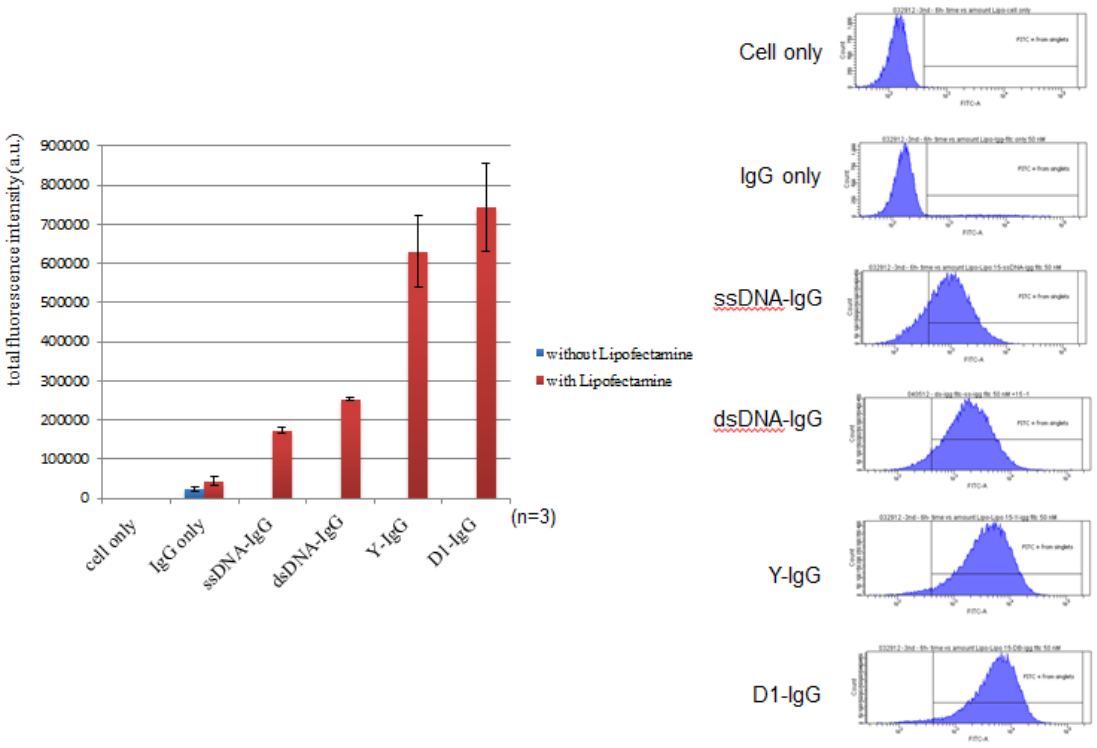

Figure 5.6. DNA-assisted IgG antibody intracellular delivery with Lipofectamine-2000. The IgG antibody materials were incubated with HeLa cells at 50 nM with or without 1.5 µl of Lipofectamine for 5h at 37^{o}C. Branched DNA-IgG complexes (Y-IgG, D1-IgG) showed much better uptake compared to linear DNA (ssDNA-IgG, ds-IgG). Some representative flow cytometry data of samples with Lipofectamine are shown in the right handed side graphs. The error bars were obtained from 3 separate experiments.

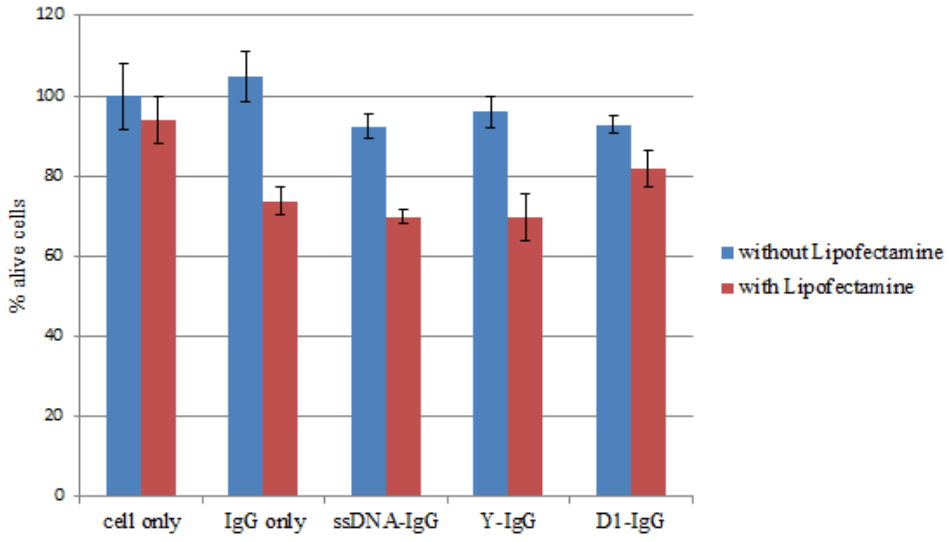

Figure 5.8. Cytotoxicity of Lipofectamine-2000 and DNA-protein materials to cells. 1.5 µl of Lipofectamine was used with 50 nM of materials at 37^{o}C for 5h. MTT assay was performed, and the data was normalized to cell only without Lipofectamine. Lipofectamine-2000 itself at 1.5 µl is not toxic to cells when compared to cell only without Lipofectamine. DNA-protein hybrid materials also have low cytotoxicity. The error bars were obtained from 3 separate experiments.

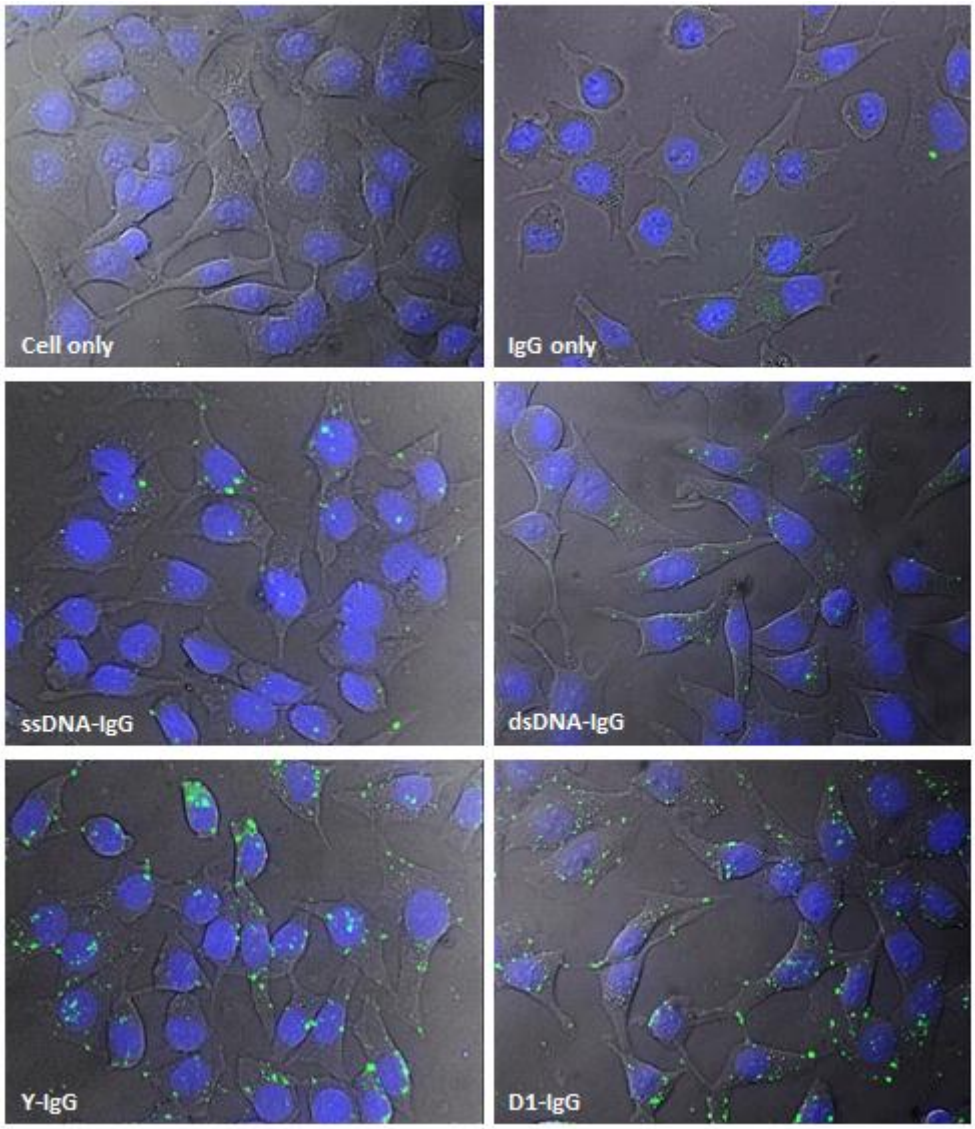

Figure 5.9. Fluorescence microscope images of DNA-assisted IgG antibody delivery with Lipofectamine-2000. 10 nM of materials were used with 1.5 µl of Lipofectamine at 37^{o}C, 5h. Clearly, the images confirms flow cytometry results that branched DNA-protein can deliver proteins intracellulary in high efficiency. Also, Zstack series of images from confocal microscope confirmed that the IgG antibodies are inside the cells (data not shown).

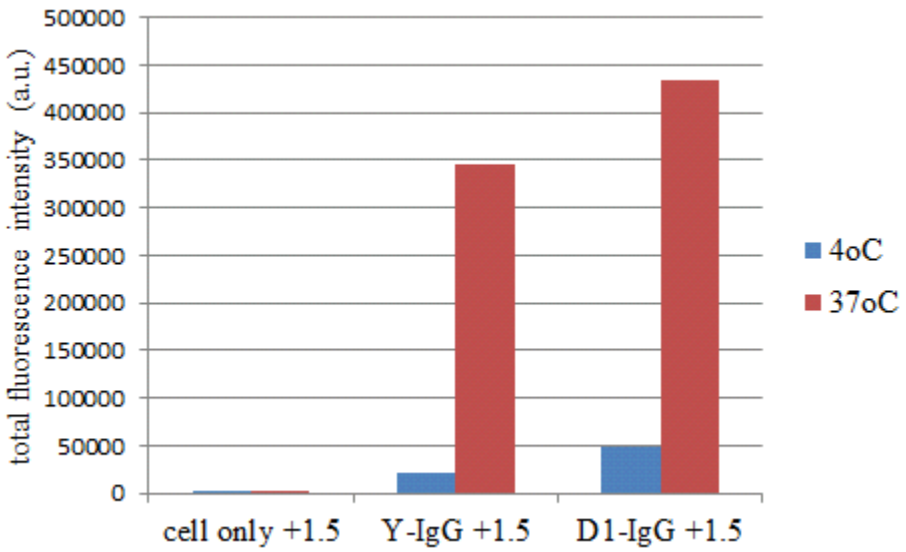

Figure 5.10. Endocytosis is the main uptake mechanism of branched DNA-protein complexes with Lipofectamine.

5.4. Conclusions

Branched DNA (Y, and D1) has proved to be very efficient in protein intracellular delivery with DNA transfection reagents such as Lipofectamine-2000. In particular, since EZZ protein can bind to almost all IgG antibodies, the system can be easily extended to IgG antibody intracellular delivery. Using DNA-protein conjugation methods, any proteins now can be delivered efficiently inside the cells with the support of DNA transfection reagents. Besides, branched DNA allows multiple proteins to be delivered simultaneously. Furthermore, not only proteins, but any moieties which can be attached with DNA can be delivered inside cells also, for example, lipids, polymers, gold nanoparticles, etc. This novel approach may lead to the new discovery of drugs and treatments for currently uncured diseases due to the limitations of current delivery methods.

References:

1. Gu, Z., Biswas, A., Zhao, M. & Tang, Y. Tailoring nanocarriers for intracellular protein delivery. *Chem. Soc. Rev.* **40**, 3638-3655 (2011).

2. Brown, L. R. Commercial challenges of protein drug delivery. *Expert Opin. Drug Deliv.* **2**, 29-42 (2005).

3. Lu, Y., Yang, J. & Sega, E. Issues related to targeted delivery of proteins and peptides. *AAPS J.* **8**, E466-78 (2006).

4. Kelloff, G. J. & Sigman, C. C. Cancer biomarkers: selecting the right drug for the right patient. *Nat. Rev. Drug Discov.* **11**, 201-214 (2012).

5. Leader, B., Baca, Q. J. & Golan, D. E. Protein therapeutics: a summary and pharmacological classification. *Nat. Rev. Drug Discov.* **7**, 21-39 (2008).

6. Roh, Y. H. *et al*. Photocrosslinked DNA Nanospheres for Drug Delivery. *Macromolecular Rapid Communications* **31**, 1207-1211 (2010).

7. Lee, J. B. *et al*. Multifunctional nanoarchitectures from DNA-based ABC monomers. *Nat. Nanotechnol* **4**, 430-436 (2009).

8. Walsh, A. S., Yin, H., Erben, C. M., Wood, M. J. & Turberfield, A. J. DNA cage delivery to mammalian cells. *ACS Nano* **5**, 5427-5432 (2011).

9. Li, Y. *et al*. Controlled assembly of dendrimer-like DNA. *Nat. Mater.* **3**, 38-42 (2004).

10. Lu, F., Wu, S. H., Hung, Y. & Mou, C. Y. Size effect on cell uptake in well-suspended, uniform mesoporous silica nanoparticles. *Small* **5**, 1408-1413 (2009).

Chapter 6: Conclusions and Future directions

6.1. Accomplishments

Three methods, SNAP tag, sulfo-SMCC, and sortase A, were successfully used to conjugate DNA and proteins together without any loss of function in either the protein or DNA. The conjugation between DNA and EZZ proteins (such as EZZ-SNAP-DNA (ESD) and EZZcys-DNA conjugates) served as universal adapters to interface between DNA and IgG antibodies, affording the construction of versatile platforms for IgG antibody-based protein detection and IgG antibody intracellular delivery.

For multiplexed protein detection, IgG antibody-based DNA nanobarcodes (IgG nanobarcodes) have been successfully used to detect proteins efficiently and with high specificity across different systems, such as microbead-based assays, dot blotting, and immunofluorescence staining. In addition, by using DNA-modified quantum dots instead of DNA nanobarcodes, the complexes could be used to detect proteins from western blotting as well. Similar to prelabeled primary IgG antibodies, the IgG nanobarcode system gives a convenient approach to detect proteins with fewer steps in the procedure, while maintaining high efficiency and specificity. Moreover, IgG nanobarcodes can be generated in a one-pot reaction, simply by mixing individual components (IgG antibodiess, ESD conjugate, and DNA nanobarcodes) at 1:1:1 molar ratio – a significantly easier and simpler approach compared to the procedures to prepare prelabeled primary IgG antibodies.

For the first time, branched DNA (Y, D1 structures) has been used as a platform to deliver proteins and IgG antibodies intracellularly with high efficiency.

6.2. Limitations and Future directions

Since the EZZ protein cannot bind to some IgG antibodies, the choice of antibodies that can be used in IgG-based protein detection and delivery is somewhat limited. For protein detection, DNA nanobarcodes are not sensitive enough to have signals detected by western blotting. Quantum dots with much stronger fluorescence intensity and stability can be used to replace fluorescence dyes, but it requires complicated and expensive systems for signal read-out; for example, filters with narrower bandwidths can be utilized in the detection system in order to utilize the multiplexing capacity. Monovalent DNA-modified quantum dots can be used in place of the fluorophores in DNA nanobarcodes but their synthesis is not a trivial process. Besides, quantum dots are relatively large (about 15 nm) which may not suitable to replace small fluorophore molecules (20-100 atoms) due to steric hindrance effects.

Nevertheless, the main goal of this work is to develop DNA as a material platform for interfacing with proteins. In spite of advances in protein synthesis and engineering, there has yet to be a general customizable approach towards adding functionality onto proteins in a modular fashion. DNA, on the other hand, has been engineered as a material for a broad range of applications due to excellent control over its size, structure and anisotropicity. Here, we have developed a convenient approach to interface DNA with proteins, thus affording the ability to modify proteins and IgG antibodies without resorting to protein engineering techniques that requires skilled

personnel. Proteins and IgG antibodies now can be labeled with fluorophores, quantum dots, nanoparticles, or any moieties that can be modified with DNA, in a single mixing step, requiring no chemical reactions. Besides, proteins can be arranged in a specific configuration by DNA either on microarrays or rationally designed structures by incorporating novel structures made available through DNA nanotechnology. Moreover, we envision that new proteins with desired functions can be engineered by bringing different protein domains together using DNA as a linker. We expect that this approach will open up new avenues for engineering proteins without going through complicated steps or relying on the predictions of amino acid sequences to tertiary structures to functions of proteins.

Furthermore, with the demonstration of the versatility of IgG nanobarcode systems, DNA-protein conjugate provided a platform not only for fluorescence-based protein detection system, but it can also be expanded to other detection systems such as label-free, using optical and electrical properties of gold nanoparticles. Similarly, for the development of protein delivery, or for the discovery of new drugs, protein drugs now will not stand alone in the battle of uncured diseases. With the interfacing of DNA and the supports from other DNA nanotechnology, protein drugs can be combined with any other moieties such as lipid, polymers, nanoparticles, etc. to create "super" drugs. More importantly, the drugs will not just target at the surface of the cells, which all current protein drugs do, but they will be delivered efficiently inside the cells using DNA transfection reagents which are well developed for more than 50 years, and some are FDA-approved. We are optimistic that the development of this technology will pave the way for a future of DNA-based protein engineering, where

malfunctioned proteins inside the cells can be replaced with the healthy ones to set up again the normal functions of the cells without guessing or relying on signaling pathways to judge the effects of new drugs.